



IMPI's
50TH ANNUAL MICROWAVE
POWER SYMPOSIUM (IMPI 50)

2016 PROCEEDINGS

June 21-23, 2016

**The Caribe Royale All-Suite Hotel
& Convention Center
Orlando, Florida, USA**

ISSN 1070-0129

Presented by the
INTERNATIONAL MICROWAVE POWER INSTITUTE

PO Box 1140, Mechanicsville, VA 23111
Phone: +1 (804) 559 6667 • Email: info@impi.org

WWW.IMPI.ORG

WELCOME TO ORLANDO FOR THE 50TH IMPI SYMPOSIUM

Each year, IMPI brings together researchers from across the globe to share the latest findings in microwave and RF heating theories and applications, and this year we have an outstanding array of researchers in attendance. If you are not yet a member of IMPI, we strongly encourage you to consider joining onsite. IMPI membership connects you to microwave and RF academia, researchers, developers and practitioners across the globe. Talk to an IMPI member today to learn more about the value of joining our outstanding organization!

Thank you for joining us. We hope you learn from the technical presentations, interact with your colleagues, and enjoy the atmosphere of the Symposium. And do take the opportunity to visit the many interesting sites in and around Orlando.

Special thanks to the following partners for printing these Proceedings:



IMPI wishes to express its gratitude to the following individuals:

TECHNICAL PROGRAM COMMITTEE

Chair Ulrich Erle, Nestle R & D, USA
Co-chair Kadir Aslan, Morgan State University, USA

Members

Vladimir Bilik, S-TEAM Lab, The Slovak Republic
Raymond Boxman, Tel Aviv University, Israel
Graham Brodie, University of Melbourne, Australia
Georgios Dimitrakis, University of Nottingham, UK
John F. Gerling, GAE, Inc., USA
Satoshi Horikoshi, Sophia University, Japan
Marilena Radoiu, Independent Consultant, France
Vadim V. Yakovlev, Worcester Polytechnic Institute, USA

FOOD SCIENCE AND TECHNOLOGY COMMITTEE

Chair Bob Schiffmann, R.F. Schiffmann Associates, Inc., USA

Members

Gordan Andrews, GAMA Microwave Technology Ltd., United Kingdom
Justin Balousek, The Kraft Heinz Company, USA
Sumeet Dhawan, Nestle R & D, USA
Marie Jirsa, Tyson Foods, USA
Ric Gonzalez, ConAgra Foods, USA
Jeyamkondan Subbiah, University of Nebraska- Lincoln, USA
Juming Tang, Washington State University, USA
Mark Watts, Campbell Soup Company, USA

Purchasing Information: Copies of the Proceedings of the 50th Annual Microwave Power Symposium, as well as back issues from prior years, are available for purchase. Contact Molly Poisant, Executive Director of IMPI, at +1 804 559 6667 or molly.poisant@impi.org for details.

TABLE OF CONTENTS

MEDICAL APPLICATIONS

The Use of Microwave Power for Treatment of Cancer Augustine Y. Cheung	11
Antenna Applicators and Microwave Fields for Imaging of the Interior of Human Breasts and Heads P.O. Risman	14
Microwave-Accelerated Bioassays Enock Bonyi	16
Alternative Treatment of Gout using Metal-Assisted and Microwave-Accelerated Decrystallization (MAMAD) Technique Zainab Boone-Kukoyi	19
Crystallization of Lysozyme on Nanoparticle Surfaces using Monomode Microwave Heating Brittney Gordon	22

DIELECTRIC PROPERTIES

Use of Dielectric Properties for Agricultural Applications Stuart O. Nelson	25
Dielectric Properties of Biomass/Bentonite Clay Mixtures between 0.5 and 20 GHz Candice Ellison	28
Design of a Test Cell for Dielectric Properties Measurement Soon Kiat Lau	31

SOLID STATE

Recognizing Design Challenges of Solid-State Power Amplifiers for RF Energy Applications Klaus Werner	34
64 kW Microwave Generator Using LDMOS Power Amplifiers for Industrial Heating Applications Bob Bartola	37
Compact 1 kW 2.45 GHz Solid-State Source for Industrial Applications Roger Williams	39

TABLE OF CONTENTS

FOOD SCIENCE & TECHNOLOGY I

A Comparison of Mode Mixer vs. Turntable Upon Temperature Response of Small Samples Robert F. Schiffmann	42
Multiphysics Modeling of the Effect of Headspace Steam on Microwave Heating Performance of a Frozen Heterogeneous Meal Jiajia Chen	43
Model Food System Development for Quality Optimization of Microwave-Assisted Pasteurized Foods Ellen Bornhorst	45

INDUSTRIAL APPLICATIONS I

The Use of Microwave Energy in Reactive Powder Metallurgy Cristina Leonelli	48
A Novel Microwave-Low Pressure Process for Strengthening High Performance Concrete Paste Natt Makul	51
Improved Treatment for Wood Boards Disinfestation by Microwave Power Application A. Tatiana Zona Ortiz	54
Feasibility of Liberating Gold from Refractory Ores by Microwave Irradiation Prosper Munemo	57

MICROWAVE EQUIPMENT

Development of High Power 5.8GHz CW Magnetron -Industry's First Nagisa Kuwahara	59
Performance Description of a Cavity for Heating α-SiC at 5.8 GHz Juan Antonio Aguilar-Garib	62
Improvement of Microwave Heating Uniformity Contributed by the Screw Propeller Huacheng Zhu	65
3D Particle-In-Cell Simulation Study of Injection Locked Magnetron Yang Yang	68

FOOD SCIENCE & TECHNOLOGY II

Microwave Modelling in the Food Industry: Combined Microwave Baking and Tubular Microwave Processing of Particulate Foods Birgitta Wäppling Raaholt	71
---	----

TABLE OF CONTENTS

INDUSTRIAL APPLICATIONS II

Some Emerging Applications for Microwave Technology in Chemistry, Polymers and Waste John Gerling	73
Formation of Micro-fractures on Ludwigite Ore and its Effect on Grinding Efficiency of Ludwigite Ore under Microwave Treatment Yajing Liu	76
Development of a Coaxial Microwave Applicator for Liquid Heating over a Wide Frequency Range Tomohiko Mitani	79

FOOD & AGRICULTURE

Microwave Treatment of Garden Soil prior to Planting Raymond L. Boxman	82
Growth Stimulation System of Plants using Microwave Irradiation and Elucidation of its Molecular Mechanism Satoshi Horikoshi	85
Microwave Weed Control Graham Brodie	88
Effect of Microwave (2.45 GHz) on Agronomic Efficiency of Nitrogen in Wheat Muhammad Jamal Khan	91
Determination of Kinetic Parameters of Thermal Death of Radio Frequency Heated Red Flour Beetle (<i>Tribolium castaneum</i>) using Inverse Simulation Oon-Doo Baik	94
A Simulation Model for Microwave-Assisted Thermal Pasteurization System Deepali Jain	97

FOOD SCIENCE & TECHNOLOGY III

Magnetrons, Microprocessors and the Birth of Expert Cooking Intelligence Steven J. Drucker	100
Solid State Cooking Robin Wesson	102

PLASMA & MAGNETRONS

The Localized Microwave-Heating Paradigm and its Implementation in Solids, Powders, and Dusty Plasma Eli Jerby	105
--	-----

TABLE OF CONTENTS

Study on an Injection-Locked Magnetron Satoshi Fujii	108
Microwave Induced Plasma for Food Sanitizing in a Technological Scale M. Andrasch	111
The Plasma Boost in Semiconductor Industry Tunjar Asgarli	114
 <u>POSTERS</u> 	
Dielectric Properties of Concrete: An Experiment and New Model Approach Natt Makul	117
Microwave Aided Plasma Generation Mathias Andrasch	120
A Novel Microwave-Thermal Process for Accelerated Curing of Concrete Paste Natt Makul	123
Cooking by Microwave Fireball Excited from Salty-Water Jet Eli Jerby	126
Inversion of the Mixture Models for Materials of Required Complex Permittivity Vadim V. Yakovlev	129

NOTES

NOTES

The Use of Microwave Power For Treatment of Cancer

Augustine Y. Cheung
Medifocus Incorporated, Columbia, Maryland, USA

Keywords: Microwave thermotherapy, cancer, heat activated drug, heat activated gene therapy.

INTRODUCTION

The therapeutic potential of heat has long been recognized. However, the inability to focus heat precisely at disease sites on a reliable and repeatable basis had hampered the development of heat energy as a therapeutic modality. In the 1970s', the commercialization of the microwave oven and the emergence of high power microwave transmission systems for communication and military uses again rekindled the interests among medical communities in the use of "Microwave Heat" as a viable cancer treatment alternative. The excitement led to worldwide efforts in development and commercialization of microwave hyperthermia systems and devices for cancer treatment.

FOCUSED HEAT THERMOTHERAPY

Heat kills cells just like radiation and chemotherapy. Properly delivered and controlled, heat therapy led to tumor shrinkage or eradication. In addition, heat treatment does not induce side effects and cumulative toxicities as in the case of the other two conventional cancer treatment modalities. At high temperatures (50 degree C +), heat can ablate tumors. At medium temperatures (42-49 degree C), heat therapy combines synergistically with radiation and/or chemotherapy, leading to improved treatment outcomes. At lower temperatures (40-42 degree C), tumor targeted focused heat can be used to activate or release temperature sensitive drugs and genes directly at tumor sites, resulting in tumor-targeted gene therapy and chemotherapy. It has also been observed that modest heating to 41-45 degree C increases "Gene Expression" by hundreds of fold above baseline, significantly enhancing the therapeutic potential of gene therapy.

THERMO-DILATATION SYSTEM FOR TREATMENT OF BENIGN PROSTATIC HYPERPLASIA

The development and commercialization of "**Prolieve**", a catheter-based microwave thermotherapy system for treatment of Benign Prostatic Hyperplasia (BPH) is presented. "**Prolieve**" delivers minimally invasive microwave heat therapy in

combination with cooled balloon dilatation for BPH treatments. The procedure provides both immediate and long term BPH symptoms relief without the numerous undesirable side effects often associated with daily medication and/or other more invasive BPH treatment procedures. Clinical results from 100,000 BPH patients treated with “**Prolieve**” will be summarized.

BREAST CANCER TREATMENT SYSTEM

The APA-1000 microwave thermotherapy system (see figure 1), delivers tumor-targeted focused heat energy in combination with chemotherapy for management of early stage and advance stage breast cancers. Results from a randomized phase II clinical trial with the APA-1000 proved that tumor-targeted focused microwave heating, used in combination with neo-adjuvant chemotherapy, increased tumor shrinkage to enable breast conservation surgery. A second phase II clinical trial using the APA-1000 demonstrated that microwave heat therapy delivered by the APA-1000 selectively ablates satellite cancer cells within the tumor margin, suggesting that the treatment may become a viable approach for non-surgical management of breast cancer. The design of the APA-1000 utilizes the Adaptive phased Array technology developed by the Lincoln Laboratories of the Massachusetts Institute of Technology (MIT). The APA technology platform, originally developed for use in the “Star War Missile Defense Program” was exclusively licensed to Medifocus for the development and commercialization of focused thermotherapy systems for treatment of cancer other diseases.

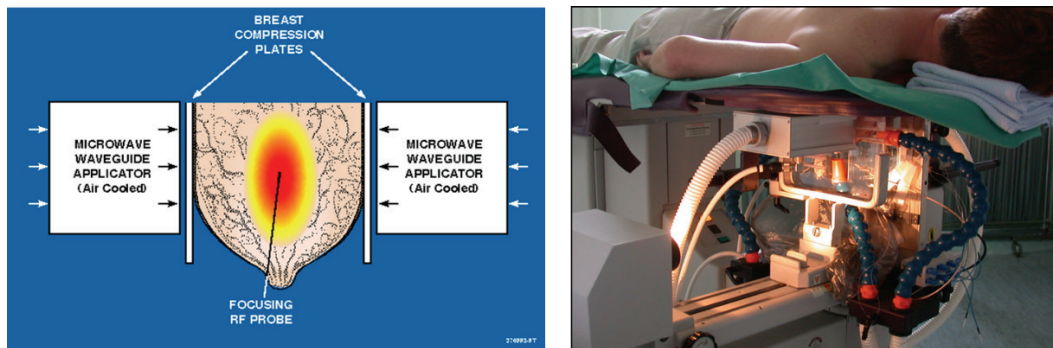


Figure 1: APA-1000 Microwave Thermotherapy System

HEAT-ACTIVATED DRUG THERAPY

The concept of heat-activated and tumor-targeted drug delivery and targeted release of cancer therapeutics directly at tumor site for cancer treatment will be introduced and discussed. The innovative design of “**Thermodox**” a heat sensitive liposomal drug encapsulating Doxorubicin will be presented as an example. In this therapeutic approach, the action of focused heating directed at the tumor will lead to

temperature elevations, which trigger the release of the encapsulated drug payload, leading to a targeted drug therapy for cancer.

HEAT-ACTIVATED GENE THERAPY

The theory behind the bio-engineering design of a **Heat-Activated Adenovirus Gene Delivery Construct** for various **Molecular and Immuno-therapeutics** will be presented. Figure 2 shows this approach for the treatment of prostate cancer, combining the “**Prolieve**” catheter-based microwave thermotherapy system with an Adenovirus carrying therapeutic genes. Preclinical data leading to the development of a heat activated Viral Delivery Construct for Tumor Targeted Immunotherapy of Cancers will be presented.

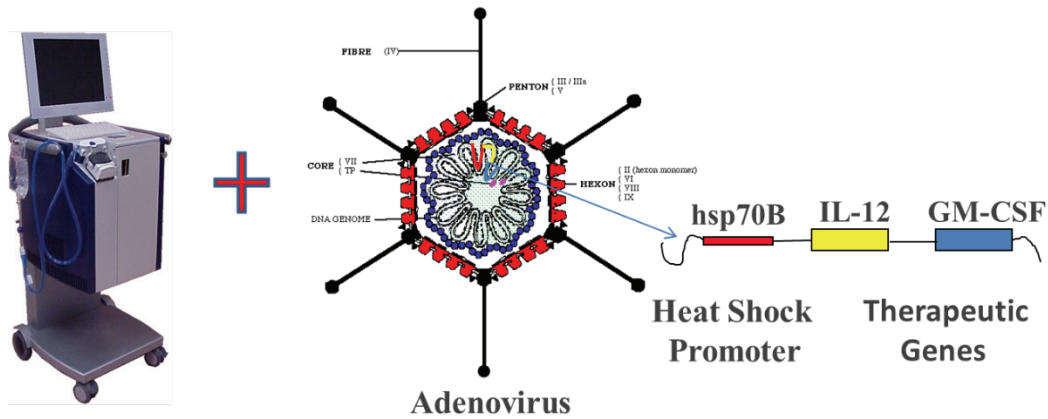


Figure 2: Principle of a heat-activated gene therapy, using a catheter-based microwave thermotherapy system and an Adenovirus.

Antenna Applicators and Microwave Fields for Imaging of the Interior of Human Breasts and Heads

N. Petrovic, M. Otterskog, P.O. Risman
Mälardalen University, Västerås, Sweden

Keywords: Microwave imaging, surface waves, magnetic wall effect and contacting antenna.

INTRODUCTION AND BACKGROUND

There are increasing R&D activities in several universities and companies towards reliable microwave-based systems complementing conventional X-ray mammography and allowing imaging closer to the ribs, thus reducing the number of false positives and negatives to the benefit of patients as well as medical resource spending. A similar application is diagnosing brain hæmorrhages versus strokes, since the medications are very different and clear diagnostics will save lives, particularly if equipment is simple to use, inexpensive and can be used very early after the attack.

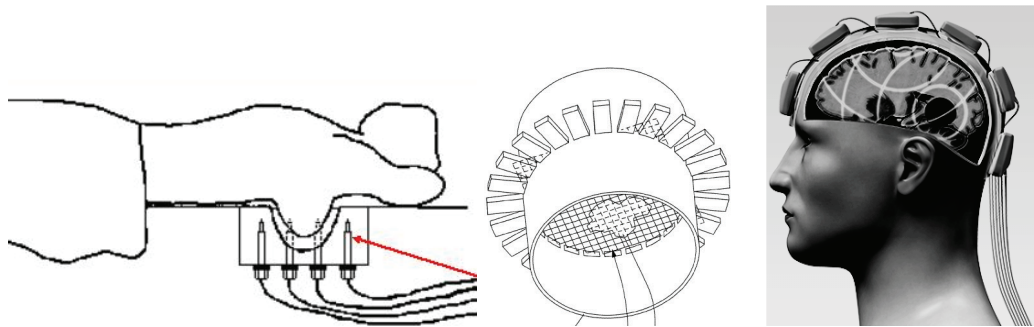


Figure 1. The Meaney *et al.* [4] multi-monopole system with the breast in a bolus liquid (left); the EMTensor [5] ceramic waveguide multiple antennas in a hood with bolus liquid surrounding a head model (mid); the Medfield [6] antenna helmet with bolus bags for hæmorrhage detection.

A way of avoiding some antenna and other problems is to use *boluses*, which are liquids contacting the object under study (OUS) and having dielectric properties similar to those of the tissue. Strong reflections and the creation of so-called surface waves are then avoided, and simple coaxial line monopole antennas around the OUS can be used. An illustration of to-day's most successful system for breast studies is shown in Figure 1 (left). The bolus liquid volume is large and the patient lies on a hollow bench just above a

liquid tank. Since the distance between the antennas and OUS is several centimeters, complicated antenna nearfield issues are avoided.

Figure 1 (mid) shows a system under development with which promising results have been obtained. There are 5 x 32 ceramic antennas in the complete system which is therefore quite expensive (in the order of US\$ 150,000).

Figure 1 (right) shows a simpler system under development, for only h emorrhage detection and intended for use in emergency vehicles, primarily for diagnostic separation from stroke.

ONGOING RESEARCH AT M ALARDALEN UNIVERSITY

In to-day's most successful system small bolus bags are used in a flexible helmet-like structure. Of course, such boluses cannot be used with heads. There is thus a need for antenna systems which can be used without boluses and do not generate surface waves. Such an antenna has been developed by us [1] [2] and is shown in Figure 2 (left).

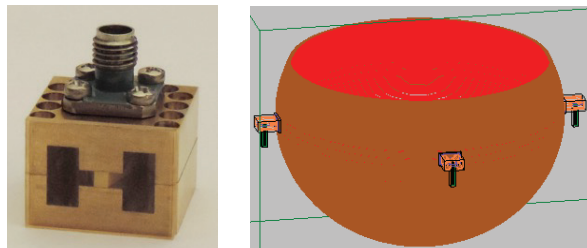


Figure 2. The applicator antenna design in our project (left); three of these antennas contacting a skull model with bone (brown) and brain substance (red) (right).

It is basically a ridged rectangular TE waveguide with a high permittivity ‘‘projectile’’ insert in the ridge, resulting in generated external field with almost no nearfield. This allows it to be directly contacting the OUS.

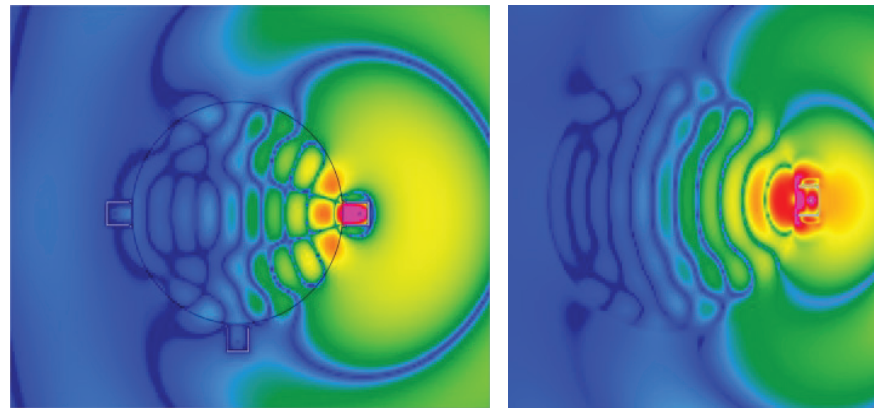


Figure 3. The total momentary electric field numerical result with the head model (without ferrites at the antenna) in the horizontal cross section (left), in logarithmic scaling; same as the left figure but know with the ferrites at the antenna (right).

Microwave-Accelerated Bioassays

Enock Bonyi, Zeenat Kukoyi and Kadir Aslan*

Morgan State University, 1700 E. Cold Spring Lane, Baltimore, MD 21251

Keywords: bioassay, nanoparticles, microwave, analytes, hybrid platform.

INTRODUCTION

Biological analytes (e.g. blood, urine) and environmental pollutants (e.g. insecticides) are detected and quantified by medical scientists and health providers, and the results used by allied policy-makers. However, many of the commercial bioassays used for either pathogen or pollutant detection are carried out in controlled environments, hence, take a long time to produce the results, and have low sensitivities. Tools and methods are needed to address these limitations. In this paper, we report the preparation of bioassay platforms by surface modification of circular poly-methyl methacrylate (PMMA) discs, paper and polyethylene terephthalate (PET) with nanoparticles (silver and indium tin oxide (ITO)). The use of these bioassay platforms in combination with microwave heating (i.e., microwave-accelerated bioassays) improved bioassay sensitivity and nanoparticle film stability, and reduced the assay time from 3 hours to 25 minutes.

MATERIALS AND METHODS

Surface modification of circular PMMA discs. The PMMA discs (2 mm) were etched using lithium aluminum hydride and later immersed in 3-aminopropyltrimethoxysilane (APTES) for NH₂ groups to attach to the roughened disc surface [1] before baking the discs for either, 1, 3, 5, 10, or 16 hours at 125^oC in a vacuum oven. The water contact angle was measured to verify the surface modification.

Hybrid Platform 1: Deposition of silver thin films (STFs) on modified PMMA surfaces. Silver thin films of 10 nm thickness were deposited in a plasma sputter coater employing a silver target onto the surface of chemically modified discs using a 21-well mask. To demarcate the wells, a 21-well silicone isolator was carefully aligned on top of each individual sputtered spot (Fig 1: with black border).

Hybrid platform 2: ITO on PET. ITO dots were punched from the ITO-coated PET film using a 1-hole punch and securely aligned with each of the individual 21 wells of the silicone isolator. The 21-well silicone isolators with the attached ITO dots were subsequently positioned and firmly pressed onto the blank circular PMMA discs (Fig 1: with blue border).

Hybrid platform 3: Incorporation of silver nanowires (SNWs) on paper. The silver nanowires were synthesized using the polyol method [2]. The SNWs were spray-coated on paper and left to dry. A one-hole punch was used to obtain silver nanowire dots which were securely attached to the 21-well silicon isolator and pressed firmly on the circular PMMA discs (Fig 1: with red border). The bioassay steps were performed on hybrid platforms 1,

2, and 3 using microwave heating at power level=1 using a 900 W Emerson microwave oven Model No MW939SB for 5 minutes.

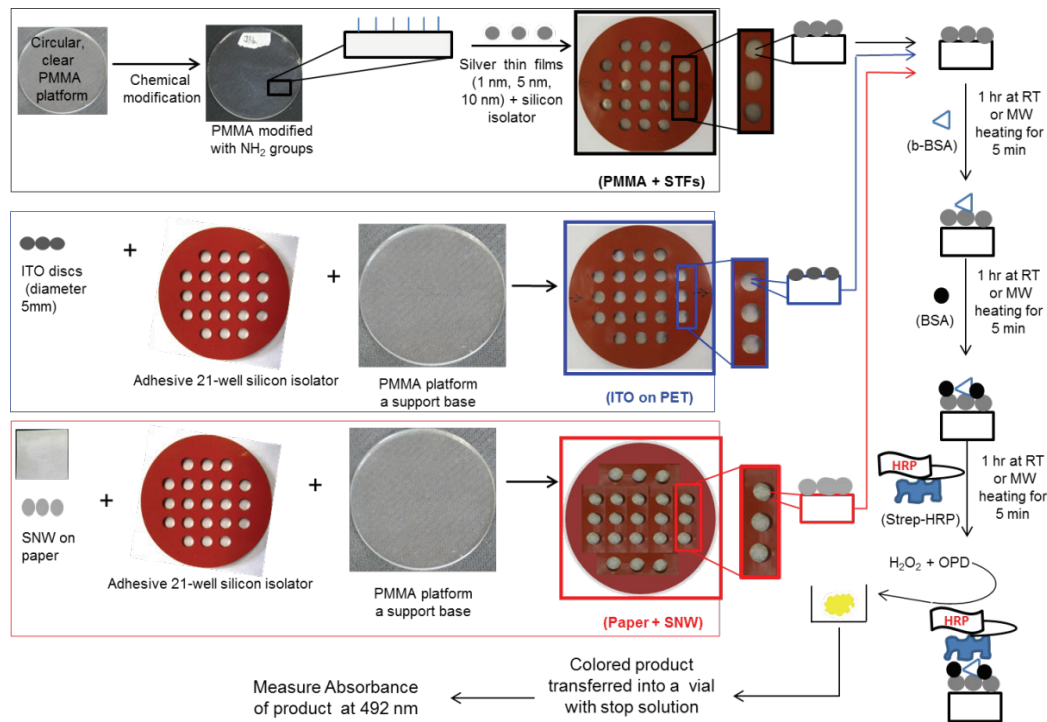


Figure 1: Schematic depiction of hybrid platforms; PMMA + silver (1 nm, 5 nm, 10 nm) (black border), Indium tin oxide (blue border) and SNW functionalized on paper (red border) and b-BSA assay (far right, vertical panel).

RESULTS AND DISCUSSION

The water contact angles for silanized and baked circular PMMA discs was $33^\circ \pm 5^\circ$ (1 hr), $43^\circ \pm 12^\circ$ (2 hrs), $27^\circ \pm 6^\circ$ (5 hrs), $25^\circ \pm 4^\circ$ (10 hrs), $41^\circ \pm 10^\circ$ (16 hrs), and $72^\circ \pm 1.5^\circ$ (control). Discs silanized and baked for 1, 5, and 10 hours showed water contact angles that agree with those published of $33^\circ \pm 4^\circ$ [3]. However, only the PMMA discs modified by baking for 1 hour demonstrated STF stability when subjected to four consecutive washes using water under microwave heating. The PMMA discs were silanized with amine groups, hence the strong association with silver. Absorbance for SNW on paper before and after bioassay was not measured due to the opacity of paper. The absorbance of the ITO film on PET was the same before and after conducting the bioassay under microwave heating. This can be attributed to the tight bonding of ITO onto PET. There was no observable change in the ITO absorbance before and after the bioassay steps, but this did not translate into higher colorimetric responses under microwave heating, an observation currently under investigation. As illustrated in Fig. 2, the sensitivity of b-BSA assay was higher under microwave heating than at room temperature. This is due to the thermal gradient that develops between the warmer bulk (protein solution) and a cooler nanoparticle film layer, causing mass transfer of biomolecules.

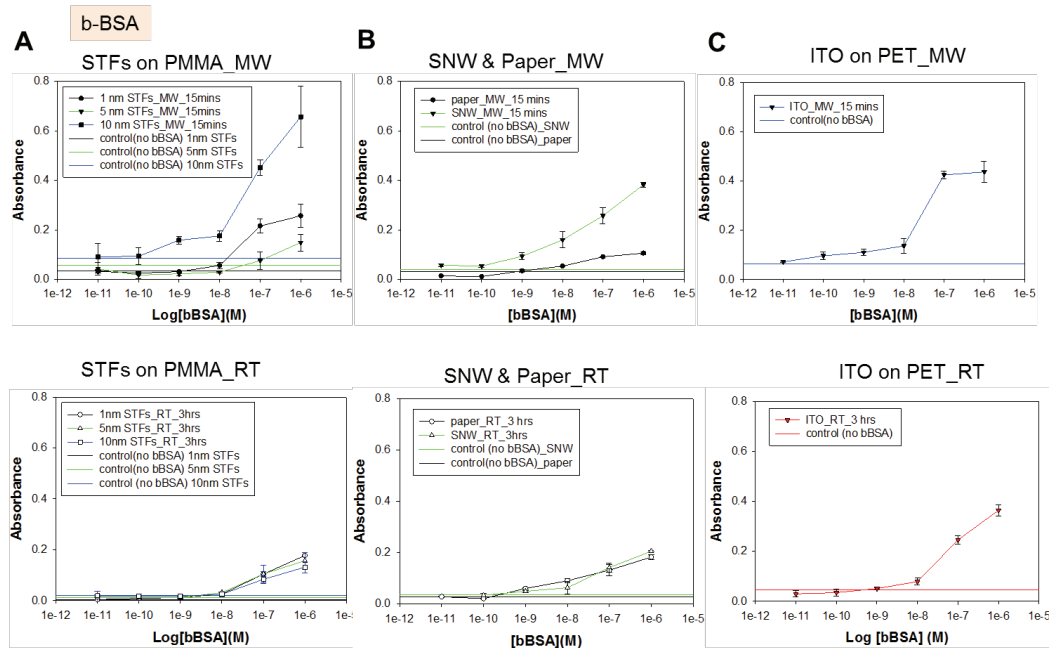


Figure 2: Colorimetric response for b-BSA assay under microwave heating (top panel) and in room temperature environment (lower panel). Modified PMMA discs + STFs (A), SNW functionalized paper (B) and ITO on PET (C).

CONCLUSION

The assay time for b-BSA assay was decreased ~ 7 fold by microwave heating. Also, the b-BSA assay sensitivity of hybrid platforms was improved using microwave heating. While PMMA+ 10 nm STFs and ITO on PET hybrid platforms had better colorimetric response than SNW functionalized on paper under MW heating, the latter platform exhibited the best linearity. These results demonstrate that microwave-accelerated bioassays can be potentially be used for real-life assays with the potential to obtain higher assay sensitivities using chemiluminescence and fluorescence detection methods in the near future.

REFERENCES

- [1] Cheng, J.-Y.; Wei, C.-W.; Hsu, K.-H.; Young, T.-H., Direct-write laser micromachining and universal surface modification of PMMA for device development. *Sensors and Actuators B: Chemical* 2004, 99 (1), 186-196.
- [2] Coskun, S.; Aksoy, B.; Unalan, H. E., Polyol synthesis of silver nanowires: an extensive parametric study. *Crystal Growth & Design* 2011, 11 (11), 4963-4969.
- [3] Henry, A. C.; Tutt, T. J.; Galloway, M.; Davidson, Y. Y.; McWhorter, C. S.; Soper S. A.; McCarley, R. L., Surface modification of poly (methyl methacrylate) used in the fabrication of microanalytical devices. *Analytical chemistry* 2000, 72 (21), 5331.

Alternative Treatment of Gout using Metal-Assisted and Microwave-Accelerated Decrystallization (MAMAD) Technique

Zainab Boone-Kukoyi, Treshaun Sutton, Raquel Shortt,
Nishone Thompson, Chinenye Nwawulu, Hillary Ajifa, Salih Toker, and
Kadir Aslan*

Morgan State University, Baltimore, Maryland

Keywords: Gout, uric acid, microwaves, monosodium urate monohydrate, gold nanoparticles

INTRODUCTION

Gout in humans is triggered due to the accumulation of monosodium urate monohydrate (MSUM) crystals in the soft tissue surrounding joints and in the synovial fluid in the joints¹. Acute gout is formed when MSUM crystals build up in soft tissue and chronic gout is exhibited with the formation of tophi masses at joints. Treatments currently available for gout are pharmaceutical therapies, such as, nonsteroidal anti-inflammatory drugs (NSAIDs), and for chronic gout surgery is often prescribed for tophi removal^{2, 3}. These treatment methods are somewhat effective, however, they were proven to have significant side effects, such as stomach ulcers and thinning bones or tragic effects like losing a limb. In this study, we demonstrated the use of a new technique, called Metal-Assisted and Microwave-Accelerated Decrystallization (MAMAD)⁴, which is based on combined use of medical microwaves and gold nanoparticles as an efficient alternate method for the decrystallization of MSUM crystals (*in vitro*) that are associated with chronic gout⁴.

METHOD

The MAMAD technique was used for rapid decrystallization of uric acid crystals and MSUM crystals *in vitro* on 2-D glass slides (a model surface). Initial studies were comprised of the crystallization of uric acid crystals (i.e., the main causative of gout), and the synthesis of MSUM crystals (prominent in gout patients) followed by the implementation of MAMAD technique for the decrystallization of uric acid and MSUM crystals. The prepared uric acid crystals and nucleated MSUM crystals were decrystallized on the model surfaces with the use of silicon isolators to demarcate sections and to quantify results. In a typical experiment, uric acid and MSUM crystals in bovine synovial fluid was

placed in the isolated sections of the model surfaces; gold nanoparticles added to the supersaturated solution, covered with a glass coverslip and low power microwaves (20 W, 8 GHz, Emblation microwave) were applied with an applicator tip, as shown in Fig.1. This method was repeated with MSUM crystals with albumin, chondroitin sulfate, collagen and phosphatidyl choline, which are factors that cause crystal nucleation and tophi formation.

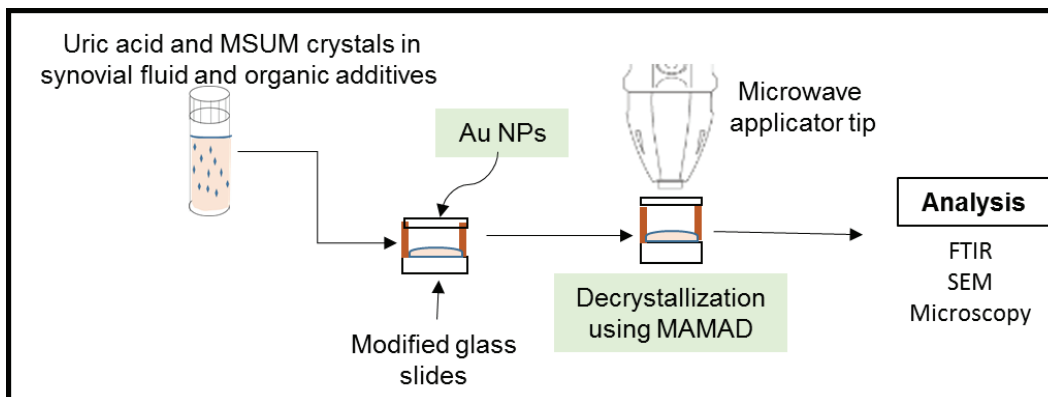


Figure 1. (a) Experimental setup of MSUM crystals for decrystallization using the MAMAD technique.

RESULTS

The use of MAMAD technique in the presence of gold nanoparticles decreased the number and size of crystals notably when exposed to microwaves for a period of 120 seconds on a 2-D glass surface. Crystal sizes were analyzed with use of optical microscopes, Scanning electron microscopes (SEM) and quantified with the use of image J (results not shown).

DISCUSSION

Gout like conditions were simulated in vitro with the growth and nucleation of MSUM crystals in a synovial fluid environment with organic additives. Fig 2 (a), illustrates decrystallization of uric acid crystals with the use of MAMAD in the presence of 20 nm gold nanoparticles on a 2-D glass platform. A significant decrease in crystal size and number was observed. Fig. 2 (b) demonstrates the decrystallization of MSUM crystals using MAMAD in the presence of 100 nm gold nanoparticles where there was also a significant decrease in crystal size (> 65%). From these observations, we postulate that gold nanoparticles act as nano bullets that chip away the crystals when activated by microwaves.

CONCLUSION

MSUM and uric acid crystals are decreased notably when exposed gold nanoparticles and microwaves for a duration 120 seconds. We have demonstrated that

MAMAD technique has the potential to be used as a non-pharmaceutical, alternate treatment for gout.

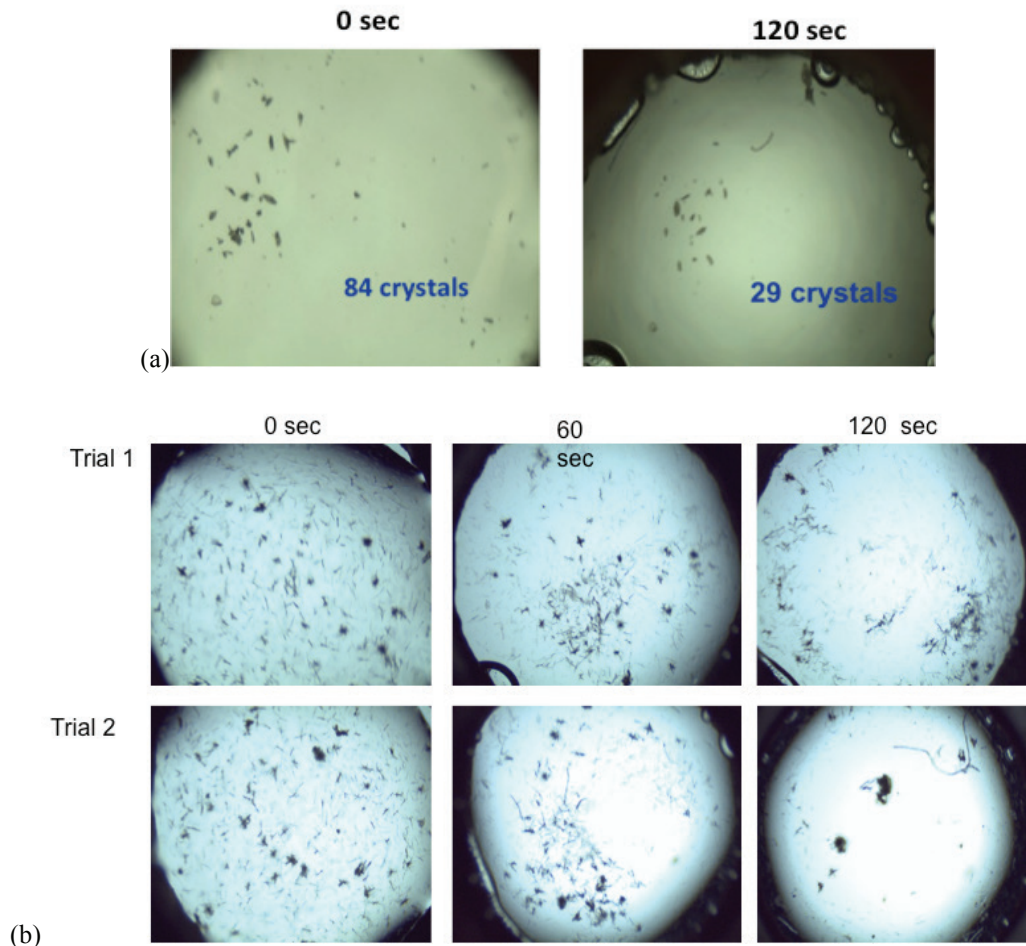


Figure 2. (a) Uric acid crystals exposed to MAMAD technique, 20 nm gold nanoparticles at 120 seconds (b) MSUM crystals decrystallized using MAMAD, 100 nm gold nanoparticles at 120 sec.

REFERENCES

1. Martillo, M. A.; Nazzal, L.; Crittenden, D. B., The crystallization of monosodium urate. *Curr Rheumatol Rep* **2014**, *16* (2), 400.
2. Manno, R. Treatment of Gout. <http://www.hopkinsarthritis.org/arthritis-info/gout/gout-treatment/>.
3. CDC Gout. <http://www.cdc.gov/arthritis/basics/gout.htm>.
4. Kioko, B.; Ogundolie, T.; Adebisi, M.; Ettinoffe, Y.; Rhodes, C.; Gordon, B.; Thompson, N.; Mohammed, M.; Abel, B.; Aslan, K., De-crystallization of Uric Acid Crystals in Synovial Fluid Using Gold Colloids and Microwave Heating. *Nano Biomed Eng* **2014**, *6* (4), 104-110.

Crystallization of Lysozyme on Nanoparticle Surfaces using Monomode Microwave Heating

Brittney Gordon,¹ Kevin Mauge-Lewis,¹ Fareeha Syed,¹ Saarah Syed,¹ Enock Bonyi,¹ Muzaffer Mohammed,¹ Eric A. Toth,^{2,3} Dereje Seifu,⁴ Kadir Aslan¹

¹ Morgan State University, Department of Chemistry, Baltimore, MD 21251, USA.

² University of Maryland at Baltimore, Department of Biochemistry and Molecular Biology, Rockville, MD 20850, USA.

³ Marlene and Stewart Greenebaum Cancer Center, University of Maryland School of Medicine, Baltimore, Maryland 21201, USA.

⁴ Morgan State University, Department of Physics, Baltimore, MD 21251, USA.

Keywords: Protein Crystallization, iCrystal System, Nanoparticles

INTRODUCTION

The crystallization of biological macromolecules has been the primary focus of researchers due to its immense application in the medical and pharmaceutical industry. With the interest in the controlled growth of pure crystals, we continue to study the rapid crystallization of biomolecules using the Metal-Assisted and Microwave-Accelerated Evaporative Crystallization (MA-MAEC) technique.¹ In this study, the MA-MAEC technique was employed to investigate the use of three different metal surfaces for the evaluation of the optimal crystallization of lysozyme on a colloidal scale, to address the continuous demand for a crystallization method which facilitates the growing attention towards nucleation kinetics, thermodynamics and modified surfaces.^{2,3} Furthermore, we report the use of metal nanoparticles on polymeric films under continuous, low wattage microwave heating produced by our iCrystal system, which is composed of a microwave cavity and a mono-mode microwave source with a power range of 0-100 W, for the rapid crystallization of lysozyme.

MATERIALS AND METHOD

Preparation of lysozyme solution. 60 mg of lysozyme powder was dissolved in 1.0 mL of sodium acetate (pH 4.6) and 500 μ L of crystallization reagent in a clean glass vial. Preparation of modified iCrystal plates. Silver nanoparticle films (SNFs, 1 nm thick), iron nano-columns (height: 50 nm, 100 nm and 200 nm) at 70^o angle, and ITO dots (5 nm in diameter) were deposited on blank iCrystal plate poly(methyl methacrylate) (PMMA) disks (**Fig. 1B**), prior to the application of a 21-well silicone isolator (**Fig. 1A4**) to yield hybrid iCrystal platforms. Crystallization of lysozyme using the iCrystal System. 15 μ L of the

prepared lysozyme solution was placed in each of the 21 wells of the silicon isolator for a blank iCrystal plate and each hybrid iCrystal platforms, with the exception of 8 μL used for the ITO-modified platform. The crystallization process progressed using continuous heating at 70 W of power (**Fig. 1A**). Temperature Measurements. Fiso multichannel fiber optic sensors were used to measure the real-time temperature inside the iCrystal system (**Fig. 1A1**). Characterization and analysis of lysozyme crystals. Optical images of the growth of the lysozyme crystals at 15 minute intervals were obtained using a Swift Digital M10L monocular light microscope at 10X magnification and Motic Images 2.0 software. X-Ray diffraction (XRD) analysis was conducted using an X-ray generator and Raxis4++ image plate detector.

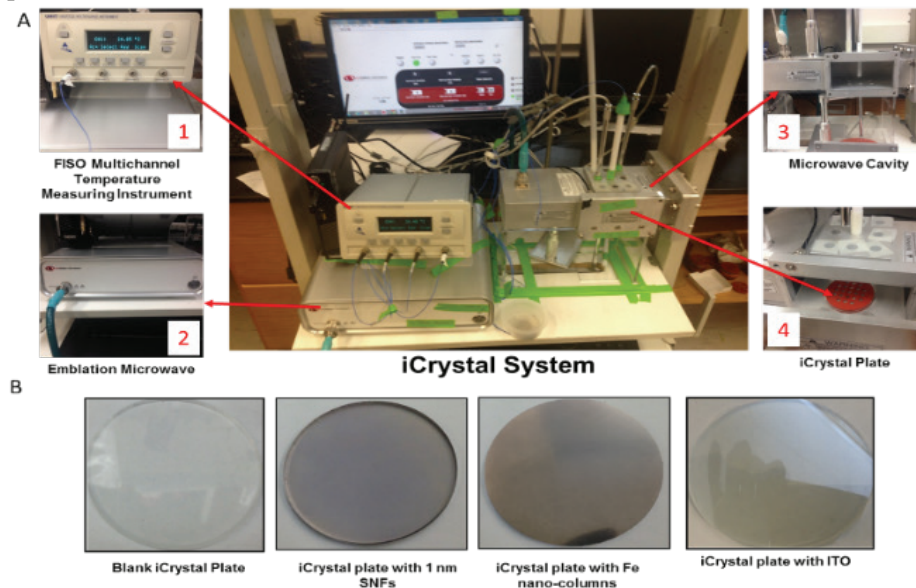


Figure 1.

Figure 1. (A) Real-color photograph of the iCrystal System and four major components: (1) Fiso Multichannel Temperature Measuring Instrument, (2) Emblation Microwave, (3) iCrystal Microwave Cavity, and (4) iCrystal Plate. (B) Real-color photographs of the four different iCrystal plate surfaces utilized for the experiments.

RESULTS AND DISCUSSION

The crystal size and distribution were significantly greater on hybrid platforms than blank iCrystal platforms. The average crystallization time for blank, deposited SNFs, iron nano-columns and ITO was 555 ± 77 minutes, 527 ± 28 minutes, 510 ± 45 minutes, 370 ± 36 minutes, respectively (**Table 1**). These findings are indicative of metal nanoparticles decreasing the rate of crystallization of lysozyme on iCrystal platforms. In addition, the increase in the number and size of lysozyme crystals on hybrid platforms, imply that the metal nanoparticles serve as a more effective nucleation site for lysozyme during the crystallization process, than the blank surface. Additionally, while the blank, SNFs and iron nano-column modified platforms exhibited fairly similar average crystallization time, ITO-modified iCrystal platforms resulted in a significantly shorter crystallization time and

the largest size range of lysozyme crystals. This is as a result of the homogenous surface of the ITO films, which provides a more extensive area for potential nucleation sites. Furthermore, there was a 5-fold difference in the number of crystals and a greater crystal size distribution under the MA-MAEC technique than those grown at room temperature. Therefore, MA-MAEC technique facilitated the generation of a thermal gradient due to the significant difference in the thermal conductivity of the solvent and the metal surfaces (SNFs, iron nano-columns, and ITO), which expedited the mass transfer of proteins from a region of higher temperature (solvent) to a region of lower temperature (metal surface), leading to the faster crystallization of lysozyme.

iCrystal System at 70 W	Initial Crystallization Time*, minutes	Crystallization Time**, minutes	Size Range (min-max), μm	Average Number of Crystals***
Blank PMMA	<15	555 \pm 77.0	43.0 – 268	305 \pm 49.0
ITO	<15	370 \pm 36.0	56.0 – 584	73 \pm 13.0
Fe (50 nm)	<15	510 \pm 45.0	26.0 – 262	461 \pm 83.0
Fe (100 nm)	<15	845 \pm 22.0	18.0 – 347	286 \pm 42.0
Fe (200 nm)	<15	810 \pm 51.0	42.0 – 460	111 \pm 26.0
SNFs (1 nm)	<15	527 \pm 28.0	41.0 – 248	435 \pm 117

Table 1. Summary of results for the crystallization of lysozyme on iCrystal plates using the MA-MAEC technique with continuous heating at 70 W of power. *Initial crystallization time: the time of appearance of first crystal detectable by our optical microscope. **Crystallization time: the time when lysozyme crystals stopped their growth. ***Average number of all observable crystals counted on 21-well iCrystal plates.

CONCLUSIONS

We have demonstrated MA-MAEC technique's capability of decreasing the crystallization time of lysozyme, while retaining crystal quality. Moreover, crystal growth facilitated by the modified surfaces (SNFs, iron nano-columns and ITO) yielded a shorter crystallization time, with ITO yielding the shortest crystallization time.

REFERENCES

- [1] Pinard, M. A.; Aslan, K., Metal-assisted and microwave-accelerated evaporative crystallization. *Crystal growth & design* **2010**, 10, (11), 4706-4709.
- [2] Young, T. M.; Roberts, C. J., Structure and thermodynamics of colloidal protein cluster formation: Comparison of square-well and simple dipolar models. *The Journal of chemical physics* **2009**, 131, (12), 125104
- [3] Mohammed, M.; Syed, M. F.; Bhatt, M. J.; Hoffman, E. J.; Aslan, K., Rapid and selective crystallization of acetaminophen using metal-assisted and microwave-accelerated evaporative crystallization. *Nano biomedicine and engineering* **2012**, 4, (1), 35.

Use of Dielectric Properties for Agricultural Applications

Stuart O. Nelson, and Samir Trabelsi

U. S. Department of Agriculture, Agricultural Research Service
Athens, GA

Keywords: Dielectric heating, quality sensing, dielectric properties, agricultural products, moisture sensing, pest control

INTRODUCTION

The use of dielectric properties for applications in agriculture can be divided into two general categories, dielectric heating and product quality sensing. Dielectric heating of agricultural materials, through application of high-frequency and microwave electric fields, has been considered for several applications. These include drying of products such as grain and seed, controlling stored-product insects, seed treatment to improve germination, improving nutritional value of products, controlling product-borne plant and animal pathogens, and inactivating weed seed and plant-infecting organisms in soils. Product quality sensing applications have included the use of dielectric properties of agricultural products for rapidly sensing moisture content and other quality attributes of selected products.

DIELECTRIC HEATING

Loose smut is a fungal disease that can cause significant yield loss in small grains. Because it is an internal seed-borne pathogen, the smut is difficult to control with surface fungicide treatments, and tedious hot water treatments with critical temperature control, to avoid damaging seed viability, are used to rid seed lots of the disease. Therefore, radio-frequency (RF) dielectric heating has been studied for potential control of the seed-borne pathogens, but RF treatments were not successful for controlling the fungi without damaging the viability of the seed [1].

The production of sprouts from alfalfa and other seed for human consumption is a substantial industry. However, there have been several outbreaks of illness associated with sprouts contaminated with bacteria, *Salmonella* and *Escherichia coli*. The potential for controlling human bacterial pathogens on alfalfa seed by dielectric heating was studied by exposure of alfalfa seed contaminated with these bacteria and *Listeria* to RF dielectric heating treatments at 39 MHz [1]. Although significant reductions in bacterial populations were observed, the desired levels of reduction were not achieved without severe reductions in germination of the alfalfa seed.

Insects that infest grain after harvest and in storage account for tremendous losses of cereal grains and other similar crops around the world. Grain storage sanitation practices and chemical controls have been relied upon to limit such losses, but losses are

still substantial, and health hazards of chemical residues are of concern. Raising insect body temperatures to lethal levels is one means for controlling them. However, temperatures of these levels generally produce damage to the host product. If selective heating of the insects in relation to the grain they infest were possible, dielectric heating would offer an advantage over conventional heating. Experiments have shown that many insect species that infest grain and cereal products can be controlled by short exposures to RF electric fields that do not damage the host material [1]. Generally, for successful RF insect-control treatments, resulting temperatures in host materials of this kind range between 40 and 90 °C, depending upon the characteristics of the host material, the insect species and developmental stage, and the nature of the RF or microwave treatment. RF and microwave methods have not been practical, because they are too costly compared to conventional chemical and physical control methods.

Problems with poorly or slowly germinating seeds have plagued growers of numerous plant species in production of field crops, horticultural crops, ornamentals, nursery materials for landscaping, and forest trees. Use of RF dielectric heating treatments has been studied, and the germination responses of seeds of more than 80 plant species have been summarized [1]. No improvement in germination was achieved with many kinds of seed, but many others responded favorably, either with increases in germination or accelerated germination. Particular success was achieved in the treatment of alfalfa seed and that of some other small-seeded legumes that exhibited impermeable seed-coat problems. Benefits of alfalfa seed treatment were retained in storage for 10 to 21 years after treatment [1]. Several of the vegetable and ornamental species did not show any improvement, but some, such as okra, garden peas, and garden beans responded favorably. Germination of spinach was consistently accelerated. In general, seeds of woody plants and tree species did not respond very well. Results with field crops such as corn, cotton, and wheat were mixed, with acceleration and increased growth being noted in some lots but not in others. Practical aspects of RF seed treatment have been discussed [1]. The increased germination achievable in some kinds of seed and the proven long-range safety of the treatment indicate that the method might be considered for further study and economic analysis where practical benefits might be realized.

Over the past 50 years, the use of microwave energy has been proposed frequently as an alternative method for controlling pests in the soil, such as weed seeds, insects, nematodes, and soil-borne plant pathogens. Upon considering the basic principles of microwave energy absorption by dielectric materials and the experimental work that has been reported, there appears to be little probability for the practical application of microwave power for field use in controlling pests in soil [1].

Some experiments have been conducted to determine the influence of RF dielectric heating and microwave heating on quality attributes of agricultural products. These included RF drying of chopped alfalfa forage, RF and microwave heating of raw soybeans to improve nutritional value, and RF dielectric heating for quality maintenance in stored pecans. Dielectric heating of alfalfa forage, while not practical for field application, might be useful as a means for inactivating carotene-destroying enzymes in laboratory procedures or field testing. RF heating of soybeans at 42 MHz and microwave heating at 2,450 MHz were effective in reducing trypsin inhibitor, urease, and

lipoxygenase activities to low levels, whereas peroxidase activity remained relatively high, all of which are desirable characteristics [1].

Dielectric heating of freshly harvested pecan nuts showed promise for maintaining quality of pecans in storage, and dielectric heating treatments offered the advantage of maintaining desirable color of the pecan kernels [1].

QUALITY SENSING APPLICATIONS

Moisture content of cereal grain and oil seed determines suitability for harvest and storage and is usually measured whenever grain and seed are traded. Because standard and reference methods for determining moisture content in grain and seed involve tedious laboratory procedures and long oven-drying periods, rapid methods for moisture measurement have been essential in the grain and seed trade. Electrical measurements have been developed that provide rapid grain and seed moisture testing through correlations between their dielectric properties and moisture content. The dielectric properties, or permittivities, of grain and oilseed vary with the frequency of the applied electric field, the moisture content of these materials, and their temperature, and bulk density. Instruments operating at frequencies of 1 to 20 MHz have been used for moisture testing for many years. More recently, higher frequencies have been investigated, and use of grain and seed permittivities at microwave frequencies show promise for the simultaneous sensing of moisture content and bulk density in both static and flowing granular materials [1]. Because of the advantages of higher frequencies, commercial development of microwave moisture meters for grain and seed will improve the reliability and utility of such instruments in the grain and seed industries.

New, nondestructive techniques for sensing quality of fresh fruits and vegetables would be helpful to producers, handlers and consumers. Dielectric properties of many fruits and vegetables have been measured over wide ranges of frequency and attempts were made to correlate these properties with quality factors [1]. So far, no practically useful correlations were found for detecting maturity, sweetness in fruits such as apples and melons, or quality changes during apple storage. Some potential was noted for detecting moisture content in onions associated with changes during the curing process [1]. Also, sensing of moisture content in dates through capacitance measurements at 1 and 5 MHz on parallel-plate electrodes with a single date between them showed promise for potential application in the automatic sorting of dates to reduce skilled-labor requirements in manual sorting and grading processes [1].

CONCLUSION

With further research, useful applications of dielectric properties can be expected for both quality sensing and dielectric heating applications in agriculture.

REFERENCES

- [1] Nelson, S. O. (2015) *Dielectric properties of agricultural materials and their applications*. Elsevier - Academic Press, 2015.

Dielectric Properties of Biomass/Bentonite Clay Mixtures between 0.5 and 20 GHz

¹Candice Ellison, ²Murat McKeown, ³Samir Trabelsi, ¹Dorin Boldor

¹Louisiana State University, Baton Rouge, LA, USA

²University of Georgia, Athens, GA, USA

³USDA ARS, Athens, GA, USA

Keywords: Dielectric properties, microwave absorber, biomass mixtures, microwave-assisted pyrolysis

INTRODUCTION

Thermochemical conversion processes, such as pyrolysis and gasification, can be used to convert lignocellulosic biomass feedstocks into useful fuels and other value-added chemicals. Microwave heating is volumetric and selective offering many advantages and greater temperature control compared to conventional heating methods for this application. Knowledge of the dielectric properties of a material is important for the design and optimization of microwave systems for dielectric heating. In general, dry biomasses are poor microwave absorbers (low dielectric loss materials) and cannot reach the high temperatures (400-700 °C) required by pyrolysis. A microwave absorbing material, characterized by high dielectric loss, may be mixed with biomass feedstocks to increase heating rates of thermochemical processes. In this study, bentonite clay is investigated for its microwave absorbing capabilities. Bentonite is a naturally occurring aluminosilicate with a large surface area and acid sites making it a potential candidate for in situ catalytic microwave pyrolysis [1]. The extent to which its mixture with biomass will increase the heating rate of the feedstock under microwave radiation is quantified in this study via measurement of dielectric properties. There is a lack of studies in the literature characterizing the permittivities of biomass/catalyst mixtures of any type.

METHODOLOGY

In this experiment, the dielectric properties of different biomass and bentonite mixtures were measured at microwave frequencies. Four different lignocellulosic biomasses were chosen for this study including sawdust, Chinese tallow tree wood, energy cane bagasse, and switchgrass. The following five mixtures of biomass and bentonite clay were prepared for each biomass: 0, 25, 50, 75, and 100% wt bentonite. Samples were ground and sieved to a fine particle size (<500 µm) and the moisture content of each sample was measured using the oven drying method (ASTM E871-82). Dielectric constant (ϵ') and dielectric loss factor (ϵ'') were measured at room temperature

from 500 MHz to 20 GHz for each sample using an open-ended coaxial-line dielectric probe (Agilent 85070) and vector network analyzer (Agilent N5230C PNA-L). Measurements were made at 101 frequency points on a logarithmic scale between 500 MHz and 20 GHz. To reduce possible errors, samples were packed tightly into the sample holder and pressed firmly with the probe during measurement to ensure contact between the sample and the probe. Measurements were taken in triplicates to confirm consistency of the data.

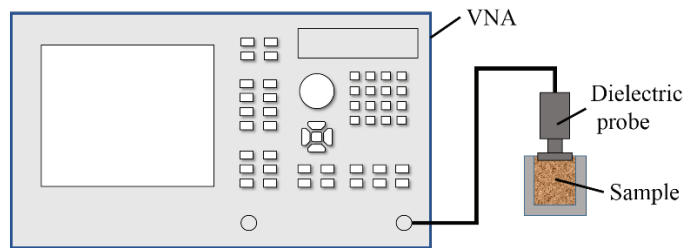


Figure 1. Diagram of dielectric measurement setup consisting of a vector network analyzer, open-ended coaxial-line dielectric probe, and stainless steel sample holder

RESULTS

Results from this study show a dependence of permittivity (dielectric constant and dielectric loss factor) on frequency and bentonite content. Dielectric constant for all samples decreases with frequency. For all biomasses, permittivity increases with increasing bentonite content indicating the microwave absorption potential of bentonite. Loss tangent ($\tan \delta = \epsilon'' / \epsilon'$) and penetration depth were evaluated from the measured data. Loss tangent shows a quadratic increase with bentonite content and penetration depth decreases linearly with bentonite content.

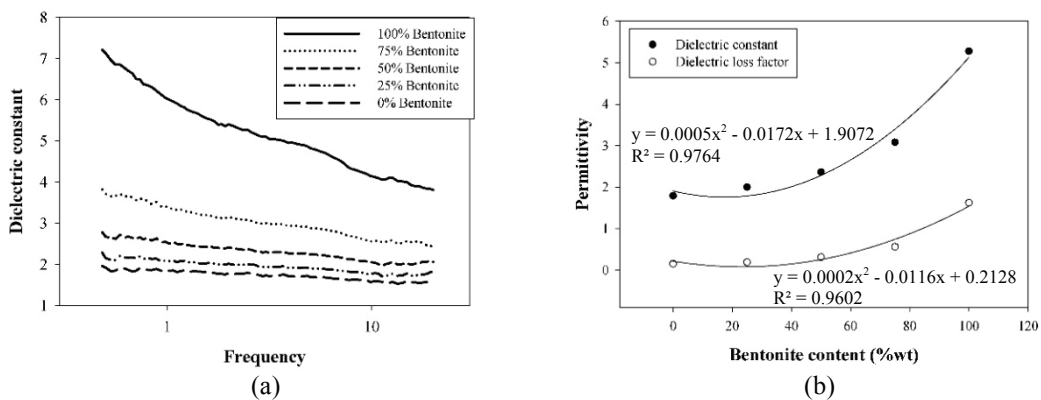


Figure 2. Permittivity measurements of switchgrass/bentonite mixtures as a function of (a) frequency and (b) bentonite content measured at 2.45 GHz.

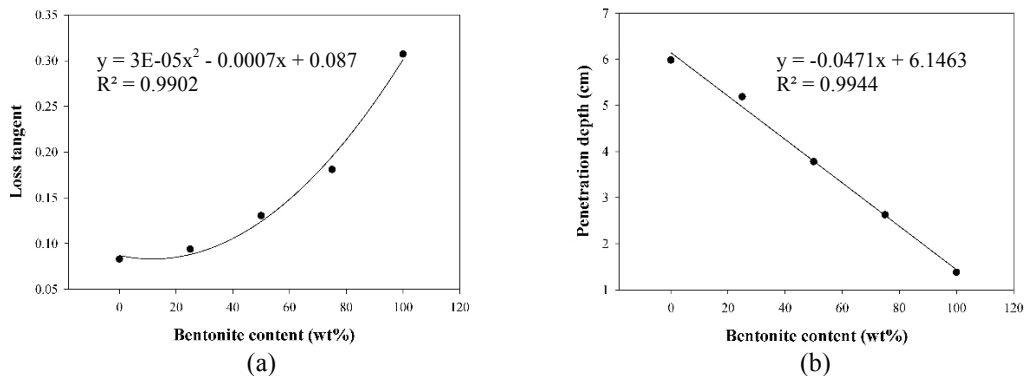


Figure 3. Evaluated parameters for switchgrass/bentonite mixtures at 2.45 GHz. (a) loss tangent and (b) penetration depth as a function of bentonite content

DISCUSSION

Increasing the amount of bentonite in the mixture increases the dielectric constant and dielectric loss factor of the overall mixture. This trend is also reflected in the dielectric loss tangent, which quantifies the dissipation of energy (as heat) within the material. An increase in bentonite content results in a quadratic increase in loss tangent. Penetration depth, the depth at which the power density is reduced to $1/e$ of its original value, is inversely proportional to bentonite content. A shorter penetration depth corresponds to a greater reduction in power density. Results indicate that a greater bentonite content yields shorter penetration depth confirming that bentonite can dissipate/absorb a greater amount of energy than biomass alone. Therefore, mixing bentonite with the biomass feedstock has the potential to increase microwave heating rates during pyrolysis.

CONCLUSION

In this study, addition of bentonite to biomass feedstocks was shown to increase the dielectric permittivity of the overall biomass/bentonite mixture, demonstrating the usefulness of bentonite clay as a microwave absorber for biomass heating applications. The results from this study can assist in designing reactors, modeling, and simulating the dielectric heating of biomass materials.

REFERENCES

- [1] Mohamed, B. A., Kim, C. S., Ellis, N., & Bi, X. (2016). Microwave-assisted catalytic pyrolysis of switchgrass for improving bio-oil and biochar properties. *Bioresource Technology*, 201, 121-132.

Design of a Test Cell for Dielectric Properties Measurement

Soon Kiat Lau¹ and Jeyamkondan Subbiah¹

¹University of Nebraska-Lincoln, Lincoln, United States of America

Keywords: Dielectric properties, test cell, vibration, impedance analyzer.

INTRODUCTION

The measurement of dielectric properties of food materials for the radiofrequency heating and microwave heating frequencies (20 MHz ~ 3 GHz) is usually performed using the open-ended coaxial probe method. For temperature-dependent measurements, the probe and food sample are normally contained within a test cell which is then cooled or heated with liquid or air. Using air as the cooling/heating medium is an attractive solution because it is not limited by freezing/boiling points and the entire test cell can be cooled/heated evenly. However, placing the test cell within a temperature-controlled chamber introduces vibration from the fans and refrigerator compressor, which could potentially affect measurements [1]. In addition, the probe should be positioned in such a way to avoid formation of air bubbles on the probe for liquid samples (**Figure 1**). This paper describes an attempt to address these issues by designing a test cell with vibration isolators and a probe insertion port at the bottom.



Figure 1. The formation of air bubble in a horizontally oriented test cell: (a) air bubble formed near the coaxial probe during solidification of agar gel and (b) the horizontal setup.

METHODOLOGY

The test cell is a pipe made of 316 stainless steel to resist corrosion from acidic food materials. EPDM gaskets were chosen due to their resistance to low and high temperatures. The probe enters the test cell from below to reduce the formation of air bubbles and ensure that the probe is always in contact with the sample due to gravity. A spring loaded block at the top also presses the sample against the probe. A thermocouple

within the block allows temperature measurement of the sample. The test cell is suspended on a metal plate with legs. The contact between the metal plate and legs is vibrationally-isolated with silicone gel dampers. Foam pads are also adhered to the legs to further dampen vibrations. This initial design of the test cell is shown in **Figure 2**. The vibration isolating capabilities of the test cell were measured by comparing its vibration to that of the chamber itself using the accelerometer of a cellphone (Google Nexus 5). In addition, the test rig was also subjected to 10-second cycles of the refrigeration compressor to determine if the test rig helped to maintain measurement accuracy.



Figure 2. Initial design of the vibration-isolated test cell.

RESULTS

The vibration isolating capability of the test rig was measured in terms of the magnitude of acceleration (**Figure 3**). The refrigeration compressor was turned on at 1.5 s, allowed to run until 8 s, and then turned off. The dielectric constant of water measured immediately after calibration, after one 10-second cycle, and after five 10-second cycles is shown in **Figure 4**.

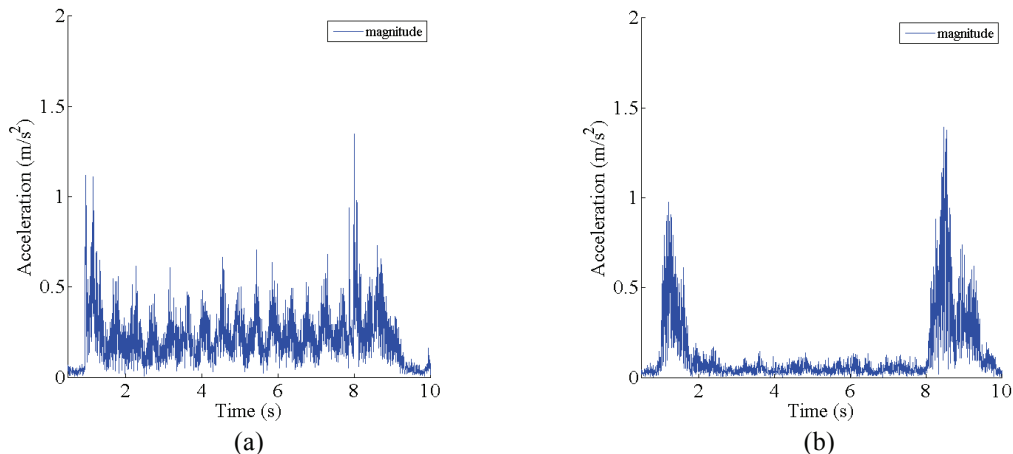


Figure 3. Vibration measurements in terms of acceleration magnitude for: (a) the floor of the temperature-controlled chamber and (b) the vibration-isolated test cell.

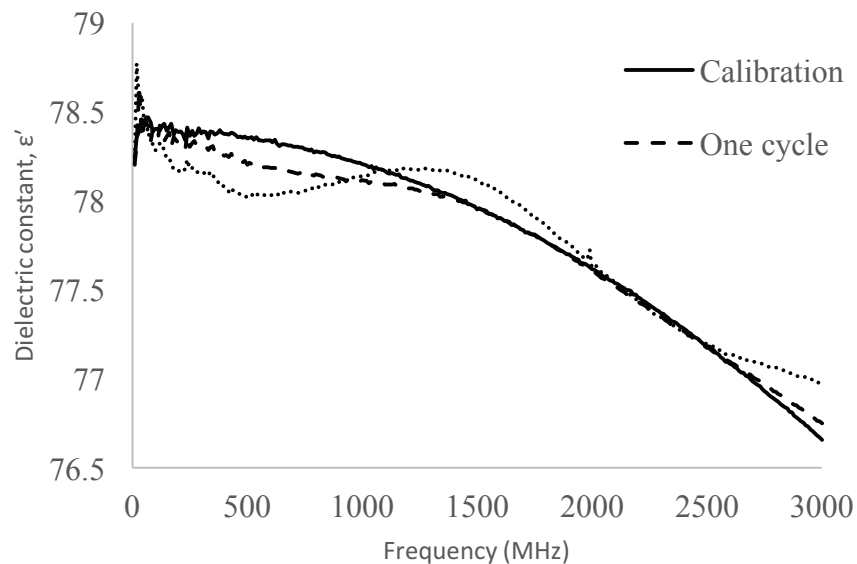


Figure 4. Vibration measurements in terms of acceleration magnitude for: (a) the floor of the temperature-controlled chamber and (b) the vibration-isolated test cell.

DISCUSSION

From **Figure 3**, it is observed that there was a spike in vibration when the compressor was turned on (1.5 s) and off (8 s) whether the test rig was used or not, however, the test rig almost eliminated vibration when the compressor was running between 1.5 s to 8 s. Therefore, the test rig helped to reduce small and constant vibrations, but was unable to reduce the large vibration spike when the compressor was turned on/off.

In **Figure 4**, the dielectric constant measurement of water appears to deviate more from its actual value (calibration) as the test rig is subjected to more 10-second cycles. The vibration spikes during the on/off phase of the compressor most likely contributed to this behavior. Although the deviation from the calibration after five cycles was only at most 0.33, the trend was noticeably affected. **At the time of writing, a second design of the test rig has been developed and is being tested for its vibration-isolation capabilities.**

REFERENCES

- [1] Agilent Technologies, *8 Hints for Successful Impedance Measurements*, 2014. Accessible at <http://literature.cdn.keysight.com/litweb/pdf/5968-1947E.pdf>.

Recognizing Design Challenges of Solid-State Power Amplifiers for RF Energy Applications

Dr. Klaus Werner

RF Energy Alliance, Beaverton, Oregon 97003 USA
www.rfenergy.org

Keywords: Solid state RF power amplifiers, RF energy applications, design, industrial heating, microwave furnaces, RF Energy Alliance

INTRODUCTION

The advantages of solid-state radio frequency (RF) technology are well known in the communications industry, however, the technology is beginning to expand into heating and power delivery application areas. Solid-state RF energy technology can already be found within medical and professional applications, though industrial and consumer uses (replacing antiquated magnetron tubes) are only slowly taking hold or currently under development. Cost concerns and engineering knowledge gaps are the primary reasons for the delay in magnetron replacement within the industrial and consumer markets.

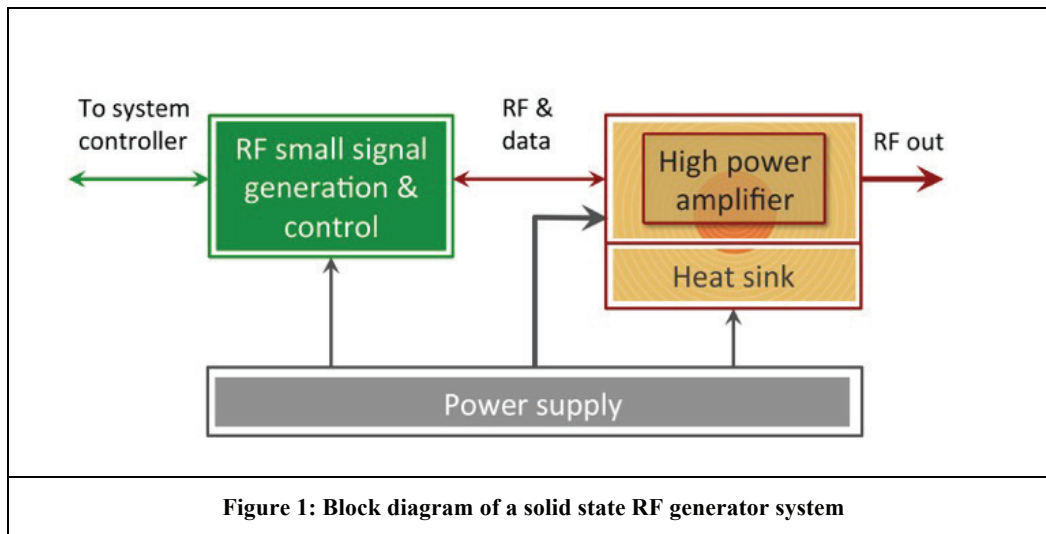
My presentation at IMPI 2015, “Economics of Solid-state Power Amplifiers for High Volume RF Energy Applications,” discussed the economic barriers to solid-state RF technology adoption in high volume, consumer-oriented markets as well as the RF Energy Alliance’s steps to facilitate a cost reduction breakthrough. As a follow up in the series, this paper will focus on various technical challenges associated with the design of solid-state RF energy systems and the work being done to address those concerns.

DISCUSSION

A complete solid-state RF generator (sub-) system typically consists of:

- Small signal generation part optionally co-located with a microcontroller
- High power amplifier (basically a gain-block) connected to a heat sink
- Power supply to deliver the various voltages and currents to drive the respective electronics

Figure 1 depicts a block diagram for such a system. The “RF out” connection leads into an RF applicator – that is a cavity or otherwise confined environment, which holds the medium to absorb the RF radiation and provides the necessary EMC shielding.



Overall, the solid-state RF power generator allows complete freedom and control over the frequency, output power level, phase, and “modulation” of the RF signal. “Modulation” here means switching the RF signal (on/off) over time and/or changing the output power level – both can happen very quickly; within microseconds. Furthermore, feedback on forward and reflected RF power is usually built into the amplifier; in some more evolved cases, even phase measurements can be carried out for complex S-parameter measurements.

Solid-state RF energy system design requires engineering knowledge, which is not generally available due to RF (power) engineers being occupied with “linearized amplifier” systems for data transmission purposes or concerned with magnetron sources for heating applications. Clearly, there is a general lack of design knowledge with respect to applying solid-state RF generation to RF energy systems.

When it comes to conceiving an RF energy system, a system architect must cover the “usual suspects” like power supplies, thermals, digital interfaces, microcontrollers and firmware, as well as the intricacies around RF signal generation, amplification and “injection” into the applicator. This paper will concentrate on and discuss the challenges facing the following RF system aspects, rather than the more common ones:

- Applicator used
- Number of RF channels
- RF signal generation (frequency, gain, phase, resolution, etc.)
- Total RF power required
- Power Amplifier (PA) thermals
- RF operation
- Ruggedness
- Homogeneous energy distribution
- Real-time process control

CONCLUSION

There is a great opportunity to develop a new industry revolving around RF energy applications, and an equally impressive number of potential job opportunities to deploy this technology. The technologies are available, and a number of novel, promising applications are under development. If done correctly, we will soon find this clean, efficient, highly controllable, contact-less and selective energy source in many facets of our daily lives, bringing remarkable convenience, energy savings and improved user experiences.

The challenges to build those systems are numerous, requiring significant knowledge on electromagnetics, control and application aspects. The overall application is an intricate interplay of RF sources, with an applicator and a variable load/processing conditions in the cavity. The above treated design ingredients hold for all kinds of RF energy systems. Be it an automotive plasma ignition source or an industrial heater, the RF source needs to continuously adapt to the changing cavity/load/resonance conditions to “stay tuned.”

64 kW Microwave Generator Using LDMOS Power Amplifiers for Industrial Heating Applications

Bob Bartola¹, Ken Kaplan² and Roger Williams¹

¹Ampleon, Inc., Smithfield, RI, USA

²Cellencor, Ankeny, IA, USA

Keywords: Microwave generator, solid state, LDMOS, semiconductor, heating, drying, cooking.

INTRODUCTION

Ampleon (formerly NXP Semiconductor) and Cellencor have collaborated [1] on a 64 kW 915 MHz microwave power generator based on a discrete 500W LDMOS transistor. Pallet amplifiers have been designed based on this device and tested with 66% drain efficiency. These pallets are combined in multiple stages to provide a single 64 kW output. This solid state microwave power generator is designed to replace CW magnetrons that suffer from short lifetime and high replacement cost, while providing controllability and reliability not available from magnetrons.

915 MHZ PALLET MODULE

915 MHz pallets have been designed and tested at the module level, and then integrated into the 64 kW generator system. Each pallet is driven with a 10W LDMOS driver and both stages are liquid-cooled via an aluminum base plate. Both stages have temperature compensated gate bias.

Figure 1 shows a photo of the test of a single pallet. At 3dB compression, $P_{out} = 57.0$ dBm, Gain = 16.2 dB, and Drain efficiency = 66%. These measurements were made with a 25°C base plate water temperature. Table 1 shows a summary of results from these tests.

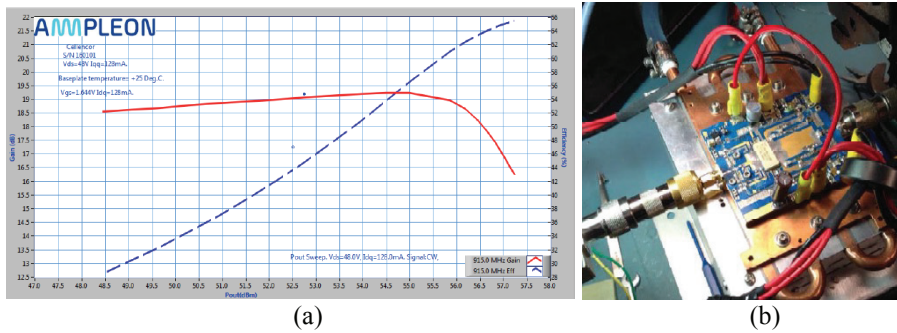


Figure 1. (a) Plot showing performance of pallet module with output power exceeding 500W CW. (b) Photo of pallet module under test.

Frequency (MHz)	Output Power (W)	Drain Efficiency (%)	Gain (dB)	Drain Voltage (V)
915	500	66	16.2	48

Table 1. (a) Power, efficiency and gain measurements.

DISCUSSION

This solid state generator has many applications in the area of industrial heating. It has frequency agility, permitting electronic load matching and stirring, and uses a high efficiency switch mode 48 V DC power supply. The full system is currently being integrated and tested, and system results will be presented in the IMPI 50 symposium.

CONCLUSION

This 64 kW microwave generator is the first high power solid-state microwave source designed specifically to supplant industrial magnetrons. Improvements in LDMOS power and efficiency, coupled with significant recent reductions in cost, have opened the door for solid-state sources to quickly begin to serve many industrial microwave power applications at both 915 MHz and 2.45 GHz.

REFERENCES

- [1] K. Kaplan, M. Romero, A Solid State High Power Microwave Generator for Industrial Heating Applications, *Proc. 49th IMPI Microwave Power Symp., San Diego, CA, June 2015.*
- [2] Gunasekaran, S and Yeng, HW, “Effect of experimental parameters on temperature distribution during continuous and pulsed microwave heating”, *Journal of Food Engineering*, vol. 78, pp. 1452–1456, 2007

Compact 1 kW 2.45 GHz Solid-State Source for Industrial Applications

Roger Williams¹ and Brad Lindseth¹

¹Ampleon, Smithfield, RI, USA

Keywords: Microwave, generator, semiconductor, LDMOS, heating, drying

INTRODUCTION

Over the past decade, LDMOS microwave power transistor technology has experienced remarkable gains in frequency range, power, and efficiency, while simultaneously decreasing in cost. All of this results from high-volume manufacturing driven by base station requirements, which enables continuous improvement of the LDMOS technology [1]. More recently, the potentially huge volumes in emerging microwave energy markets such as solid-state cooking and automotive microwave plasma ignition have driven the development of lower-cost packaging and integrated power amplifier modules. The result of these two trends is an unprecedented performance/price ratio for LDMOS devices, which expands the practical application of solid-state microwave technology into applications currently dominated by magnetrons [2].

We have developed a compact (20 x 20 x 5cm) water-cooled 1 kW, 2.45 GHz modular source (Figure 1) to demonstrate the capabilities of LDMOS technology. This presentation describes the architecture, design details, performance, and economics of this source. Components, subsystems, and manufacturing details are available to others who wish to make or purchase their own sources.



Figure 1. The packaged 1 kW source includes water cooling, MCU control and monitoring.

ARCHITECTURE

The source (Figure 2) is built around four 250 W LDMOS power amplifier pallets (Figure 3). Each two-stage pallet has 36 dB of gain, so less than 20 dBm (100 mW) of input power is needed to produce 250 W of output power. Its typical 1 dB compression point is 320 W, so there is adequate power margin to compensate for losses in the output combiner

and power drop at elevated temperatures. Each pallet includes an isolator to provide protection against reflected power. The pallets and output combiner are mounted directly on a copper-tubing cold plate which also provides the base for the source package.

The combiner is a simple in-phase microstrip structure using quarter-wave impedance transformers. The isolators on each pallet allow the use of a simple combiner without interaction between individual power amplifiers. It includes a printed directional coupler to monitor forward and reflected power.

The microwave signal is generated by a small-signal RF ASIC, which contains a 2.4-2.5 GHz synthesizer, switch, and variable-gain output amplifier which can deliver up to 500 mW. This signal is delivered to the four pallets through a simple in-phase splitter.

The source includes a microcontroller responsible for front-panel and USB control, calibration, temperature and current monitoring, and real-time measurement and display of forward and reflected power.

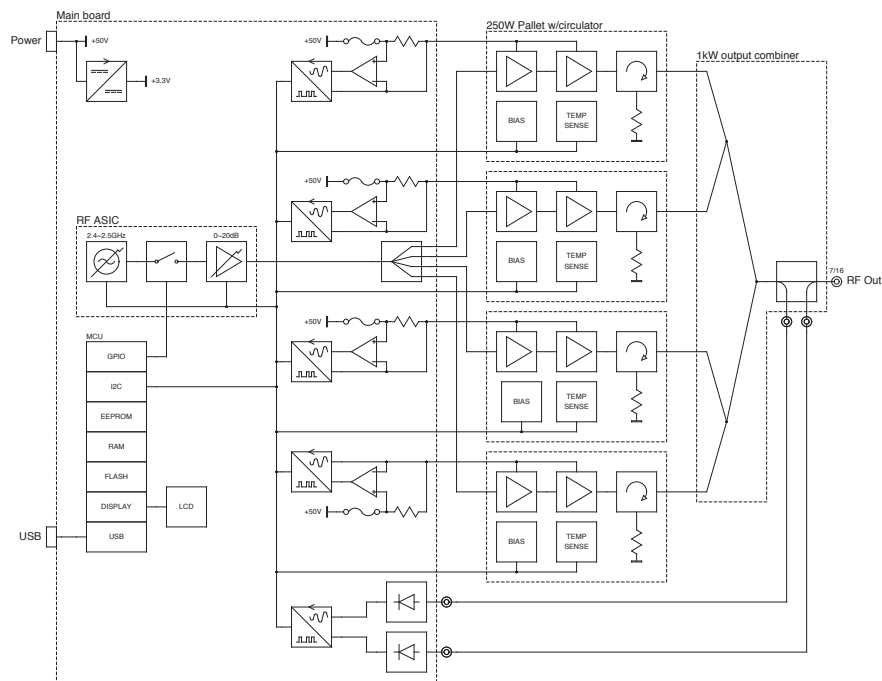


Figure 2. Simplified block diagram of the 1 kW source.

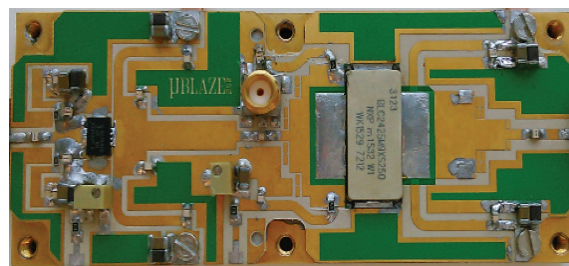


Figure 3. Two-stage 250 W pallet has 36 dB gain, 58% efficiency.

RESULTS

The preliminary module-level performance and cost is summarized in Table 1.

Frequency (GHz)	Output Power (W)	Efficiency (%)	Supply Voltage (V)	Supply Current (A)	Total Parts Cost (\$)
2.450	1150	55.4	28	74.1	490 (1k)

Table 1. CW performance for complete module at 20°C cooling water temperature.

DISCUSSION

In comparison to current magnetron generators, a solid-state source has many advantages including higher reliability and safety, reduced maintenance, and a lower lifetime cost. It also allows precise control of power and high-speed modulation, and is powered by low-cost switching DC power supplies.

Because of the pallet-level isolators and the ability to phase-lock the sources from a common 1 or 10 MHz frequency reference, this 1 kW source can be easily combined into larger systems without giving up the control and protection provided by distributed microcontrollers. The availability of pallets and all design information makes this source attractive as both a development tool and a reference for commercial products.

CONCLUSION

Much attention has been given to the “near future” economics of LDMOS in high-volume consumer microwave energy applications, such as solid-state cooking [2]. This source demonstrates that LDMOS can be successfully applied today to industrial microwave energy applications, at a final generator cost as low as \$1/W.

REFERENCES

- [1] Theeuwens, S. J. C. H., and J. H. Qureshi. "LDMOS technology for RF power amplifiers." *Microwave Theory and Techniques, IEEE Transactions on* 60.6 (2012): 1755-1763.
- [2] Werner, K. "Economics of solid-state power amplifiers for high volume RF energy applications." *IMPI: Proceedings of the 49th Microwave Power Symposium* (2015): 82-83.

A Comparison of Mode Mixer vs. Turntable Upon Temperature Response of Small Samples

Robert F. Schiffmann

R. F. Schiffmann Associates, Inc. New York, U.S.A.

Keywords: Microwave oven, small samples, mode mixers, mode stirrers, turntables' uniformity

ABSTRACT

The lack of uniformity of EM-field distribution in microwave ovens is well known and is a major focus of microwave-oven engineers constantly striving to improve this condition. While it is a problem when heating any object in a microwave oven, in many cases, especially with larger objects, such as an 8-ounce entrée, other factors such as dielectric and thermal properties, as well as shape and volume may be of greater influence. However, it is especially problematic with smaller objects on the order of approximately an ounce or less. In testing non-food products consisting of waxes or oils I found that the temperature developed in the sample was extremely sensitive to location in an oven, and that varies oven-to-oven. For example, in ovens A & B, the highest temperatures achieved in the sample after one minute of microwaving differed by over 100°C, but were highest in the center of the turntable of oven A, but highest at the edge of the turntable in oven B. This was the subject of my paper "Small-sample Positional Effects in Microwave Ovens" presented at IMPI 49 in 2015.

In this paper, I report on the influence, in terms of small-sample heating, of a turntable vs. mode mixer, vs. a combination of the two, or none of them, tested in a single microwave oven.

Multiphysics Modeling of the Effect of Headspace Steam on Microwave Heating Performance of a Frozen Heterogeneous Meal

J. Chen¹, K. Pitchai¹, S. Birla², D. Jones¹, R. Gonzalez², J. Subbiah¹

¹University of Nebraska-Lincoln, Lincoln, NE

²ConAgra Foods, Omaha, NE

Keywords: microwave, heat and mass transfer, headspace steam, heterogeneous meal, heating uniformity, modeling.

INTRODUCTION

Multiphysics models have been used in the food industry to assist in understanding microwave heating process and designing novel microwaveable food products. In a longer duration microwave heating process, steam is generated in the food product and often causes moisture loss and food splash, which deteriorate the food quality considerably. A plastic film with a slit is usually used on the top of the package to release the steam and prevent the splashing of food. In this study, a three-dimensional microwave heating model was developed to study the generation, movement and venting of steam in the food system, and to understand the effect of the steam in the headspace on the heating performance of the microwaved food product.

METHODOLOGY

The multiphysics of electromagnetics, heat and mass transport of species (water, vapor, and air) in the food product, phase change of water evaporation in the food product, and laminar flow and heat transfer of steam in the headspace were incorporated together to fully describe the microwave heating process. The model was validated by heating a tray of 550 g of a frozen heterogeneous meal – lasagna from -10 °C on a rotating turntable in a 1200 W domestic microwave oven for 6 minutes.

RESULTS

The simulation results showed good agreement with the experimental validation of transient point temperature, spatial surface temperature profile and total moisture loss. Compared to the simulation results without headspace steam (without covering film on top), the headspace steam could help increase the average temperature by 27.8%, reduce moisture loss by 34.6%, and improve microwave heating uniformity (standard

deviation/average temperature) by 24.5%. Therefore, the headspace steam could help improve the food quality considerably.

DISCUSSION

The model can be used to help food product developers in designing novel food products that can take advantage of the steam generated in the product during the microwave heating process, so that the microwaveable food quality and safety can be improved.

CONCLUSION

A multiphysics model was developed to understand the effect of headspace steam on microwave heating performance of a frozen heterogeneous meal. The results showed that the headspace steam could help improve the temperature and reduce the total moisture loss.

Model Food System Development for Quality Optimization of Microwave-Assisted Pasteurized Foods

Ellen R. Bornhorst¹, Juming Tang¹ and Fang Liu¹

¹Washington State University, Pullman, WA, USA

Keywords: mashed potato, green pea, model foods, quality, microwave pasteurization

INTRODUCTION

A single mode, 915 MHz Microwave Assisted Pasteurization System (MAPS) has been developed at WSU to thermally pasteurize prepackaged food, yielding products that are both safe and have a high quality [1]. Process optimization for the MAPS is in progress; the goal is to obtain the best quality while maintaining safety. Process and product development and optimization for all food products of interest is time consuming and expensive; to address this issue, model foods can be used to represent a variety of food products. Model food systems have been an effective tool in heating pattern visualization and cold-spot determination to assess process lethality for microwave-assisted thermal sterilization (MATS), in the temperature range 110-130°C [1]. However, model food systems used for sterilization are not optimal for pasteurization because of the large difference in processing temperature. Previous work on model foods for pasteurization temperatures (70-90°C) focused on only egg white gel [2]. In addition, all the past research on model food systems for both microwave sterilization and pasteurization applications was aimed at process lethality determination and not quality optimization. Therefore, the objective of this study was to develop additional model foods for quality optimization at pasteurization temperatures, especially for MAPS.

METHODS AND MATERIALS

Color changes in food during heating are an indicator of a decrease in food quality; in this study, model foods for quality optimization utilized this concept. Green pea puree and mashed potato model foods were selected for this study based on preliminary results. Bench-top experiments were performed in triplicate to determine the reaction kinetics of the model foods' color change. Model food samples were heated inside custom-designed aluminum test cells with a 1 mL sample capacity at 80, 90, or 100°C for 0 to 90 minutes. These time-temperature combinations were selected to be relevant to pasteurization with short time MAPS and conventional pasteurization methods; longer heating times were also needed to find the saturation of color change. Color was quantified in CIELAB (L*a*b*) color space using a computer vision system (CVS) that included a digital camera, light pod, and image analysis.

Initial pasteurization tests were conducted with 8 oz. trays of mashed potato and green pea model foods processed in the MAPS and conventional method (hot water). Both processes aimed to achieve a 6 log reduction at the cold spot for non-proteolytic *C. botulinum*, the target food pathogen in this study; this equates to a thermal treatment of 90°C for 10 minutes [3]. The MAPS process (Figure 1) included 30 minutes of preheating in 61°C water, 2.3 minutes of microwave heating (5 kW generator) with trays in 93°C water, 9 minutes of holding in 93°C water, and 5 minutes of cooling in 23°C water. The hot water process included 30 minutes of heating in 93°C water and 10 minutes of cooling in 0°C water. After processing, model foods were sliced horizontally at ¼ and ½ the sample thickness (quarter and middle layers). The color of the quarter and middle layers was analyzed using the CVS described above. During the image analysis, color mapping was performed to visualize the heating pattern; the a* values in the image were transformed to a jet color scale.



Figure 1. Pilot-scale microwave assisted pasteurization system at Washington State University.

RESULTS


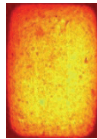
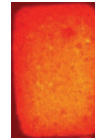

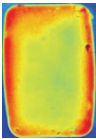
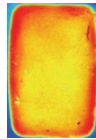

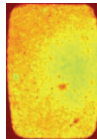
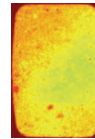

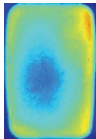
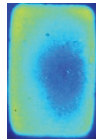
During heating, green pea and mashed potato model foods’ color change was quantified using image analysis. For both green pea and mashed potato, a* showed significant change during heating that fit to first order kinetics. D-values at 90°C and z-values (80-100°C) for a* color change were 79.1 min and 31.1°C for green pea and 80.0 min and 20.7°C for mashed potato, respectively. Table 1 shows the RGB and color transformed images for green pea and mashed potato models during heating at 90°C.

Table 1. Green pea and mashed potato model foods during heating at 90°C with RGB and color mapped images.

Min at 90°C	0	10	20	30	60	90
Green pea RGB						
Color mapped						
Mashed potato RGB						
Color mapped						

The pasteurization test with the MAPS process achieved a thermal treatment equivalent at the cold spot of 90°C for 11.3 min (F_{90} =11.3 min) and the hot water heating process achieved only 5.1 min (F_{90} =5.1 min). Table 2 shows the green pea and mashed potato RGB and color mapped images of the MAPS and hot water processed trays.

Table 2. Green pea and mashed potato model foods after hot water and MAPS pasteurization.

Process	Green pea model food			Mashed potato model food		
	RGB	Color mapped		RGB	Color mapped	
	Middle layer	Middle layer	Quarter layer	Middle layer	Middle layer	Quarter layer
Hot water						
MAPS						

DISCUSSION

During heating, a^* increased for both foods; the color was moving from the green to red range. Both model foods had similar D-values at 90°C, which means that it took about 80 minutes to achieve a one log increase in the a^* color value. The hot water process (F_{90} =5.1 min) yielded more color change in the middle and quarter layers than the MAPS (F_{90} =11.3 min). Overheating of the quarter layer was apparent in the hot water process, but was not significant in the MAPS.

CONCLUSION

Green pea and mashed potato model foods were developed for pasteurization temperatures. The MAPS processed model food trays had less color change and a less overheated quarter layer, even though the thermal treatment at the cold spot was more than double the hot water processed trays. This implied that the tray pasteurized with the MAPS may have had a better quality than the hot water processed tray.

REFERENCES

- [1] J. Tang. Unlocking potentials of microwaves for food safety and quality. *J. Food Sci.*, vol 80, no 8, pp. E1776-93, 2015.
- [2] W. Zhang, J. Tang, F. Liu, S. Bohnet, and Z. Tang. Chemical marker M2 (4-hydroxy-5-methyl-3(2H)-furanone) formation in egg white gel model for heating pattern determination of microwave-assisted pasteurization processing. *J. Food Eng.*, vol 125, pp. 69-76, 2014.
- [3] J. Peng, J. Tang, D. M. Barrett, S. S. Sablani, N. Anderson, and J.R. Powers. Thermal pasteurization of vegetables: critical factors for process design and effects on quality. *Crit. Rev. Food Sci. Nutr.*, pp. 00, 2015.

The Use of Microwave Energy in Reactive Powder Metallurgy

Roberto Rosa, Cristina Leonelli, Paolo Veronesi

University of Modena and Reggio Emilia, Department of Engineering “Enzo Ferrari”, via P. Vivarelli 10, 41125 Modena, Italy

Keywords: Microwaves; combustion synthesis; intermetallics; high entropy alloys.

INTRODUCTION

The use of microwave energy in powder metallurgy has become a well-established practice due to the recognized advantages of direct microwave-matter interaction with respect to conventional heat transfer mechanisms. Indeed, the possibility for microwaves to rapidly and selectively heat micrometric metallic powders is a significant advantage in preparing advanced materials, by exploiting reactions among metallic powder precursors. In this framework, the term "reactive powder metallurgy" is intended to designate processing of metallic powder compacts or loose powders like combustion synthesis or reactive synthesis of new alloys, and to differentiate it from simple sintering.

This paper presents recent advances in the use of microwave energy to ignite combustion synthesis (CS) reactions. The effects of electric and magnetic field components in the synthesis of intermetallic compounds were investigated, together with the effects of different incident microwave frequencies (2.45 vs. 5.8 GHz). Moreover, research aimed at obtaining high entropy alloys (HEA) starting from pure metals is described in detail. HEA have been studied in just published paper [1], but starting from a mixture of metal oxides.

EXPERIMENTAL APPARATUS AND PROCEDURE

Most of the microwave heating experiments were conducted in a single mode TE103 microwave applicator, operating at a frequency of 2.45 GHz. The applicator was based on the rectangular WR-340 waveguide geometry. Heating experiments performed at 5.8 GHz used a single mode microwave applicator based on the WR-159 waveguide geometry. The reactive powder mixture was prepared according to the stoichiometry of the desired compounds (or HEA), starting from high purity elemental metal powders. Cylindrical samples were prepared and positioned in the centre of the applicator. When investigating the role of H-field component, the sample was positioned near the short side of the applicator.

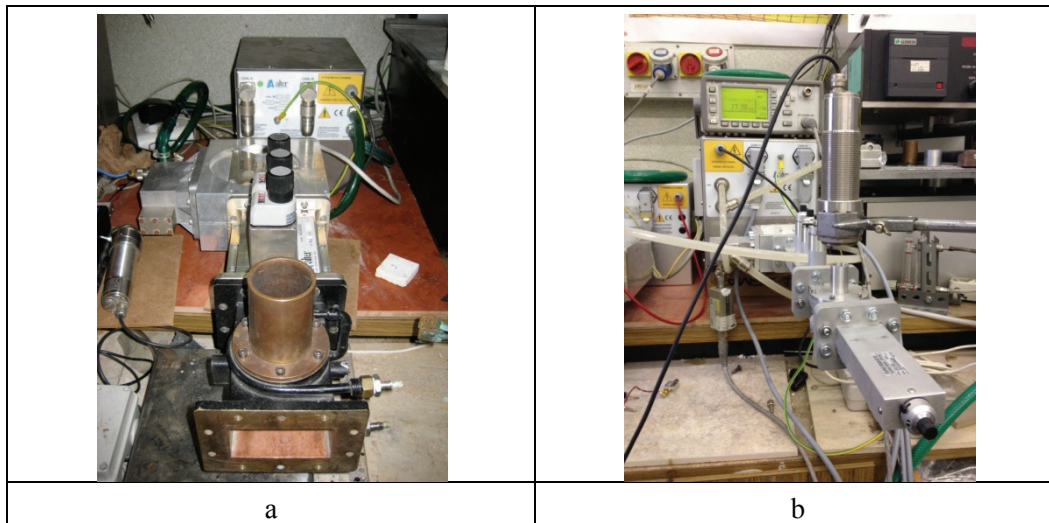


Figure 1. Two single-mode microwave applicators, operating at (a) 2.45 GHz and (b) 5.8 GHz, fed by magnetron generators through circulators and 3-stub tuners, terminated with shorting plungers.

RESULTS AND DISCUSSION

The direct interaction of microwave energy with reactive powder mixtures, belonging to the systems Ni-Al, Co-Al, Fe-Al and Ni-Ti, was successful in igniting combustion synthesis reactions. The final products were characterized, and it was found that the corresponding intermetallic compounds were formed. Particularly, it was found that the reactivity of less exothermic systems (i.e. Fe-Al and Ni-Ti) could be increased by exploiting the H-field component of the incident microwaves. Its interaction with the reactive system allowed reaching a heating rate significantly higher than E-field ignition, thus prolonging the residence time at high temperatures and favoring completion of the reaction. [2] The heating and cooling rates, and thus the microstructure and the composition of the products, were also modified by changing the input frequency, from the widely used 2.45 GHz to the less employed 5.8 GHz.

Microwave irradiation was also successful in preparing high entropy alloys by powder metallurgy strategies, particularly FeCoNiCuAl, FeCrNiTiAl, FeCoCrNiAl_{2.5} and Si-modified Mn₂₅Fe_xNi₂₅Cu_(50-x) [3,4] HEAs were prepared using microwave heating of stoichiometric powder compacts. Additionally, different components of the electromagnetic wave as well as different available frequencies were employed and opportunely selected in order to optimize the syntheses and to obtain homogenous structures without further annealing. In particular, the powder precursors were directly heated by the microwaves, until the ignition conditions were reached (melting point of aluminum). Microwave heating allowed altering the cooling rate after synthesis, and thus extended the time at high temperature. This was particularly evident when the sample was located in regions of the applicator, where the magnetic field was dominant. The temperature and duration of the microwave-assisted process at atmospheric pressure were significantly less than in conventional powder metallurgy processes. The microwave

processed samples had generally less segregation, but they had unwanted porosity. The addition of auxiliary microwave absorbers allowed rapid preparation of HEAs from the liquid state, with results very similar to conventional arc melting techniques.

CONCLUSION

Direct interaction of microwave energy with micrometric metallic powders is advantageous in preparing intermetallic compounds and high entropy alloys. It significantly reduced processing times, leading to products with unique characteristics (reduced segregation), and allowed controlling their microstructures, mainly by acting on the cooling rates after synthesis.

REFERENCES

- [1] T. Wang, J. Kong, B. Chao, Microstructure and mechanical properties of FeCoNiCuAl high-entropy alloy prepared by microwave-assisted combustion synthesis, *Fenmo Yejin Jishu/Powder Metallurgy Technology*, vol. 29, pp. 435-438+442, 2011.
- [2] R. Rosa, P. Veronesi, A. Casagrande, C. Leonelli, Microwave ignition of the combustion synthesis of aluminides and field-related effects, *J. Alloys Compds.*, vol. 657, pp. 59-67, 2016.
- [3] P. Veronesi, R. Rosa, E. Colombini, C. Leonelli, Microwave-assisted preparation of high entropy alloys, *Technologies*, vol. 3, pp. 182-197, 2015.
- [4] P. Veronesi, E. Colombini, R. Rosa, C. Leonelli, F. Rosi, Microwave assisted synthesis of Si-modified Mn₂₅Fe_xNi₂₅Cu(50-x) high entropy alloys, *Mater. Letters*, vol. 162, pp. 277-280, 2016.

A Novel Microwave-Low pressure Process for Strengthening High Performance Concrete Paste

Natt Makul

Department of Building Technology, Faculty of Industrial Technology, Phranakhon Rajabhat University, 9 Changwattana Road, Bangkok Bangkok, 10220, Thailand

Keywords: Concrete, Paste, Microwave, Processing, Low-pressure, Strength

INTRODUCTION

The use of microwave (MW) energy to make high performance concrete paste (HPC), which is associated with a low pressure system, is an innovative method that will become increasingly important in the near future in the production of HPC. Research in this area is necessary to understand the processing mechanism with dielectric properties and to establish the characteristics of HPC.

The concept for determining the parameters of MW processing and the vacuum system of HPC is based on the hydration reaction of HPC, which comprises three main periods: [1,2]

- Period 1: The early period, which is also referred to as the dormant period, begins with contact between the cement grains and the water molecules.
- Period 2: The accelerated or middle period begins with the formation of calcium and hydroxide ions until the system is saturated. Once the system has become saturated, the calcium hydroxide begins to crystallize.
- Period 3: The final period is referred to as the decelerated or late period. In this period, the hydrate products begin to slowly form and continue to form so long as both water and unhydrated silicates are present.

As noted in the conceptual outline, two principal parameters are employed to control the hydration reaction of HPC: the time-dependent dielectric properties of HPC throughout the hydration process and the water–cement (w/c) mass ratio; the latter influences the temperature (i.e., causes it to increase) and the properties of the MW-cured HPC.

METHODOLOGY

Type 1 Portland cement (ASTM C150) was mixed with deionized water with a pH of 7.5 in specific water–cement (w/c) mass ratios of 0.22, 0.38, and 0.60. MW was used to assist the processing as shown in Fig. 1. The MW power was generated at a frequency of 2.45 GHz, and the power setting was calibrated at 780 W. The MW power was conveyed via a rectangular waveguide to a 0.13 m³ metallic low-pressure cavity, in which the

materials were rotated by a rotary drum. The drum was composed of polypropylene with a diameter of approximately 30 cm and a length of approximately 50 cm, and had a full load capacity of 30 kg. The drum rotation speed was 10 rpm. The maximum low-pressure level was approximately 30 kPa.

The work pieces were maintained at a specific maximum temperature; for the HPC with w/c ratios of 0.22, 0.38, and 0.60, these temperatures were 96.8°C, 70.4°C, and 52.8°C, respectively). After obtaining the given maximum temperatures, the work pieces were maintained at these temperatures for 60 min, i.e., until the MW processing was completed. After step 3 was completed, the work pieces were cooled at room temperature, and the pressure was simultaneously reduced to normal using a convection method that was based on air flow.

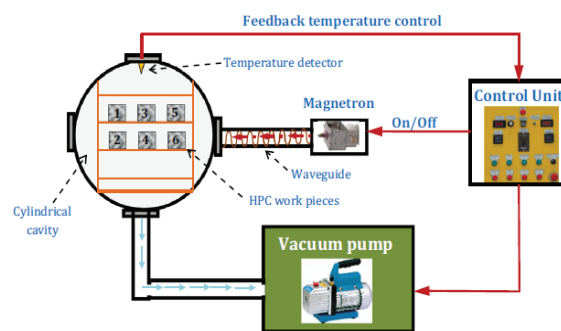


Figure 1 A combined unsymmetrical MW and vacuum system

RESULTS

The compressive strengths of the HPC work pieces with w/c ratios of 0.22, 0.38, and 0.60 after the application of MW processing are shown in Fig. 2. When cured at elevated temperatures, HPC can rapidly develop strength. At the age of 2 hours after MW curing, the HPC work pieces with a w/c ratio of 0.22 attained a compressive strength of 20.1 MPa (129% higher than the compressive strengths of the water-cured HPC). At 24 h of curing, the compressive strength of the MW-cured HPC was 35.3 MPa; at 7 days and 28 days, the compressive strengths were 45.2 and 42.6 MPa, respectively. However, for subsequent 7-day and 28-day stages, the compressive strengths of the MW-cured work pieces were 21.1 to 41.9% lower than the compressive strengths of the water-cured HPC due to a reduction of less than 0.25 in the w/c of the MW-cured HPC. When the water content is 0.25, all water molecules exist as gel and combined water in the C-S-H structure, that is, no capillary water exists after complete hydration has occurred. However, some capillary pores should be preserved as paths through which water molecules can enter and react with cement grains near the pores. These pores can serve as a space for the gel to expand. The existence of a few capillary pores may support the structure and strength of the hardened concrete paste, which is consistent with our experimental results, that is, if the w/c ratio is less than 0.40, full hydration of the cement may not occur and the strength development is undermined.

With regard to the HPC with a w/c ratio of 0.22, the compressive strength of the water-cured HPC work pieces almost continuously developed, because the remaining w/c

for the work pieces exceeded the minimum w/c (0.25). Consequently, the strength continuously developed compared with the water-cured HPC at a subsequent age. In the case of the work pieces with a w/c ratio of 0.60, the strength development at subsequent ages (7 and 28 days) was lower than the strength development of the water-cured HPC because high w/c ratios affect the high porosity of the internal structure of HPC. As a result, the water with high HPC content can be transported from the work pieces, causing a decrease in compressive strength.

CONCLUSION

MW heating of HPC produced compressive strength that was higher than that produced by normal water curing.

ACKNOWLEDGMENTS

The author appreciates the financial support of the Thailand Research Fund (Contract No. TRG5780255). The author is also grateful for the permission and facilities extended by Professor Dr. Phadungsak Rattanadecho.

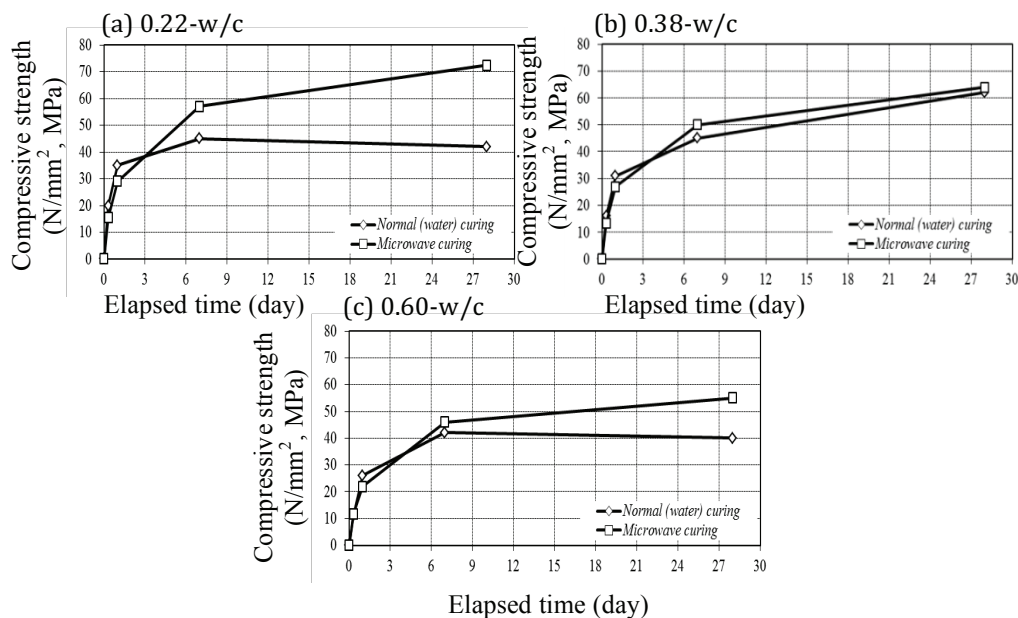


Figure 2. Compressive strength development of HPC with w/c ratios of 0.22, 0.38, and 0.60 after application of MW power at 780 watt for 15 min and low pressure of 30 kPa compared with compressive strength development with normal (water) curing.

REFERENCES

- [1] Neelakantan, T. R.; Ramasundaram, S.; Vinoth, R. Accelerated curing of M30 grade concrete specimen using microwave energy. *Asian Journal of Applied Sciences* 2014, 7, 256–261.
- [2] Xuequan, W.; Jianbo, D.; Mingshu, T. Microwave curing technique in concrete manufacture. *Cement and Concrete Research* 1987, 17, 205–210.

Improved Treatment for Wood Boards Disinfestation by Microwave Power Application

A. Tatiana Zona-Ortiz¹, B. Juan V. Balbastre², C. Eva Pérez-Marin³ and
D. Antonio Martínez⁴

¹ Universidad Santo Tomás, Cra 9 # 51-11, Bogotá, Colombia.

² ITACA -Instituto de las Aplicaciones de las Tecnologías de la Información y de las Comunicaciones Avanzadas, Universitat Politècnica de València, Camino de Vera s/n, 46022 Valencia, España.

³ IRP- Instituto de Restauración del Patrimonio, Universitat Politècnica de València, Camino de Vera s/n, 46022 Valencia, España.

⁴ Desinsección y secado 3D, s.l., Avda.Mare Nostrum 7, 46120 Alboraya, Valencia, España.

Keywords: Electromagnetic heating, Microwave heating, Wood disinfestation.

INTRODUCTION

Nowadays, severe damage in wood buildings, furniture and artistic or historical heritage has been reported, since woodworms build tunnels during the growing process which causes structural problems. A detailed comparison of the most widely used methods for controlling woodworm attacks in buildings can be found in [1] and [2]. As the public interest in non-chemical treatments has increased, microwave energy could be seen as an alternative, like in agricultural products [3],[4],[5],[6].

Much work has been done to date about the feasibility of microwave disinfestation of wood and less to determine the exact lethal dosage or treatments. What this research deals with is the establishment of an improved treatment for wood boards by estimation of the extermination rate and comparison between the extermination rates obtained with linearly and circularly polarized prototypes.

METHODOLOGY

The samples used were wild pine wood (*Pinus sylvestris*) with tangential and radial sections, their dimensions were 20x20x2.5 cm. The disinfestation system was controlled and the sample monitored from the outside of the chamber. Woodworm larvae (*Hylotrupes bajalus*) were artificially placed inside the samples in pairs at the three locations shown in figure 1. The larvae orientation was not relevant because of the circular polarization, thus they were always placed parallel to the grain in order to compare the result obtained with the ones in [7]. In the first experiment, the infested samples were treated with central application at different treatment durations: 20, 30 and 40 seconds. In the second

experiment, the infested samples were treated with overlapping applications at 20, 25 and 30 seconds, 40 seconds treatment duration was not evaluated in order to conserve safety the overlapped areas. At the end, 60 larvae were treated and 20 observed as a control. The extermination rate was evaluated after each procedure.

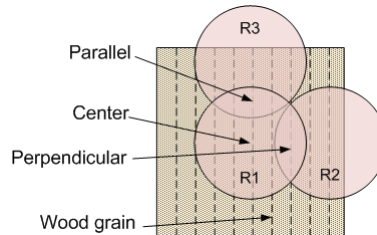


Figure 1. Experimental procedures and locations. For central application only R1 was applied, and for overlapped application R1, R2 and R3 were applied. The perpendicular and parallel directions are related to the wood grain.

RESULTS

In the central application case the effectiveness at the peripheral areas was not improved, when the treatment duration increased, but it was in the overlapping one. The effectiveness for 30 seconds was poor in central application at peripheral areas; otherwise it was highly effective in overlapping application at those areas.

On the other hand, the 25 seconds treatment duration in overlapping application had a good effectiveness, but it was not effective enough for the perpendicular orientation. To summarize, the best treatment for mode 1 seems to be 30 seconds with overlapping application.

Table 1 shows the comparison between the extermination rates of the effective treatment found above and the one found in [7]. Both were highly effective, but the treatment found with the circularly polarized prototype improved the effectiveness at the perpendicular location.

Table 1. Extermination Rate comparison between effective treatments for both prototypes in mode 1 with overlapping application.

	Linearly Polarized. 20 s	Circularly Polarized 30 s
Parallel	12/12	2/2
Central	12/12	2/2
Perpendicular	20/40	2/2

DISCUSSION

This research attempted to asses a more effective treatment for wood boards by changing the polarization. A treatment for 30 seconds in mode 1 and overlapping application with the circularly polarized prototype has promise as a guide to establish a

highly effective procedure to exterminate woodworms in wood boards, depending on the piece size.

In order to get similar effectiveness with the circularly polarized prototype, the treatment duration had to be increased. Additionally, the circularly polarized prototype guaranteed that the difference between peripheral locations was minimum. This is the reason why the effectiveness was improved in perpendicular location in relation to the results found in [7].

This study has taken a step in the direction of defining a standard procedure for wood disinfestation. It is possible, of course, that other wood kinds, different piece sizes, changing applicator or the microwave sources, other woodworm kinds or the same in another stage may produce different results. In addition, it is important to emphasize that the number of woodworms was reduced to 60 larvae because of their high price.

The approach outlined in this study should be replicated in other types of wood as well as in other piece sizes in order to establish a standard procedure. Additionally, it is important to research about the safety in the application of these methods.

CONCLUSION

The current results demonstrate that the treatment is more effective with the circularly polarized prototype because of the heating uniformity, although it was necessary to increase the treatment duration. The best treatment found was for 30 seconds in mode 1 and overlapping application with the circularly polarized prototype, which was highly effective.

REFERENCES

- [1] V. R. Lewis, "Evaluation of six techniques for control of western drywood termite (Isoptera:Kalotermitidae) in structures", *Journal of Economic Entomology*, vol. 89, no. 4, pp 922-934, August. 1996.
- [2] V. R. Lewis, "Alternative control strategies for termites". *Journal of Agricultural Entomology*, Vol. 14 no. 3, pp. 291-307, July. 1997.
- [3] A. Díaz-Morcillo, P. J. Plaza-González, J. V. Balbastre, J.M. Osca, and D. Sánchez-Hernández. (2003, September). Commercial rice disinfestation unit using microwave energy. Proceedings of 9th International conference on microwave and high frequency heating 2003.
- [4] S. L. Halverson, W.E. Burkholder, T.S. Bigelow, E.V. Norsheim, and M.E. Misenheimer, "High-power microwave radiation as an alternative insect control method for store product", *Journal of economic entomology*, vol. 89, no. 5, pp 1638-1648, October. 1996.
- [5] S.O. Nelson, "Review and assessment of radiofrequency and microwave energy for store-grain insect control", *Transactions of the ASEE*, vol. 39, no. 4, pp. 1475-1484, Month. 1996.
- [6] H.H. Webber, R.P. Wagner, and A.G. Pearson, "High frequency electric fields as lethal agents for insects", *Journal of Economic Entomology*, vol. 39: pp 487-498, August. 1946.
- [7] V. Vivancos, E. Perez-Marín, L. Nuño, J.V. Balbastre, and A.T. Zona. (2006, June). Microwave treatment for woodworm disinfestation in large-format Works of art. Proceedings of the international conference on heritage, weathering and conservation, vol. II pp. 707-712 2006.

Feasibility of Liberating Gold from Refractory Ores by Microwave Irradiation

P.Munemo¹, SW Bhero²

¹Harare Polytechnic, Harare, Zimbabwe

²University of Zimbabwe, Harare, Zimbabwe

Keywords: Microwave, irradiation, refractory ores, gold leaching

INTRODUCTION

Microwave irradiation has been known of late to bring about certain metallurgical effects in mineral processing, which include liberating gold locked up in ores. The gold in a complex with ferric oxides hardly be extracted by standard leaching processes. In this project the feasibility of microwave irradiation of a refractory roast dump prior to leaching was investigated. The refractory dump in question amounts to 300 000 tonnes of residue from roasting of sulphides, the product of which was conventionally leached in cyanide. However, tailings have remained rich with an assay grade ranging from 3 to 20 g/t gold. The objective of this project was to determine the amount of gold recoverable by direct cyanidation and to investigate the characteristics of the refractory ore after exposure to microwave irradiation. .

METHODOLOGY

Chemical analysis was carried out on samples obtained from the dump for most elements present and fire assay was used to determine the amount of gold present. Agitation leaching of samples was carried out before and after irradiation with a 2450MHz, 750W domestic microwave for 1 minute and 5 minutes with the leach residues being fire assayed to determine the residual gold and thus establish the amount of gold liberated and leached out.

RESULTS

The chemical analysis showed that the elements present included copper, iron, zinc, arsenic and antimony, the main element being iron, 31.85%. The average assay of gold in the tailings dump was found to be approximately 8,14g/t, the maximum gold recoverable by simple cyanide leaching of the ore was about 13 % at lime and cyanide consumption rates of 4.0g/t and 6,03g/t respectively. After microwave irradiation gold recoveries were approximately 33% and 40% after exposure for 1min and 5 minutes respectively at reagent consumption rates for lime and cyanide being 4,5g/t and 5,4g/t respectively for 1min exposure and 5,0g/t and 5,3g/t respectively for 5mins irradiation.

DISCUSSION

Microwave irradiation improved the irradiation of gold as shown by the increase of liberation of gold from 13% by simple cyanidation to 40% after irradiation with microwaves.

CONCLUSION

It is possible to liberate gold from refractory ores using microwave irradiation as shown by the increase from 13% to 40%..

REFERENCES

- [1] Johnstone R.F, Biological Treatment of Bendigo Refractory ores, www.batemanbv.com/pdfs, (20/05/2009)
- [2] Marsden J and House I, *Chemistry of Gold Extraction*, EllisHorwood limitedGraet Britain,1992.
- [3] Muir A,Mitchell J, Flatman S.R, Sabbagha C, A Pactical Guide to Retreatment of gold Processing Residues, , *Minerals Engineering, Vol 18, Issue 8, 2005*
- [4] Xia D.K and Pickles C.A , Application of Microwave Energy in Extractive Metallurgy, CIM Bulletin, 90(1), p99-107, 2006

Development of High Power 5.8GHz CW Magnetron-Industry's First

Nagisa Kuwahara¹, Takanori Handa¹

¹Panasonic corporation, Kusatsu City, Shiga, Japan

Keywords: continuous wave magnetron, 5.8GHz, high power.

INTRODUCTION

Up to present the output power of 5.8GHz CW magnetrons has been less than 1kW; higher power is requested for industrial uses. However, higher power levels have been impractical because the filament temperature rises too high and hence, shortens that magnetron lifetime and makes its operation unstable. This study presents our new high power 5.8GHz CW magnetrons which can achieve 1.5kW output at lower filament operating temperature.

METHOD

When the output power of 750W magnetrons is augmented to 1.5kW, the back-bombardment increases and the filament temperature rises. This leads to shorter magnetron lifetime and instable operation. To decrease the back-bombardment, we expanded the dimensions of the interaction space, which lowered the electronic density minimizing the decrease of oscillation efficiency. In addition, to study the relation between the output power and the filament temperature, we made a special magnetron which enabled the measurement of the filament temperature (Figure 1). The measurements helped to optimize the diameter of wire and the length of the filament to minimize the temperature.

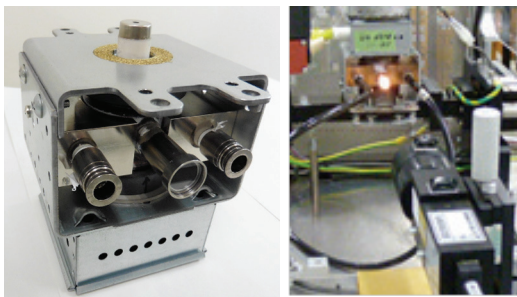


Figure 1. Magnetron for temperature survey and measurement system.

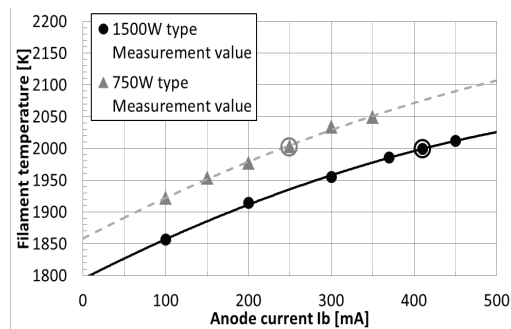


Figure 2. Measurement value of the filament temperature.

RESULTS

Figure 2 shows the relation between the anode current and the filament temperature of the 750W magnetron. The anode voltage of 750W is 4.5kV, and the standard anode current is 250mA; the filament temperature at 250mA is ~2000K. Accordingly, 1.5 kW requires 500mA, which leads to filament temperatures in excess of 2100K. To avoid the high temperature, we optimized the dimension of the interaction space. Thus, as shown in Figure 2, we succeeded in decreasing the 1.5kW filament temperature by ~70K compared to the 750W magnetron. Figure 3 presents the measured temperatures versus the wire diameter and the filament length as a function of the filament temperature. Based on these results, we built the 1.5kW output power

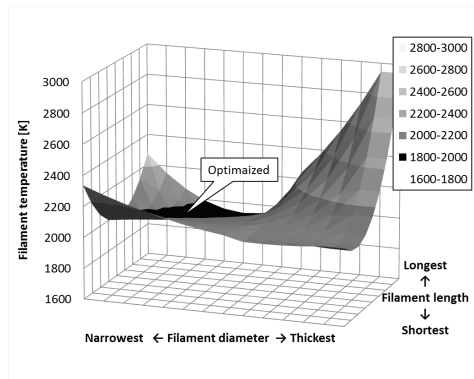


Figure 3. Optimization of Filament diameter and length to reduce the filament temperature

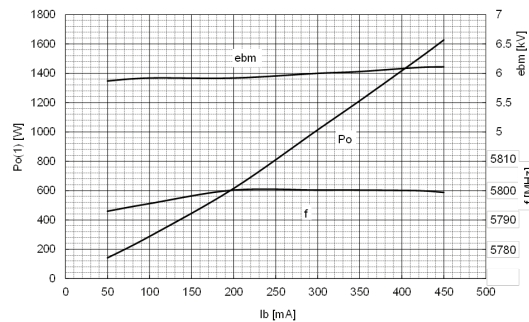


Figure 4. Performance chart of 1.5kW, 5.8kW CW magnetron

magnetron with 6.1kV anode voltage and 420mA standard anode current; the filament temperature of this magnetron is ~2000K. The performance of the magnetron is shown in Figure 4.

DISCUSSION

The use of the 1.5kW, 5.8kW CW magnetron provided some unique effects, e.g. 1) the skin effect is utilized; 2) can be used to thaw thin or small articles; 3) absorbed energy is increased; 4) possible to generate super-heating^[1]; 5) foot print of equipment is smaller. We succeeded to develop the 5.8GHz CW magnetrons producing high output power which has been previously difficult to manufacture due to semiconductor elements availability. It means that we can expand the possibility to verify the effects of higher frequency in different applications. Our high power magnetrons operate at lower filament temperature, and hence provide a longer life-time which is mandatory for the industrial users. It is necessary to note that the 1.5kW, 5.8GHz magnetrons must be handled more carefully than the 2.45GHz ones, due to their sensitive assembling accuracy and electrical performances related to their higher operating frequency.

CONCLUSION

This study proves that we succeeded in developing the industry's first high output power 5.8GHz CW magnetron. We expect the magnetrons to be used in various fields such as heating, plasma, etc.

REFERENCE

- [1] S. Horikosh, N. Serpone, (A. de la Hoz, A. Loupy; Eds.), *Microwaves in Organic Synthesis*, Chapter 9, Wiley-VCH Verlag, Weinheim, Germany, 2012.

Performance Description of a Cavity for Heating α -SiC at 5.8 GHz

Juan Antonio Aguilar-Garib and Karina Cabriaes-Gómez

Universidad Autónoma de Nuevo León, Facultad de Ingeniería Mecánica y Eléctrica,
San Nicolás de los Garza, NL, México

Keywords: Cavity, microwave, silicon carbide.

INTRODUCTION

Microwave engineering inventive is sometimes underestimated because it is easy to assume that the process is reduced to just placing a material in a microwave oven that is built to heat, overriding the conditions that must be matched for achieving such purpose. One important aspect is the description of the electric field distribution in the cavity, which is related to its geometry, microwave frequency and permittivity of the material. Reports about applicators and cavities for 2.45 GHz are found in literature more frequently than for 5.8 GHz applications. Therefore, a cavity for this late frequency was characterized in terms of its thermal distribution assumed to be a consequence of the electric field, and compared to another one designed for 2.45 GHz

METHODOLOY

The comparison method consists in obtaining the thermal profiles of one cavity for 2.45 GHz (cavity A) and another, scaled as the microwave guide, for 5.8 GHz (cavity B). α -SiC in a crucible that was moved, as a thermal probe, around different locations in the cavities, and exposed to microwaves while its temperature was measured.

EXPERIMENTAL

The cavities used for the experiments were fabricated with aluminum frames and walls of metallic mesh for being able to measure temperature optically through them. The cavity A is based in a kitchen oven design of 40 cm X 35 cm X 30 cm, and the cavity B was scaled, using the WR284 to WR215 (1.8) ratio, to 23 cm X 24 cm X 18 cm (Figure 1). The probe sample was an alumina crucible of 5.1 cm external diameter, 3.5 cm internal diameter, 3.55 cm height, and 26.9 cm³ capacity, filled to the top with approximately 30 g of powdered α -SiC. The exposition power of the probe and time were defined in such a way that temperature increased enough to generate a measurable profile; heating too fast will show hot spots only, while heating too slow would produce a profile that would be affected by convection heat transfer. Therefore, from preliminary tests it was decided to use an exposition power of 260 W for the cavity A (2.45 GHz), and 400 W for the cavity B (5.8 GHz), measured with the arrange of waveguide and directional coupler for feeding the cavity. The exposition time was 5 minutes for both cavities.

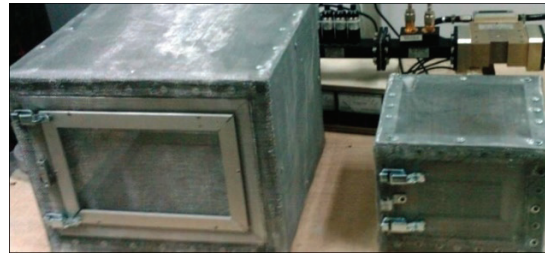


Figure 1. Cavity A for 2.45 GHz (left) and B for 5.8 GHz (right).

RESULTS AND DISCUSSION

The probe was moved around 60 locations in the cavity A (Figure 2) and the maximum temperature found was 122°C, it was reached in the location 9 at 6.5 cm height and 10 at 9.5 cm. Microwaves entrance is on the right in the following figures.

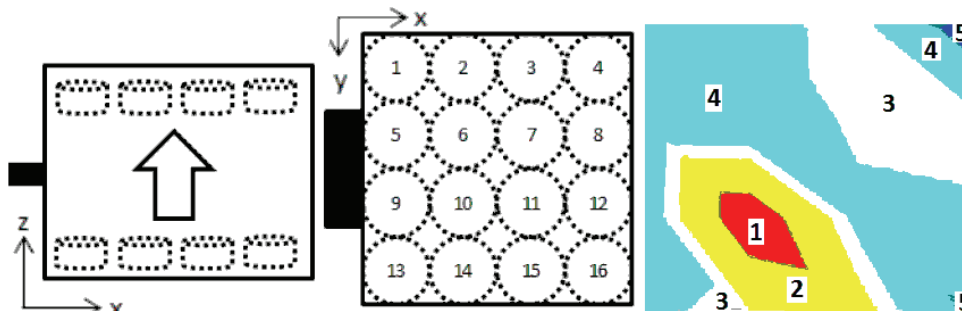


Figure 2. Cavity A (2.45 GHz). Side view (left), top view (center), and a thermogram at 9.5 cm height. Temperatures: 1) 110-120°C, 2) 90-110°C, 3) 70-90°C, 4) 50-70°C, 5) <40°C.

Observing the thermograms at different heights in the cavity A (Figure 3), which is complementary to Figure 2 (right), it is noticeable that the hottest locations are mostly in front of the microwave entrance, also certain temperature uniformity can be appreciated around the hot spots. Cavity modes can be appreciated, better shown at middle heights. This pattern is similar to that found during heating of meals, and as separated comment, the usefulness of a turning table is clearly understood.



Figure 3. Thermograms of cavity A. 6.5 cm height (left), 13 cm (center), and 16.5 cm (right). Temperatures: 1) 110-120°C, 2) 90-110°C, 3) 70-90°C, 4) 50-70°C, 5) <40°C.

In the case of cavity B, the probe was moved around 80 locations in it (Figure 4), and the maximum temperature was 220°C in the position 4 at 8.5 cm height. Figure 5 shows complementary thermograms at 6 cm, 10.5 cm, and 11 cm height. This cavity does not show the same multimode characteristic than cavity A.

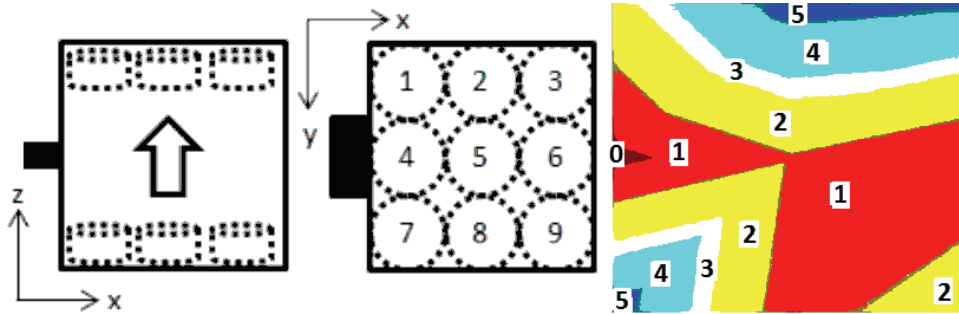


Figure 4. Cavity B (5.8 GHz). Side view (left), top view (center), and a thermogram at 8.5 cm h. Temperatures: 0) >120°C, 1) 175-200°C, 2) 150-175°C, 3) 125-150°C, 4) 100-125°C, 5) <100°C.

A comparison of the thermograms of Figures 2 and 4, shows that a larger portion of the cavity was heated in the late. A simple thermal balance shows that in this case the higher frequency combined with the cavity resulted in higher microwave power dissipation in the α -SiC sample.



Figure 5. Thermograms of cavity B. 6 cm height (left), 10.5 cm (center), and 11 cm (right). Temperatures: 1) 175-200°C, 2) 150-175°C, 3) 125-150°C, 4) 100-125°C, 5) <100°C.

CONCLUSION

A method for estimating thermal field distribution in cavities was presented, and the results suggest that for a cavity fed with microwaves at 5.8 GHz for heating α -SiC, is better than a 2.45 GHz one. This conclusion could be extrapolated to other materials with similar properties than α -SiC.

ACKNOWLEDGEMENT

The authors express their gratitude to CONACYT for the scholarship granted to K. Cabriaes and to PAICYT-UANL for its support.

Improvement of Microwave Heating Uniformity Contributed by the Screw Propeller

Huacheng Zhu, Jinghua, Ye, Xing Chen, Yang Yang, Kama Huang¹

¹Sichuan University, Chengdu, China 610064

Keywords: Uniformity, Screw propeller, Microwave heating.

INTRODUCTION

To overcome inhomogeneous heating when microwave energy is applied in the industrial application, a continuous flow applicator with screw propeller for microwave heating liquid was proposed. The structure of the continuous flow microwave heating applicator is shown in Figure.1.

As shown in Figure.1, water flows into the pipeline from one side and flows out on the other side. The rotation of the screw propeller will make the material rotating and moving forward at the same time. Hence the location of the material will change both in axial and radial directions. This will improve the uniformity of microwave heating inside the pipeline.

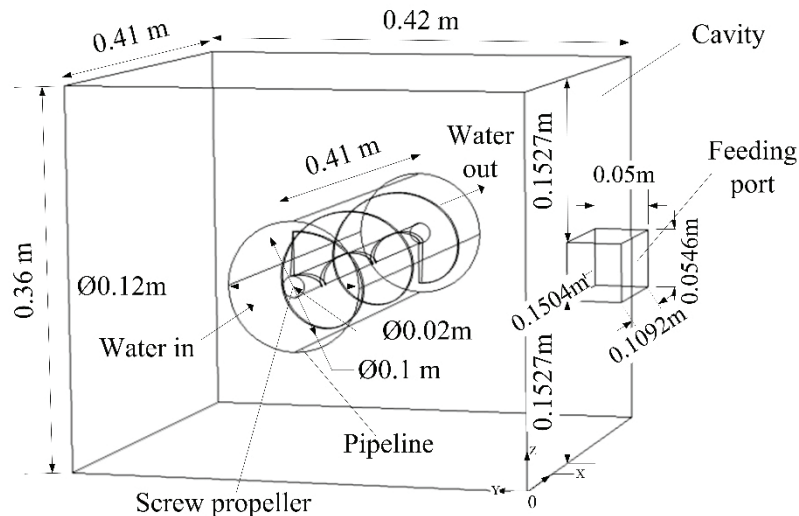


Figure.1 The structure of the continuous flow microwave heating applicator

METHODOLOY

The simulation of this heating process is achieved by using COMSOL Multiphysics 5.1 and MATLAB. First, time-averaged electric field strength and dissipated power density were calculated by solving Maxwell’s electromagnetic wave equations for a defined time step in the entire space domain ^[1]. Secondly, the Navier-Stokes equation formulated in a rotating coordinate system, mass conservation equation and heat conduction equation with dissipated power density obtained earlier were coupled together to obtain the velocity and temperature distribution of the pipeline ^[2]. Then, the pipeline was rotated to the next position by using moving mesh method ^[3]. Electromagnetic properties are updated based on the new temperature field, after that we perform the first step again at each rotational step. This cyclic process continues until a desired heating time is reached ^[1].

RESULTS

When the microwave input power is 2kW, inlet water flow rate is 1670ml/min, rotating speed of the screw propeller is 6r/min, the simulation results show that the outlet temperature reached a steady state after heating for about 200s, and the outlet temperature uniformity of water has been greatly improved compared with the case without a screw propeller. The schematic diagrams of the outlet temperature variation are shown below.

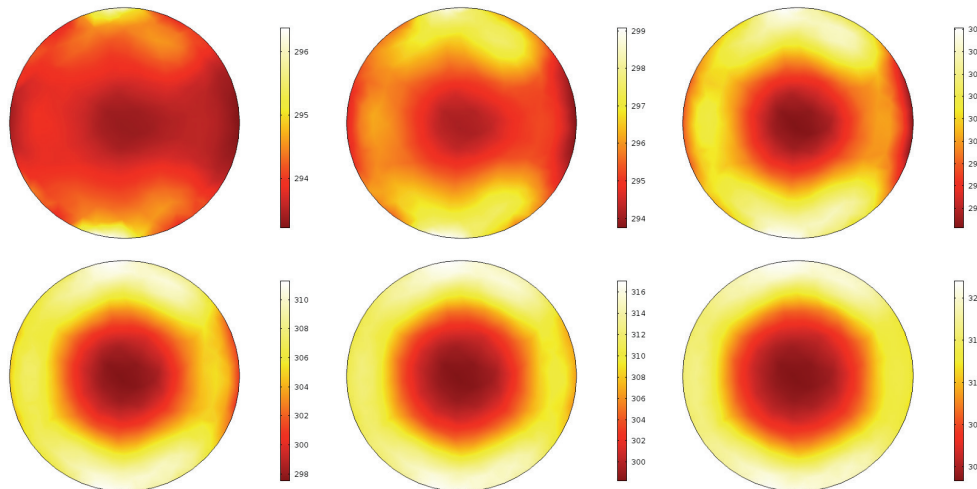
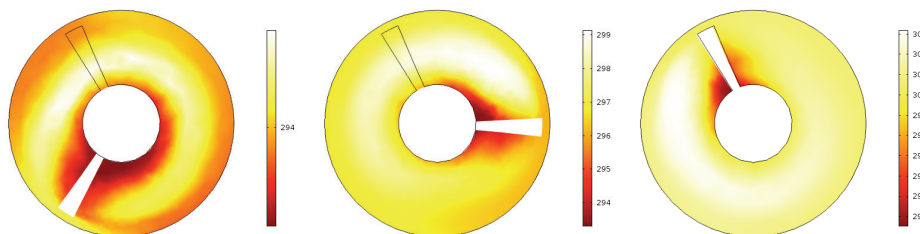


Figure 2. The schematic diagram of outlet temperature variation (without a screw propeller, heating time: 20, 40, 80, 120, 160, 200 s).



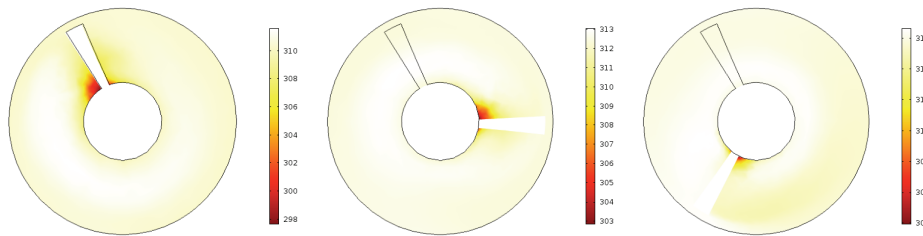


Figure.3 The schematic diagram of outlet temperature variation (with a screw propeller, heating time: 20, 40, 80, 120, 160, 200 s)

DISCUSSION

The simulation results indicated that the hot spot and inhomogeneous heating which occurred in the pipeline without screw propeller can be avoided. The outlet temperature's coefficients of variation (COV) are 0.007 and 0.019 corresponding to the case with a screw propeller and without a screw propeller, respectively, which means outlet temperature's coefficient of variation is increased by 63.2% because of the effect of screw propeller.

CONCLUSION

The results indicated that the screw propeller can improve the microwave heating uniformity greatly. The work will be helpful for the design of microwave heating reactor for industrial application.

REFERENCES

- [1] Pitchai K, Chen J, Birla S, et al, A microwave heat transfer model for a rotating multi-component meal in a domestic oven: Development and validation, *J. Journal of Food Engineering*, 2014, 128(128):60–71.
- [2] Salvi D, Ortego J, Arauz C, et al. Experimental study of the effect of dielectric and physical properties on temperature distribution in fluids during continuous flow microwave heating, *J. Journal of Food Engineering*, 2009, 93(2):149-157.
- [3] J. Yan, X. Yang, and K.-M. Huang. Numerical analysis of the influence of stir on water during microwave heating, *J. Progress In Electromagnetics Research C*, Vol.17, 105-119, 2010.

3D Particle-In-Cell Simulation Study of Injection Locked Magnetron

Yang Yang, Wenjun Ye, Xing Chen, Kama Huang, and Huacheng Zhu*

Sichuan University, Chengdu, China

Keywords: Magnetron, particle-in-cell simulation, injection locking, frequency spectrum

INTRODUCTION

Magnetrons are widely applied to the rapidly developing microwave industries as microwave sources. However, the free-running magnetron's applications in power-combining and scientific fields are limited because of its unstable frequency and wideband spectrum. Therefore, injection locking technique is employed to improve the performance of magnetron so that magnetron's applications could be extended.

Particle-in-cell (PIC) simulations studies are mostly concentrated in free running magnetron [1-3]. There are few studies of the PIC simulation of injection locked magnetron [4]. Reference [4] has simulated an injection locked magnetron by using an injection dipole. They have reached the phase locking in simulation. Simulation of injection locked magnetron is meaningful for researching the locking condition with the DC voltage and the character of the output antenna. In this paper, a 10-vanes injection locked magnetron is performed by PIC simulation. A magnetron with an input voltage of 4.2 kV and magnetic field of 0.19 T is presented. The output power of the magnetron operating in pi-mode is 8 kW. The pi-mode frequency spectrum shows that the magnetron freely oscillate at 2.457 GHz.

In our simulation of the injection locked magnetron, the DC input voltage is applied in two ways. One way is to getting the electronic field of the input voltage firstly and then applying the electromagnetic field in the simulation setup. The other way is to loading the DC voltage in the input port of the magnetron. In simulation, the electronic field is isochronous with the DC voltage. The second method is more similar to the real work stage of the magnetron. In addition, this method can also simulate the effects of the ripple in DC voltage. We simulate both ways and compare the results.

Two injection models of magnetron are presented in this paper. The traditional injection locking model by using several current sources in symmetric gaps is simulated. We emphasis on injecting the external signal through the output antenna of the magnetron. The latter method is more convenient to control the injection power and it is not affected by the position of the current source. Results show that the frequency of magnetron is injection locked by both two injection methods.

SIMULATION MODEL AND RESULTS

The two methods of DC input voltage are shown in Figure 1. Figure 1 (a) shows the traditional method of DC voltage in simulation. The anode which is colored in red is 0 V. The cathode which is colored in blue is -4200 V. In the process of simulation, the static electric field between the anode and the cathode is calculated firstly. Then the PIC simulation starts and uses the static electric field. Figure 1 (b) shows another method of DC voltage. The DC voltage is applied in the input port of the magnetron by using waveguide port.

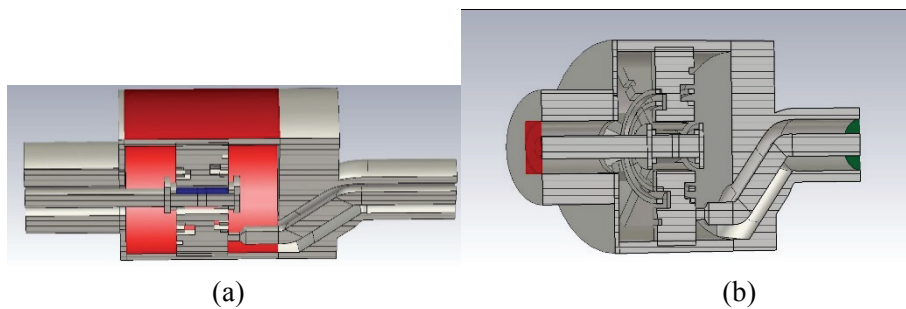


Figure 1. The two methods of DC input voltage: (a) DC voltage is added between the anode and the cathode, (b) DC voltage is applied in the input port of the magnetron.

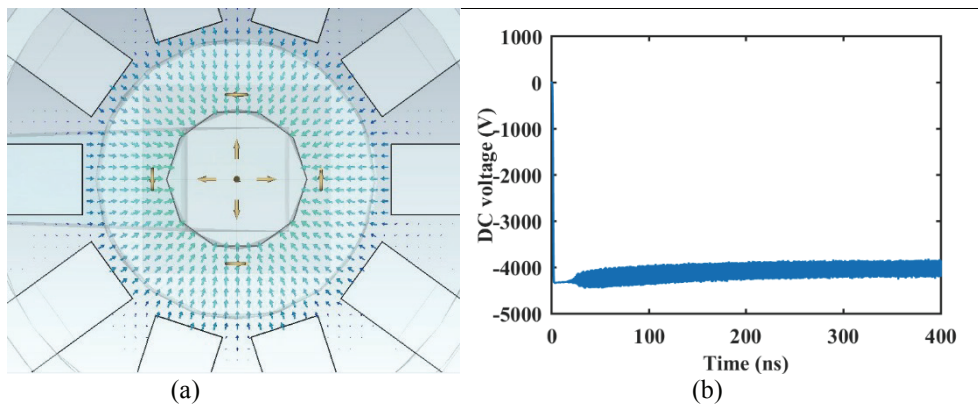


Figure 2. (a) The static electric field, (b) The DC voltage produced by the waveguide port.

Figure 2 compares the two results by the two methods. The static electric field make the simulation very stable. The voltage produced by the waveguide port is more similar the real-world signal with some ripples.

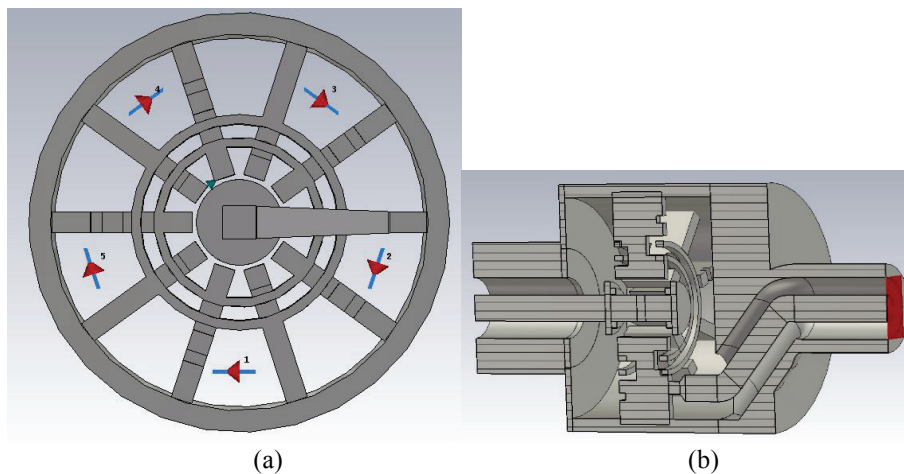


Figure 3. Two injection locking magnetron model.

Two injection locked magnetron model are also shown in Figure 3. In Figure 3 (a), 5 current sources are used as injection signals. This method can make the injection signals evenly distributed in the cavity. However, the injection power is hard to control and estimate in this method. So, we apply the other model as shown in Figure 3(b). A waveguide port is applied in the output antenna of the magnetron. The injection signal is injected to cavity through the antenna. The injection power can be controlled conveniently. This method is consistent with the actual situation of injection locked magnetron.

CONCLUSION

Two methods of DC voltage in injection locked magnetron simulation model are presented. Injection signal is also injected to the magnetron by two different ways. In this paper, we make the simulation more realistic.

REFERENCES

- [1] D. Andreev and S.L. Birla, Review of particle-in-cell (PIC) simulations of an oven magnetron, *15th IEEE Intern. Vacuum Electronics Conference*, p. 497, Apr. 2014.
- [2] S.K. Vyas , S. Maurya, and V.P. Singh, Electromagnetic and particle-in-cell simulation studies of a high power strap and vane CW magnetron, *IEEE Transaction on Plasma Science*, vol. 42, no. 10, p. 3373, Oct. 2014.
- [3] N.N. Esfahania, M. Tayarania, and K. Schünemann, Design and simulation of a $\pi/2$ -mode spatial-harmonic magnetron, *AEU – Intern. Journal of Electronics and Communications*, vol. 67, no. 5, pp. 426-432, 2013.
- [4] X. Chen, M. Esterson, and P.A. Lindsay, Computer modeling of phase locking in magnetrons, *SPIE's 1996 Intern. Symp. on Optical Science, Engineering, and Instrumentation. Intern. Soc. for Optics and Photonics*, pp. 47-56, Aug. 1996.

Microwave Modelling in the Food Industry: Combined Microwave Baking and Tubular Microwave Processing of Particulate Foods

Birgitta Wäppling Raaholt¹

¹SP Food and Bioscience, RISE, Göteborg, Sweden

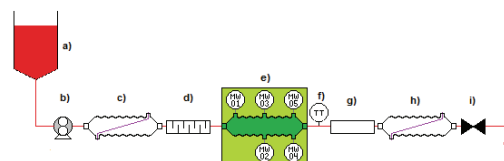
Keywords: microwave modeling, combined microwave baking, bread, tubular microwave processing, particulate foods.

INTRODUCTION

Microwave modelling is exemplified for two applications: combined microwave-infrared (IR) baking [1] and tubular microwave processing [2], in order to visualize some of the benefits of using mathematical modelling. Modelling, combined with lab-scale and/or pilot-scale trials, is often useful in feasibility studies before up-scaling and industrial implementation. Moreover, it could reduce the amount of experimental work considerably and increase the level of understanding for different types of food processes.

METHODOLOGY

A mathematical model of combined microwave-infrared (IR) baking of bread, developed to describe the mechanisms that occur within the bread during baking, was developed. The model includes heat and mass transfer with source terms for microwave and IR radiation, as well as a diffusion model for transport of water and gas. It could be used to illustrate how changes in process conditions may affect the physical phenomena in bread during baking, which in turn is directly related to control of product quality. The model will be exemplified for baking of white rolls in laboratory scale. Reduced processing time and energy consumption will be illustrated and compared to conventional baking. Moreover, results from microwave baking of a bakery product, followed by convective post-drying, will be described in terms of reduced energy consumption and processing time.



Microwave in-flow processing of pumpable foods, which offers an alternative way to produce e.g. high-quality particulate foods. The system is pressurized and equipped with a robust control system to facilitate microwave heat treatment of particulate foods at temperatures up to 140 °C (284°F). The microwave heating part of the system consists of two types of cavities, each one with appropriately selected microwave modes. Results from using a simplified model for tubular microwave heating of pumpable foods will be presented. Radial heat transfer and an assumed velocity profile are included in the model. Measurements in a tubular microwave heating system developed by SP in pilot-scale will be presented for comparison.

RESULTS AND DISCUSSION

The model of combined baking could be used to predict the developed water distribution in bread during baking, as well as the temperature distribution. The studied process of combined microwaves and IR baking offers advantages such as: reduced processing times and less energy consumption compared to traditional baking technologies. Baking times were reduced down to approximately 1/3 (of the baking time used traditionally) for microwave-IR baking in lab-scale. Microwave baking of a bakery product, followed by convective post-drying, will also be illustrated at pilot-scale.

Tubular microwave processing of foods at 2450 MHz was modelled by combining a radial model for microwave heating with a mathematical description of the flow profile. The selected combinations of power levels at each type of cavity contribute to a more uniform microwave heating over the cross-section of the tube. Examples of the resulting achieved temperature distribution show larger degree of temperature uniformity compared to measurements in a pilot-scale system. Appropriate combinations of microwave power levels at each of the cavities contributed to a more uniform microwave heating over the tubular cross-section. Moreover, results from implementing a multi-physics model of tubular microwave heating of homogeneous foods will be presented.

CONCLUSION

Modelling of the two types of microwave processes illustrates benefits in terms of reduced processing times and an increased level of understanding of phenomena occurring during processing. Modelling of baking and post-drying processes often offers valuable tools for process optimization and evaluation, with resulting process designs which corresponds to improved food quality. Additionally, modelling enables a time-efficient means of feasibility studies, in terms of up-scaling to industrial scale.

REFERENCES

- [1] B. Wäppling Raaholt and B. Waldén. (2011), Modelling of a combined microwave-infrared baking process of bread, *Proc. 13th AMPERE conference on Microwave and High-Frequency Heating, Toulouse, France, September*, pp. 340-343.
- [2] B. Wäppling Raaholt, S. Isaksson, L. Hamberg, A. Fhager, and Y. Hamnerius, (2015) Continuous tubular microwave heating of homogeneous foods: evaluation of heating uniformity, submitted to *J. Microwave Power and Electromagnetic Energy.*, submitted Nov 16, 2015; accepted for publication, Jan. 19, 2016. DOI: 10.1080/08327823.2016.1157318.

Some Emerging Applications for Microwave Technology in Chemistry, Polymers and Waste

John Gerling¹, Tunjar Asgarli², Klaus Baumgaertner², and Markus Reichmann²

¹MUEGGE-GERLING, Modesto, USA

²MUEGGE GmbH, Reichelsheim, Germany

Keywords: Pyrolysis, recycling, heating, drying, solid-state, compact head.

INTRODUCTION

The evolution of mankind with time has forced it to find a common interface with smaller and smaller units. While in relatively recent past large metal pieces were used to cut through flesh, nowadays microscopic devices took over the medical field with negligible failure risk. By similar analogy, the integration of short wavelength microwave can be easily observed by recognizing the escalated number of applications around us. The following includes a brief summary of new and emerging applications in which Muegge GmbH is involved.

APPLICATIONS AND DISCUSSION

It is obvious that as microwave power generation and transmission becomes more affordable, the number of its applications is increasing. The straightforward example for the integration of microwave is the food industry. Besides the general household consumer microwave oven, the technology has found use for other applications in the food industry. The possibility of electronic re-arrangement of the power in microwave technology, thus supplying different range of temperatures in the defined space enables microwaves to be used in different fields of food industry such as (re)heating, baking, tempering, dehydration, pasteurization and even popping. In contrast to classical variants of applications there is a constant demand for new dietary varieties in modern food industry that can be implemented quickly and efficiently by means of microwave energy. Amongst these may mentioned the popping up of cereals and cheese products, the preparation of dried meat chips as well as the preservation of fish and meat products by microwave assisted brine injections.

Furthermore, heating ability was utilized in production fields, namely rope, rubber and wood. In contrast with conventional ovens, microwave resonators can adapt to increase the efficiency in the production line. A relatively new production application for microwave heating is the so called conti-press, with microwave warming integrated in the

pressing area, for the production of light-weight building boards for doors and cupboard systems. Another is robot-guided microwave generators for the selective drying of moisture nests in multilayer sanitary ceramic parts. Microwave heating is further adapted to bio and pharmaceutical industry. In these industry sectors the microwave technology is predominantly used for drying and disinfection applications in batch processes. The possibility for sterilization with microwave technology by proper refinement has created a large market as an alternative technology in latter fields.

Microwave technology, which is still sometimes not preferred because of safety cautions and radiation effects, is evolving to supply a healthier environment to mankind. Promising microwave applications in the future are related to the chemical industry, namely pyrolysis and recycling. Microwave pyrolysis application, which is already well understood and has the current status of being optimized, opens a possibility for production of many products for inputs such as bio/plastic waste. After a process enhancement in the area of batch systems, continuously working facilities for pyrolysis enabling future-proof and continuous provisioning with “green energy” in industrial scale are now being developed. One of challenges here is the infeed of microwave energy into the process chamber, that has to be carried out via dirt-proof, atmosphere-separating window system within the waveguides. In other areas of the chemical industry, relevant for climate and environment, highly efficient microwave systems are used for heating processes during the production of extruded, bio-soluble plastic films of metal-free poly-lactic-acids and for the foaming and stabilization of polyurethane and melamine foams with very low density that are used as heat and sound insulation.

Another emerging application of microwave technology is recycling. In such systems, production of expensive fluorine species and new PTFE/PEEK materials is intended from unmixed recyclate of PTFE and plastics. Several high power microwave generators in an eddy current reactor that is enriched with a susceptor material in a chemically highly reactive steam pressure atmosphere are used to achieve a swift warming and reprocessing of the fluorine species.

A further new area of application is the drying and hardening of fiber-reinforced composites directly during the production of fiber-reinforced composite profiles in the process of pultrusion, in contrast to batch process mentioned earlier. The microwave located in the mold is utilized for a preheating and hardening of resins and coatings.

Microwave technology is also the basis for integration with emerging plasma technology applications such as diamond growth. The microwave generator technology is expected to supply a preeminent consistency concerning stability of frequency and performance over a long period of time that is essential for growing of crystals. A partitioned geometry of the resonator and an application specific wave propagation enhances the plasma guidance to achieve improved performance.

Rephrasing the initial idea, miniaturized units are gaining fame in the market. Adapting to the concept, shrinking large standard components in microwave technology into small dimensions for size optimization and cost effectiveness is a main focus for equipment development. Future product developments are related to solid state components, establishing small-size and inexpensive solutions to all of the previously discussed microwave applications. A main reason for the implementation of the solid state

technology is a fundamental minimizing of service costs thanks to omitting the magnetron tubes working with limited service life, in the power generators. Presently, power output of 400 Watts can be achieved with only one or two transistor devices, which can be further amplified to 2-3 kW with multi-device arrays.

CONCLUSION

Industrial heating by microwaves is required for processing of an emerging number of novel materials in a large variety of application areas. Different demands and specifications call for individual and customized solutions concerning coupling of the microwave to the material, necessary microwave power level, and microwave frequency to be applied. As the avoidance of down-time is more and more relevant, recent developments in solid state components will lead to increasing use of solid state technology in microwave power supplies. Consequently, new concepts towards multi-channel processing based on solid state power supplies will have to be developed for facilitating high-power microwave applications with this technology.

ACKNOWLEDGEMENTS

Part of the work related to the results that are referred to in this paper received funding from the German Ministry of Education and Research (BMBF) and from the European Commission.

Formation of Micro-Fractures on Ludwigite Ore and its Effect on Grinding Efficiency of Ludwigite Ore under Microwave Treatment

Yajing. Liu¹, Tao. Jiang^{1,2}, Junpeng. Wang¹, Zhaohui. Tang¹, Mi. Zhou¹ and Xiangxin. Xue¹

¹Northeastern University, Shenyang, China.

²Liaoning key laboratory for recycling science of metallurgy resources, China.

Keywords: Ludwigite ore, microwave treatment, micro-fractures, grinding efficiency.

INTRODUCTION

Energy consumed in comminution can be as high as 50-70% of the total process energy and it is difficult for Ludwigite ore to reach effective dissociation. Kingman [1-2] studied microwave pretreatment significantly improved mineral grindability. In this paper, it mainly studied the micro-structures and the effect of microwave treatment on grinding efficiency of Ludwigite ore.

METHODOLOY

The schematic diagram of the microwave and equipment is shown in Figure 1. Samples were treated using a 2.45GHz microwave oven (Mobilelab workstation mode, Tangshan Nano Source Thermal Instrument Manufacturing Co., Ltd). The samples were microwave-treated with varying exposure times, which allowed to cool to room temperature in the microwave oven.

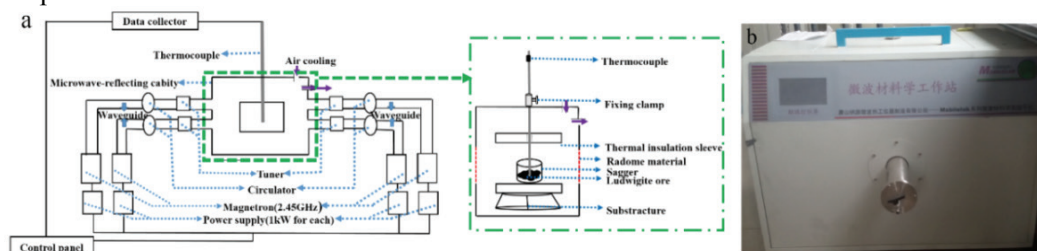


Figure 1. Schematic diagram of the microwave (a) and equipment image (b).

Phase identification, micro-fractures and particle size distributions of the ore was performed by the Panalytical X'PER TPRO MPD/PW3040 X-ray diffractometer (XRD), Ultra Plus scanning electron microscope (SEM) and a laser diffraction size analyzer (Mastersizer2000, Malvern Instruments Ltd., UK).

RESULTS

The microwave absorption property of Ludwigite. As shown in Figure 2, Ludwigite was heated rapidly and the temperature increases with the time of microwave radiation. It is due to the presence of magnetite, which belongs to microwave-absorbed components.

Formation of micro-fractures on Ludwigite after microwave treatment. Figure 3 was shown that micro-cracks produced on Ludwigite along boundaries of magnetite and gangue minerals and sometimes through gangue after microwave radiation. The longer was the exposure time, the more and deepen cracks formed fast. Obviously, it is easy to liberate the valuable minerals from the other part of the ore.

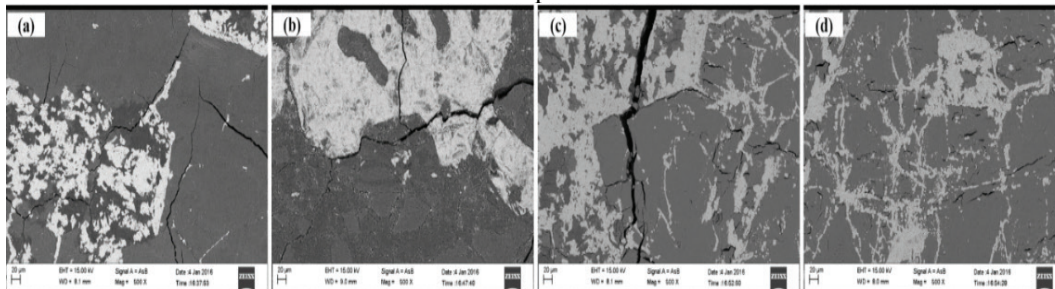


Figure 3. SEM images of microstructure of microwave-treated samples for various heating times. (a) for 40s (b) for 60s (c) for 80s (d) for 100s.

Effect of microwave treatment on grindability of Ludwigite ore. Figure 4 shows the mass fraction with particle diameter under 0.074mm reached 96.60%, which was 32.55% higher than untreated. Figure 5 was shown that the main minerals also didn't have obvious changes in 100s and the particle size distribution of treated sample shifted toward direction of small size obviously (Figure 6).

DISCUSSION

This improved grindability and easy comminution of the ore are attributable to the large amount of intergranular fractures which are formed along the grain boundaries of magnetite and gangue minerals on Ludwigite ore after microwave treatment.

CONCLUSION

The mass fraction of microwave treated samples with particle diameter under 0.074mm reached 96.20%, which was 32.15% higher than untreated. The particle size distribution of microwave treated ore shifted toward direction of small size.

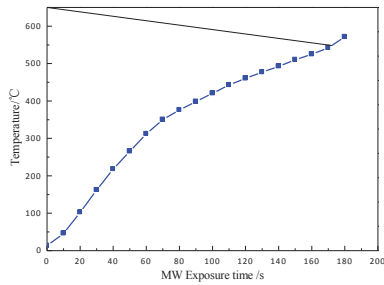


Figure 2. Effect of MW treatment on temperature of Ludwigite ore.

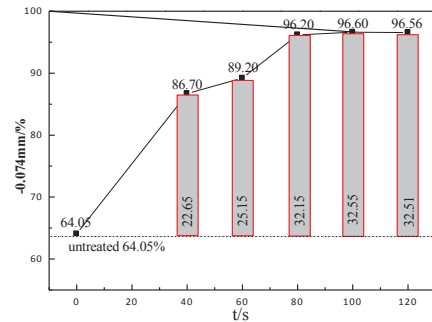


Figure 4. The effect of microwave treatment on the grindability of Ludwigite

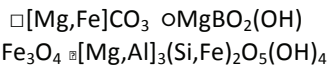
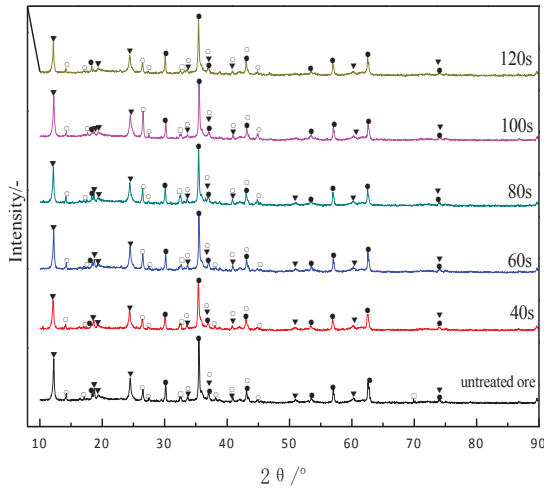


Figure 5. XRD patterns of the Ludwigite ore at various heating times.

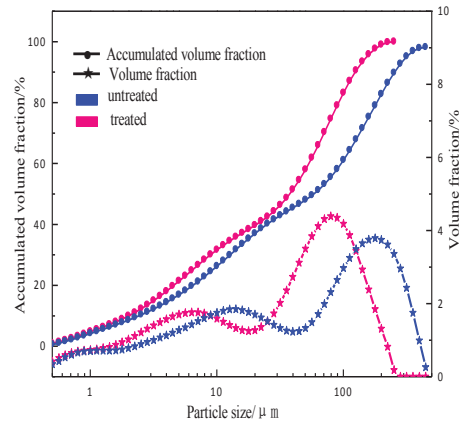


Figure 6. Particle distribution of untreated and treated Ludwigite ore.

REFERENCES

[1] S.W. Kingman, et al, Recent developments in microwave-assisted comminution, *J. International Journal of Mineral Processing*, vol. 74, no 4, pp.71-83, 2004.
 [2] S.W. Kingman, et al, The influence of mineralogy on microwave assisted grinding, *J. Minerals engineering*, vol. 63, no 2, pp.313-327, 2000.

Development of a Coaxial Microwave Applicator for Liquid Heating over a Wide Frequency Range

Tomohiko Mitani^{1,3}, Naoki Hasegawa^{1,3}, Ryo Nakajima^{1,3}, Naoki Shinohara^{1,3}, Yoshihiro Nozaki^{2,3}, Tsukasa Chikata^{2,3} and Takashi Watanabe^{1,3}

¹Kyoto University, Uji, Japan

²Japan Chemical Engineering & Machinery Co. Ltd., Osaka, Japan

³CREST, JST, Tokyo, Japan

Keywords: Microwave enhanced chemistry, Coaxial applicator, Wide frequency range.

INTRODUCTION

A coaxial microwave applicator for liquid heating, which covers two ISM bands of 915 MHz and 2.45 GHz, is described in the present study. There are no available microwave applicators over a wide frequency range; whereas the dielectric property of a material depends on frequency and temperature. The developed applicator has a coaxial transmission line structure, and electromagnetic waves propagate in the applicator in the TEM mode. Unlike the previous studies using a coaxial cable [1], [2], a liquid sample is directly poured between the inner and outer conductors of the coaxial transmission line. A truncated cone-shaped polytetrafluoroethylene (PTFE) object is inserted to reduce microwave reflection. We verify viability of the developed reactor including effectiveness of the inserted PTFE cone through electromagnetic simulations and microwave reflection measurements.

METHODOLOGY

Figure 1 shows simulation models and a photograph of the developed applicator. Microwave is input through the coaxial connector from the bottom of the applicator. The inner and outer conductors configure a coaxial transmission line structure. A liquid sample is poured into the space between the conductors. A punched metal plate is mounted on the top surface of the liquid sample in order to prevent the microwave from leaking upward through the samples and to avoid increasing the applicator inner pressure. The inner and outer conductors, the punched metal plate, and the wall of the air release area are made of stainless steel SUS 316L. The applicator volume is about 360 ml.

The applicator was designed by the 3D electromagnetic simulator, Femtet ver. 2015 (Murata software). We selected two types of liquid samples for designing: ultrapure water (henceforth water) as a dielectric sample, 0.1 M NaOH solution (henceforth NaOH)

as a dielectric and conductive sample. The dimensions of the designed applicator are shown in Figure 1(a). The punched metal plate has 20 holes with a diameter of 6 mm each.

After designing, we experimentally produced a prototype applicator, as shown in Figure 1(b). Microwave reflection measurement was conducted with a network analyzer (Agilent N5242A).

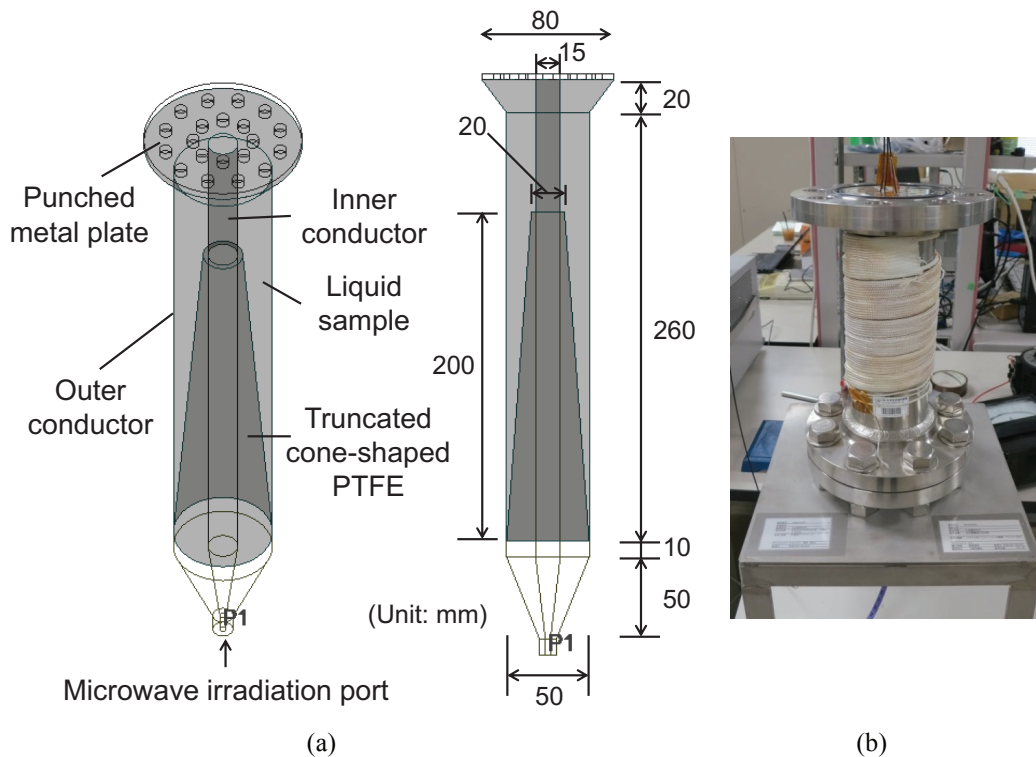


Figure 1. Simulation models (a) and a photograph (b) of the developed coaxial microwave applicator.

RESULTS

Figure 2 shows simulation and measurement results of the reflection coefficient $|S_{11}|$ of the applicator when the liquid sample temperature was 30 °C and 60 °C. The results of water and NaOH are shown in Figure 2 (top) and Figure 2 (bottom), respectively. From simulation results, we also observed non-uniformity of the power loss density in the applicator.

DISCUSSION

The measurement results show fairly good agreement with the simulation results. In the NaOH case, $|S_{11}|$ was less than -17 dB from 800 MHz to 2.7 GHz. This means the reflected power of the applicator is less than 5 % within the wide frequency range. In the water case, the reflected power was less than 10 % from 1.1 GHz to 2.7 GHz.

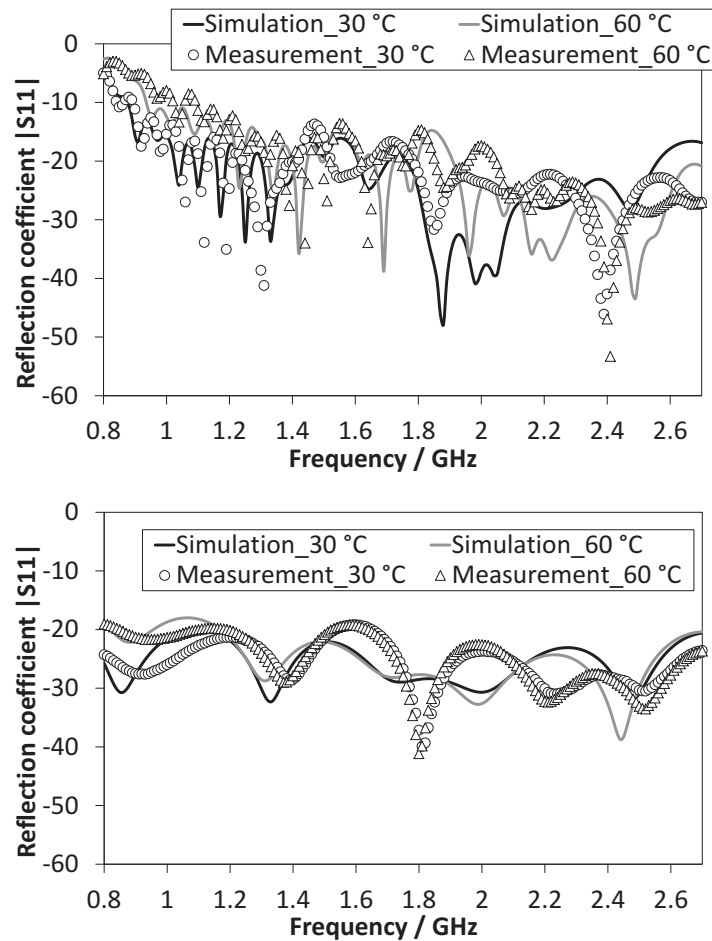


Figure 2. Simulation and measurement results of the reflection coefficient $|S_{11}|$ of the coaxial microwave applicator: water (top), NaOH (bottom).

CONCLUSION

We successfully developed a coaxial microwave applicator over a wide frequency range. Although non-uniformity of the power loss density remains as a future work, this applicator enables us to investigate microwave-enhanced chemical reaction at various frequencies without the need to replace the applicator.

REFERENCES

- [1] I. Longo and A.S. Ricci, Chemical activation using an open-end coaxial applicator, *J. Microw. Power Electromagn. Energy*, vol. 41, no. 1, pp.4-19, 2007.
- [2] G.B. Gentili, M. Linari, I. Longo and A.S. Ricci, A coaxial microwave applicator for direct heating of liquids filling chemical reactors, *IEEE Trans. Microw. Theory Tech.*, vol. 57, no. 9, pp. 2268-2275, 2009.

Microwave Treatment of Garden Soil prior to Planting

Raymond L. Boxman

ClearWave Ltd., Herzlilya, Israel
Tel Aviv University, Tel Aviv, Israel

Keywords: microwave irradiation, garden soil, weed control, germination.

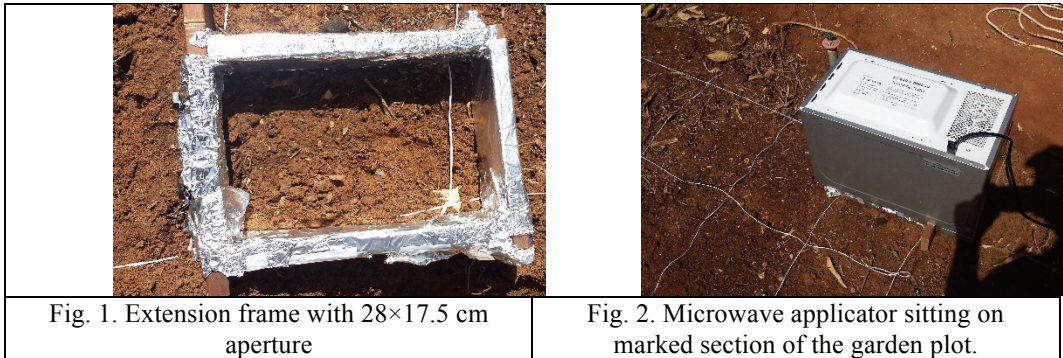
INTRODUCTION

Weed control in home gardens typically requires either extensive manual labor, or chemical treatment which can be expensive and which raises consumer safety concerns. Wayland *et al.* proposed microwave radiation with a dosage of 150-300 J/cm² to kill undesired vegetation [1]. Vidmar tested an array of 12 microwave transmitters working simultaneously at 2.45 GHz, each with an 850 W magnetron and a horn antenna, to kill weeds [2]. Recently, Brodie *et al.* showed that microwave radiation could not only kill weeds above ground, but also seeds buried up to a few cm in the ground, and produce considerably greater wheat and canola yields [3]. Such an outcome would be particularly desirable for home gardeners, but the effects of microwave radiation have not been tested in a home garden environment. The objective of this study were to determine the effects of *in-situ* microwave irradiation of garden soil on the subsequent growth of weeds and garden crops.

METHODOLOY

A microwave applicator was constructed from a domestic 17 liter 700 W microwave oven (Hemilton HEM-1330S) with its door removed, and an extension frame. The frame was constructed from wood, and covered with Al foil. It formed a rectangular 28×17.5 cm aperture with a thickness of 6.5 cm. The frame was set into the test section of the ground to a depth of ~1 cm, and the oven was mounted on the frame, with its opening towards the ground. The frame fulfilled several functions: 1) the door latch from the oven door was mounted on the frame so that the latch depressed the safety interlock on the oven, and thus allowed operation; 2) the frame lifted the oven off the ground, so that the ground did not interfere with the mechanical controls on the front panel of the oven; and 3) the frame served as an extension of the microwave cavity, so that the radiation was directed into the ground, and lateral radiation along the surface was mostly prevented.

A ~3×4 m garden plot primarily composed of *humra* soil mixed with organic compost was prepared by watering, hoeing, manually removing visible weeds, and levelling. It was partitioned into several 28×35 cm sections, which were marked with string and labeled. Adjacent sections were used for control samples **C**, and for microwave irradiation **M**. The moisture content, temperature, and pH of each ground section was measured before and after microwave irradiation, and before planting seeds. Each 28×35 cm **M** section was irradiated in two 10 min full power exposures, each on one 28×17.5 cm half-section corresponding to the frame aperture. The **M** sections were allowed to cool overnight. Then identical quantities of seeds were planted in identical patterns and at identical depths in adjacent **C** and **M** sections. The garden plot was sprinkled 3 times per week until the autumn rains began, and then as necessary.



RESULTS

Fig. 2 shows the temperature profile in the middle of the second half-section after irradiation. It may be seen temperatures between 54 C and 82 C were observed at depths of 2.5 and 5 cm, while the temperature at 7.5 cm was somewhat lower. The soil pH was 7.5 both before and after microwave irradiation.

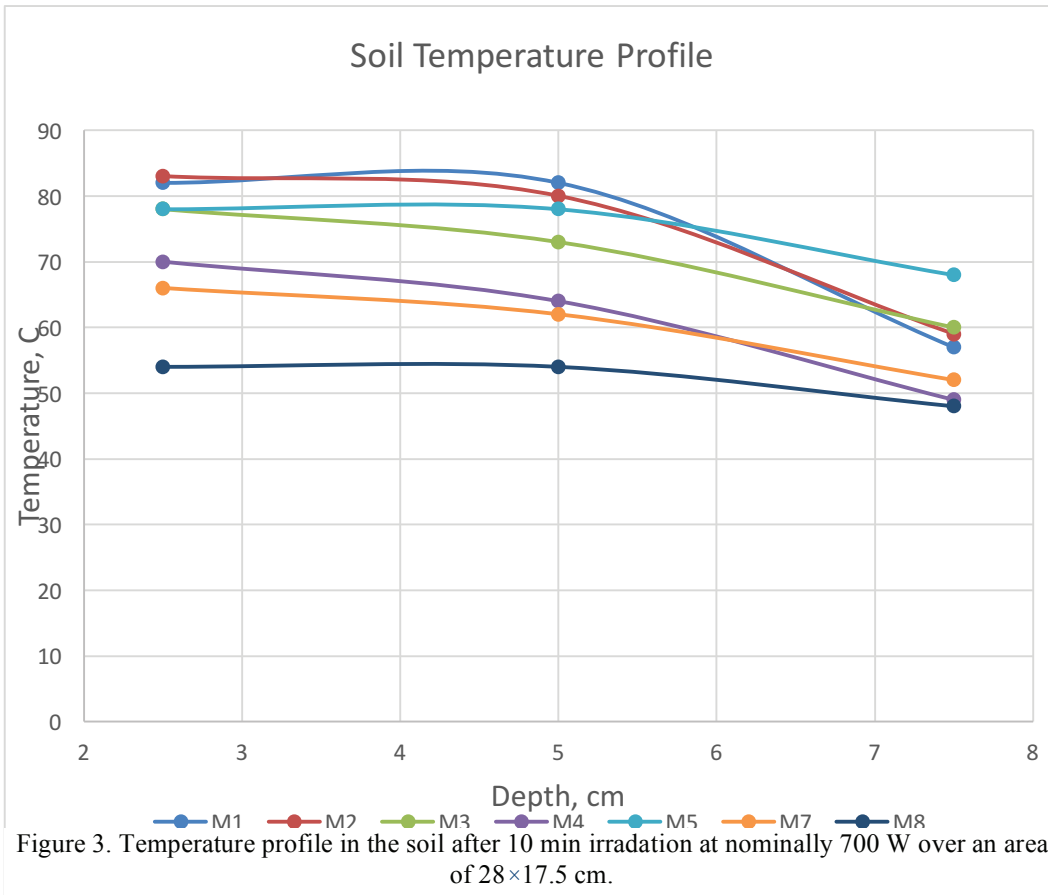


Figure 3. Temperature profile in the soil after 10 min irradiation at nominally 700 W over an area of 28x17.5 cm.



Fig. 4. Photographs of sections C1 (control) and M1 (irradiated), planted on 25 September 2015 with Burpee Salad Rose Radish seeds, at 5 days (upper left), 10 days (upper right), 40 days (lower left) and 58 days (lower right) after planting.

Fig. 4 shows a series of photographs of sections **C1** and **M1** planted with radish seeds. It may be seen that more seeds germinated, both of the crop and weeds, and that the crop plants developed better in the control section **C1**. Similar results were obtained with coriander, summer squash, green beans, and Swiss chard, whereas little difference was noted with snow peas.

DISCUSSION AND CONCLUSIONS

It should be noted that experiments in the open ground and over limited areas are difficult to control, and further testing is certainly warranted. The result that microwave irradiation of the soil apparently inhibited seed germination and subsequent plant development is surprising in light of Brodie *et al*'s results [3] which showed enhanced grain production after microwave irradiation of the soil prior to planting. Presumably in both cases microwave heating of the soil fostered breakdown of organic compounds in the soil. The breakdown products presumably depend on the soil composition and heating profile, which differed in the two studies. And possibly the different plant species tested react differently even to the same breakdown products. Given the divergent results, successful field implementation of microwave enhanced crop production will probably require optimization on a case by case basis.

REFERENCES

-
- [1] J.R. Wayland Jr, F.S. Davis, G.M. Merkle, Vegetation control, US Patent 4,092,800, 1978.
 - [2] M. Vidmar, An Improved Microwave Weed Killer, Microwave Journal, October 2005.
 - [3] G. Brodie, N. Bootes, and G. Reid, Plant Growth and Yield of Wheat and Canola in Microwave Treated Soil, Proc. 49th IMPI Microwave Power Symp., San Diego, CA, June 2015

Growth Stimulation System of Plants using Microwave Irradiation and Elucidation of its Molecular Mechanisms

Satoshi Horikoshi, Yasuhiko Hasegawa and Nobuhiro Suzuki

Department of Materials and Life Sciences, Faculty of Science and Technology,
Sophia University, 7-1 Kioicho, Chiyodaku, Tokyo 102-8554, Japan
e-mail: horikosi@sophia.ac.jp

Keywords: Microwave, growth stimulation system, *Arabidopsis thaliana*, Molecular biology

INTRODUCTION

In this lecture, the response of plants (*e.g. Arabidopsis thaliana*) to a microwave irradiation was analyzed to find the conditions that enhance the growth of plants. Microwave irradiation accelerated phase transition from vegetative to reproductive growth, and growth of inflorescence stem, as well as seed germination. Microwave irradiation, however, did not affect plant diameter. In addition, microwave irradiation enhanced the expression of a gene that regulates growth phase transition, suggesting that microwave irradiation could enhance growth of plants by modulating the expression of this gene. On the other hand, the expression of genes involved in the response of plants to heat stress were not clearly altered by microwave irradiation. Our results suggest that effect of the microwave on plant growth is besides the effect of the heat. When understanding a key factor that underlies microwave-dependent growth stimulation of plant, it's also possible to apply those to other plant growth (potato, corn, switch grass, etc).



Figure 1. Seedlings of *Arabidopsis thaliana*

METHODOLOY

A model plant, *Arabidopsis thaliana* as was grown on a potting compost (Jiffy 7, peat pellet) under the controlled conditions (21 °C and 16-hrs light) in the growth chamber. Microwave irradiation or heat treatment (40 °C) using a conventional heater was applied in the very short time on seedlings of *Arabidopsis thaliana* (**Figure 1**). Then, the cultivation was continued in the chamber once again following those treatments. Note that the atmospheric temperature and light intensity was the same to all samples. The rate of promoting growth of plant was investigated by scoring the size of leaves, stem length, timing of flowering and seed germination rate.

RESULTS&DISCUSSION

When the microwave or the conventional heat treatment was applied to the *Arabidopsis thaliana*, large influence on the growth of the leaves wasn't observed. On the other hand, a shift to reproductive stage and growth of an inflorescence stem were dramatically promoted by the microwave treatment (**Figure 2**). Because such phenomena were not observed under 40 °C high temperature condition, the thing which is the effect peculiar to microwave was expected.

When the gene expression which participates in control of growth or response to environmental stress was investigated, expression of the gene which controls the growing stage was affected by the microwave irradiation. On the other hand, expression of certain heat stress response genes was not altered.

The change for expression of CO and FT genes which control growth phase transition is indicated in **Figure 3**. Although expression of CO gene was not affected by microwave irradiation, expression of FT gene was enhanced on 4 days following the microwave irradiation. On the other hand, the genes encoding heat shock proteins or MBF1c that are involved in heat stress responses of plants did not respond to microwave. It can expect that the effect of the microwave is besides the effect of the heat.



Figure 2. Grown comparison of *Arabidopsis thaliana* with untreated (control) and microwave treatment (Microwave)

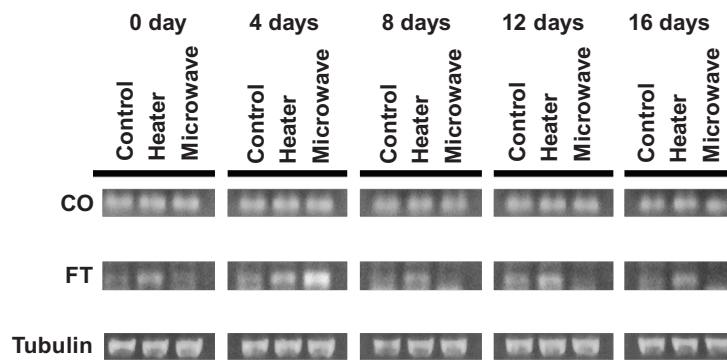


Figure 3. Changes of CO and FT gene expression after conventional heating (heater) or microwave irradiation

CONCLUSION

Plant growth can be promoted by a microwave irradiation, and it might be different from the effects caused by heat stress. This technology is also effective to other plant (detail data was discussed in presentation.).

Microwave Weed Control

Graham Brodie

¹The University of Melbourne, Dookie, Australia

Keywords: Weeds, Seeds, Microwave, Soil treatment.

INTRODUCTION

No till cropping has many benefits, including soil conservation and improved production; however these systems rely on herbicides for weed management. Herbicide resistance has become a major problem in cropping systems [1]. Microwave energy could kill herbicide resistant weeds. The objective of this paper is to present a summary of microwave energy dose studies for various weed plants and seeds, which have been undertaken over the past 10 years.

METHODOLOGY

Microwave treatment was applied using a 2 kW microwave system operating at 2.45 GHz feeding into a horn antenna with aperture dimensions of 110 mm by 55 mm. Using Huygen's principle [2], the electric field from the horn antenna can be described by:

$$E_p = \frac{E_a}{4\pi} \int_{-B/2}^{B/2} \int_{-A/2}^{A/2} \cos\left(\frac{\pi}{A} x'\right) e^{-j\beta_0 \left(\sqrt{(x-x')^2 + (y-y')^2 + z^2} + \sqrt{R_0^2 + (x')^2} + \sqrt{R_0^2 + (y')^2} \right)} \frac{1}{\sqrt{(x-x')^2 + (y-y')^2 + z^2}} \cdot dx' \cdot dy' \quad \dots (1)$$

Where x, y, and z is the Cartesian coordinates of the point relative to the centre point of the antenna's aperture and x' and y' are the Cartesian coordinates of any point in the antenna's aperture plane relative to the centre point of the antenna's aperture.

Weed seed experiments were conducted by layering either air dry or moist soil (20 % moisture by volume) into pots with sets of between 10 to 25 seeds placed into paper envelopes at depths of 0, 2, 5, 10 and 20 cm within each pot. Pots were treated for 0, 2, 5, 10, 30, 60, or 120 seconds. The paper envelopes allowed easy seed recovery from the soil after treatment so that seeds could be germinated in a growth cabinet for viability assessment. The following species were evaluated: Annual Ryegrass (*Lolium multiflorum* L.); Perennial Ryegrass; Bellyache bush (*Jatropha gossypifolia* L.); Sensitive bush (*Mimosa pigra*); Parthenium (*Parthenium hysterophorous* L.); Rubber vine (*Cryptostegia grandiflora* R.Br.); Wild Radish (*Raphanus raphanistrum*), and Wild Oats (*Avena fatua*).

In situ Plants were treated with the same microwave apparatus for 0, 2, 5, 10, 30, or 120 seconds, and evaluated 5 days after treatment to determine the number of living and dead plants. Experiments have been conducted for the following species: Annual Ryegrass (*Lolium multiflorum* L.); Barley Grass (*Hordeum vulgare* L.); Barnyard Grass (*Echinochloa crus-galli*); Fleabane (*Conyza bonariensis* L.); Marshmallow (*Malva*

parviflora L.); Prickly Paddy Melon (*Cucumis myriocarpus*); Wild Radish (*Raphanus raphanistrum*); and Wild Oats (*Avena futua*). In each case, both pot trials and *in-situ* field experiments were conducted for each species. Assuming that plant responses are normally distributed, the data was fitted to a Gaussian Error Function response curve, which is the integral of the normal distribution response:

$$S = a \cdot \operatorname{erfc}[b(\Psi - c)] \quad \dots (2)$$

Where S is the normalized survival rate for plants; Ψ is the estimated microwave energy at ground level (J cm^{-2}), calculated with the aid of equation (1), and a, b, and c are constants to be experimentally determined for each species. The relationships between applied microwave energy and seed survival were fitted to a dose response surface of the form:

$$S = a \cdot \operatorname{erfc} \left[b \cdot \left(\frac{\Psi \cdot e^{-2cd}}{g} - f \right) \right] \quad \dots (3)$$

Where d is the depth of the seeds in the soil profile (m), and a, b, c (field attenuation rate in soil), f (median seed response) and g (scaling factor) are constants to be experimentally determined for each species.

RESULTS

Table 1 shows the dose response parameters for all emerged plant species. The dose responses of these data were modelled by equation (2); however in the case of Annual Ryegrass, the relationship between applied microwave energy and plant survival was better described by:

$$S = a \cdot \operatorname{erfc}[b(\Psi - c)] + d \cdot \operatorname{erfc}[e(\Psi - f)] \quad \dots (4)$$

Data for weed seed responses were well modelled using equation (3). The various equation coefficients and goodness of fit (R^2) are listed in Table 2.

Table 1: Equation coefficients, goodness of fit (R^2), LD_{50} , and LD_{90} for weed plant survival as a function of microwave energy applied to the soil surface

Species	Regression Equation Coefficients						R^2	LD_{50} (J cm^{-2})	LD_{90} (J cm^{-2})
	a	b	c	d	e	f			
Annual Ryegrass	0.61	0.013	0	0.16	0.013	383	0.73	63	404
Barley Grass	0.517	0.005	242.7				0.97	249	427
Barnyard Grass	0.792	0.005	48.09				0.98	116	264
Fleabane	0.528	0.019	71.97				0.97	74	121
Marshmallow	0.553	0.006	176				0.98	190	334
Paddy Mellon	0.5	0.12	64.49				0.83	64	72
Wild Oats	0.51	0.009	164.3				0.98	166	266
Wild Radish	0.52	0.009	149.1				0.91	152	248

Table 2: Equation coefficients, and goodness of fit (R^2) for weed seed survival as a function of microwave energy applied to the soil surface, seed burial depth, and soil moisture status

Species	Dry						Wet					
	a	b	c	f	g	R^2	a	b	c	f	g	R^2
Annual Ryegrass	0.32	0.05	0.10	2000	1	0.92	0.42	0.01	0.05	561	1	0.99
Bellyache bush	0.56	0.04	0.02	20.3	96	0.82	0.60	0.15	0.07	4.7	96	0.80
Mimosa pigra	0.51	0.28	- 0.04	9.56	96	0.76	0.50	1.59	0.05	- 0.58	96	0.98
Parthenium	0.54	0.02	0.02	39.8	96	0.77	0.97	0.06	0.08	0.00	96	0.74
Perennial Ryegrass	0.40	0.05	0.10	2000	1	0.93	0.43	0.01	0.12	336	1	0.99
Rubber vine	0.49	0.10	0.01	18.4	96	0.73	0.61	0.08	0.05	8.0	96	0.86
Wild Oats	0.50	0.05	0.10	2000	1	0.92	0.50	0.02	0.05	445	1	0.98
Wild Radish	-	-	-	-	-	-	0.56	0.04	0.03	230	1	0.72

DISCUSSION

The economic viability of microwave weed control has yet to be determined; however it is clear that microwave treatment kills weed plants and weed seeds in the soil. Herbicide efficacy is often expressed in terms of the LD_{50} , which is the dose needed to kill half the treated population, or the LD_{90} , which is the dose needed to kill 90 % of the population. The susceptibility to microwave damage varies widely according to species; however based on the LD_{50} , growing plants are more susceptible to microwave damage than shallow buried seeds in moist soil, which are again more susceptible than dry seeds in dry soil. In all cases, seeds near the surface of the soil are more susceptible to microwave damage than seeds buried deeper in the soil.

CONCLUSION

Microwave weed treatment is effective, providing options for controlling herbicide resistant weeds.

REFERENCES

- [1] I. M. Heap, The occurrence of herbicide-resistant weeds worldwide, *Pesticide Science*, vol. 51, no 3, pp. 235-243, 1997.
- [2] F. R. Connor, *Antennas* Edward Arnold, London, 1972.

Effect of Microwave (2.45 GHz) on Agronomic Efficiency of Nitrogen in Wheat

Muhammad Jamal Khan, Graham Brodie and Dorin Gupta

The University of Melbourne, Dookie, Australia

Keywords: Microwave, Soil, Nitrogen use efficiency, Wheat yield.

INTRODUCTION

Wheat growth is primarily influenced by the nitrogen status of soil. It has been demonstrated that microwave (MW) treatment: unlocks certain nutrients into the soil solution; markedly increases the nitrification efficiency [1]; and has a minute effect on the root nodulation by Rhizobium species in the soil [2]. The mechanical effect induced by MW irradiation can stimulate the dispersal of inorganic colloids. This stimulation can increase the decomposition of non-biomass organic matter in the soil [3]. MW energy (576 J cm⁻²), applied to the soil, increases the grain yield of wheat by 189 % and in canola pods the yield was increased by 650 % compare to the control [4]. However, the bio-stimulation effect of MW energy on soil nutritional dynamics, crop growth, and crop development are not well investigated. A glasshouse study was conducted to evaluate the effect of microwave treatment (2.45 GHz) on nitrogen use efficiency, growth and grain yield of wheat.

METHODOLOGY

A two factorial, completely randomized block design glasshouse experiment was conducted with ten replicates of each treatment combination at Dookie Campus, The University of Melbourne. The microwave treatment time was T_0 = Control and T_1 = 120 sec. The four concentrations of nitrogen ($N_1 = 0 \text{ mg } ^{15}\text{N L}^{-1}$, $N_2 = 50 \text{ mg } ^{15}\text{N L}^{-1}$, $N_3 = 100 \text{ mg } ^{15}\text{N L}^{-1}$ and $N_4 = 150 \text{ mg } ^{15}\text{N L}^{-1}$) were prepared using the isotopic ammonium nitrate ($^{15}\text{NH}_4^{15}\text{NO}_3$) with 10.4 atom % ^{15}N enrichment. The soil was treated in a domestic microwave oven with cavity dimensions of 370 × 380 × 210 mm (600 W heating power and frequency 2450 MHz). The temperature range in MW treated soil was between 80 – 90 °C. Chlorophyll content of wheat was measured using the non-destructive SPAD chlorophyll meter. The agronomic efficiency (AE) of nitrogen was measured using an equation proposed in [5].

$$AE = \frac{\text{Grain yield in fertilized pot} - \text{Grain yield in unfertilized pot}}{\text{Nitrogen Applied}}$$

RESULTS

Treatment of agricultural soil using microwave energy, at 2.45 GHz, significantly increase the chlorophyll content (Figure 1), grain yield (Figure 2) and agronomic efficiency of nitrogen (Figure 3) in wheat crop under all levels of nitrogen application in a glasshouse experiment.

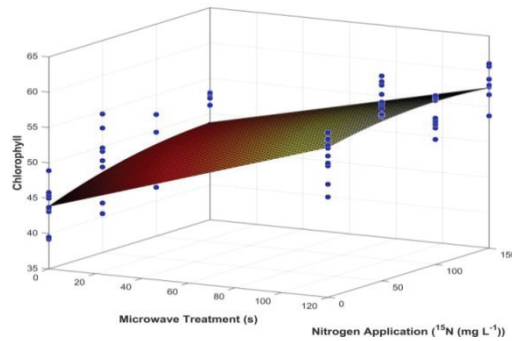


Figure 1. Relative contributions of microwave and nitrogen on chlorophyll (SPAD) content

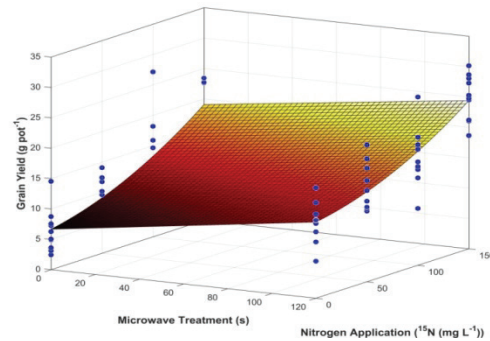


Figure 2. Relative contributions of microwave and nitrogen on grain yield of wheat.

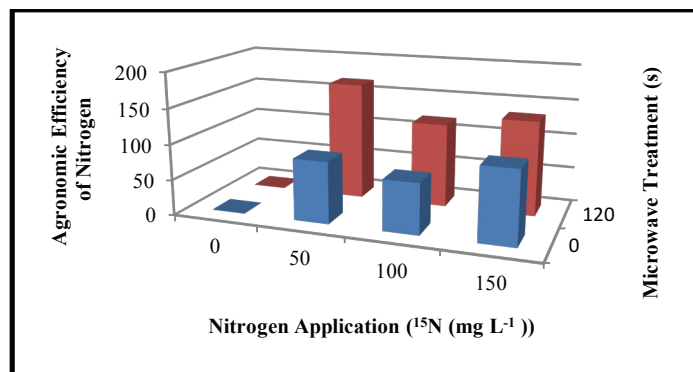


Figure 3. Agronomic efficiency of nitrogen as function of microwave and nitrogen application.

DISCUSSIONS

A 137% increase in grain yield was observed in MW treated soil at N₄ level compare to untreated control, which was consistent with the results reported by [4]. These results explain that MW treatment of soil enhanced the agronomic efficiency of nitrogen, growth and grain yield of wheat. It was interesting to know that grain yield (5.6 g) was more in MW treated pots where no nitrogen (N₁) was applied compare to N₂ (4.0 g) and N₃ (5.2 g) in untreated soil. The maximum AE of 166.9 was calculated at N₂ level followed by N₄ (133.2) and N₃ (118.5) in MW treated soil. Furthermore, the possible reason of the increase in growth related parameters of wheat may be due to the higher availability of nitrogen to plant. The results are in agreement with [6], who found that microwave irradiation increased ammonium nitrogen (NH₄⁺-N) and sulphur oxidation (SO₄⁻²-S) in soil, which may trigger both seedling vigour and plant growth.

CONCLUSIONS

This study has illustrated that MW exposure of soil could enhance crop growth and yield and may provide an alternative channel for efficient use of soil nitrogen by crop plants.

REFERENCES

- [1] M. Zieliński and M. Zielińska, Impact of microwave radiation on nitrogen removal and quantity of nitrifiers in biofilm, *Canadian Journal of Civil Engineering*, vol. 37, pp. 661-666, 2010.
- [2] M. Eglitis and F. Johanson, Control of seedling damping-off in greenhouse soils by radiofrequency energy, *Plant Disease Reporter*, vol. 54, pp. 268-271, 1970.
- [3] E. Zagal, Effects of microwave radiation on carbon and nitrogen mineralization in soil, *Soil Biology and Biochemistry*, vol. 21, pp. 603-605, 1989.
- [4] G. Brodie, N. Bootes and G. Reid, Invited Paper. Plant growth and yield of wheat and canola in microwave treated soil, In *IMPI's 49th Microwave Power Symposium*, San Diego, California, USA, 2015, pp. 40-41.
- [5] N. K. Fageria and V. C. Baligar, Methodology for Evaluation of Lowland Rice Genotypes for Nitrogen Use Efficiency, *Journal of plant nutrition*, 2003.
- [6] M. Wainwright, K. Killham and M. F. Diprose, Effects of 2450MHz microwave radiation on nitrification, respiration and s-oxidation in soil, *Soil Biology and Biochemistry*, vol. 12, pp. 489-493, 1980.

Determination of Kinetic Parameters of Thermal Death of Radio Frequency Heated Red Flour Beetle (*Tribolium castaneum*) using Inverse Simulation

Daeung Yu, Bijay Shrestha, and Oon-Doo Baik

Department of Chemical and Biological Engineering, University of Saskatchewan, 57 Campus Dr., Saskatoon, SK, S7N5A9 Canada

Keywords: Radio frequency heating, kinetics model, red flour beetle, mortality, lethal time

INTRODUCTION

One of the most common insect pests in the stored grains and oilseeds around the world is red flour beetle (*Tribolium castaneum*) [1]. RF heating based on the electromagnetic radiation is volumetric and selective heating, and this technique may avoid the problems posed by other chemical and nonchemical treatments for disinfestation of the insect pest. [2], [3], [4], [5]. There is a possibility to destroy the insect pest using RF heating without significant thermal degradation of the grains. Several kinetic models for mortalities of insect pests have been studied for thermal processing [4], [6]. Thermal death kinetics of the adult red flour beetle based on the immediately determined mortalities and temperature history of a host material (canola seeds) will be helpful to predict mortalities right after a specific RF heating time without knowing actual temperature history of insects. It can be also used to determine proper RF heating conditions for disinfestation of adult red flour beetles. Therefore, in this study, the thermal death kinetics of the adult red flour beetles infesting the stored canola seeds at various MCs and different volumes of the seeds was characterized based on dynamic temperature history of the stored canola seeds and the experimental data of insect mortalities during RF heating.

MATERIALS AND METHODS

Canola seeds (*B. napus* L.) at the initial moisture content (MC) of 7% were provided by our industrial partner Viterra Inc., Canada. Bulk canola seeds of four different MCs (5%, 7%, 9%, and 11%) were prepared. The seeds of the small ($1.96 \times 10^{-3} \text{ m}^3$) and the large ($1.77 \times 10^{-2} \text{ m}^3$) volumes were contained in RF transparent polycarbonate sample holders, then those seeds samples were RF heated. T1TM fiber optic temperature sensors were inserted at the hottest spot of the seed samples to measure the temperature of the seeds. RF exposure times (s) of the seeds were determined when the temperature of the hottest spot in the seeds reached up to each desired temperature (303K, 313K, 323K, 333K, 343K, and 353K) from 297K (initial temperature) for each MC of the seeds. The adult red flour beetles (*Tribolium castaneum*) were collected from the Agriculture and Agri-Food Canada/University of Manitoba, Canada. In brief, the insects were reared for 10 weeks in a mixture of wheat at MC of 14% and wheat germs (7:3), and collected using a suction assembly. A total of 30 adult insects were introduced at the hottest spot and its vicinity of the small volume of the seeds, and 90 adult insects at the hottest spot of the large volume of the seeds. The temperature of the infested seeds increased up to the desired temperatures at the hottest spot of the seeds. The dead and the live insects were counted immediately after RF heating to calculate mortalities. The RF heating system used in this work is shown in Fig. 1. A 1.5 kW, 27.12 MHz laboratory-scale RF system (Strayfield Fastran, Berkshire, England) was used to heat the canola seeds with the red flour beetles.

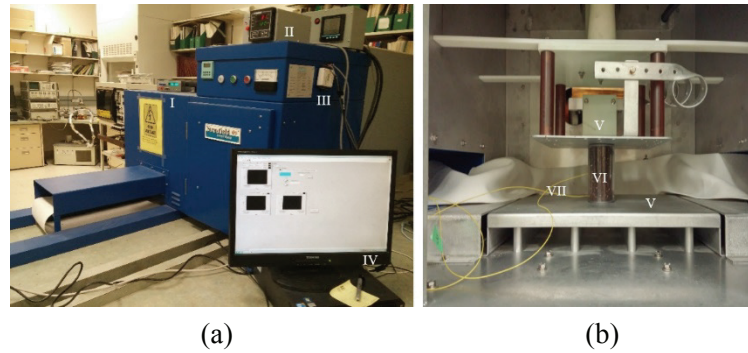


Figure 1. The side and the rear (a) and the interior (b) view of the RF heating system showing I : a reflex signal conditioner, II : a temperature controller, III : a data acquisition device, IV : a data acquisition software, V : two electrodes, VI : the canola seeds in the small sampl holder, VII : the T1TM fiber optic temperature sensors (Yu et al., 2015b).

The thermal death kinetics of the adult red flour beetles can be modeled using the following kinetics model.

$$\frac{d(N/N_0)}{dt} = -k_0 \exp\left(\frac{-E_a}{RT}\right) (N/N_0)^n \quad (1)$$

where N and N_0 are respectively the number of live insects at time and the initial number of the insects, t is the heating time (s), k_0 is the frequency factor, E_a is the activation energy (J/mol), R is the universal gas constant (8.314 J/mol·K), and T is the temperature of the bulk canola seeds (K), and n is the order of the reaction. The ordinary differential equation, Eq. (1) was solved using ODE 45 solver based on 4th order Runge-Kutta method in MATLAB R2013a (The MathWorks Inc., Natick, MA, USA). The optimum values for the parameters k_0 , E_a , and n were determined by minimizing the root mean square error (RMSE) between the values predicted from the kinetics model and the experimental values as depicted in Eq (2).

$$\text{RMSE} = \sqrt{\frac{1}{m} \sum_{i=1}^m (x_i - x'_i)^2} \quad (2)$$

where m is number of data, x_i is the measured value, and x'_i is the value predicted using the kinetics model. The unknown parameters of k_0 , E_a , and n were estimated by trial and error. The n value was almost closed to 1 in our preliminary modeling. So, we considered the order of reaction (n) to be 1. The kinetics model was also used to estimate the LTs to achieve 95% (LT₉₅) and 99% (LT₉₉) mortalities of the insects infesting the canola seeds at different MCs and volumes.

RESULTS

Table 1. The performance of the kinetics model (Eq. 5) in predicting the mortalities of the adult red flour beetles during the RF heating.

E_a (kJ / mol)	k_0 (1 / s)	n	Volume	MC (%, w. b.)	R^2	RMSE ^a	$d.f.$ ^b
100	6.73×10^{13}	1	Small	5	0.958	16.20	6
				7	0.978	11.55	6
				9	0.972	12.84	6
				11	0.741	43.32	6
			Large	5	0.975	12.30	6
				7	0.987	8.745	6
				9	0.979	11.02	6
				11	0.908	25.73	6

^a RMSE = root mean square error.

^b $d.f.$ = degree of freedom.

DISCUSSION

The temperature increment rate of the canola seeds was apparently proportional to the MC of the seeds. The RF exposure time ranged from 25 to 1200 s. In general, the survival rate of the insects decreased with increasing temperature. At any desired temperatures of the seeds, the survival rate of the insects decreased with increasing MC of the seeds, and it was attributed to increasing temperature of the seeds with increasing MC during the RF heating [8]. The survival rate of the insects was significantly affected by the MC of the seeds. The survival rate of the insects in the seeds at high MC (11%) was lower than that at low MC (5%) at the same end RF heating temperature due to more evaporated moisture from the seeds of high MC (11%). Over 84% and 99% mortalities of the insects were achieved over 333K for the small and the large volumes of the seeds, respectively.

The performance of the kinetics model in predicting the mortalities for both the small and the large volumes of the seeds is summarized in Table 1. The mortality values determined from the kinetics model agreed well with the experimental values. The determined activation energy of 100 kJ/mol for the adult red flour beetles infesting the canola seeds was similar to that for mediterranean flour moth eggs (102 kJ/mol) [9] and it was lower than that for the fifth-instar colding moth (472 kJ/mol) [6] and the fifth-instar navel orangeworm (510 kJ/mol to 520 kJ/mol) [7]. The lower activation energy indicated that the adult red flour beetle was more susceptible to the thermal death by the RF heating than the other insects infesting other food commodities. It should be, however, noted that the temperature profile of the canola seeds were used instead of that of the adult insect-body for the determination of kinetic parameters. Therefore, more accurate analysis of thermal death kinetics for the adult red flour beetle infesting the canola seeds during the RF heating could be done by implementing the temperature profile of an actual insect body. The predicted LT_{95} and LT_{99} from the kinetics model were in good agreement with those from the experiments. The differences between the LTs predicted from the experiments and the kinetics model ranged from 17.40 to 287.1 s, and 19.49 to 348.6 s for LT_{95} and LT_{99} respectively.

CONCLUSION

The thermal death kinetics model developed in this research would be useful in designing a post-harvest RF thermal process to control the red flour beetles and similar insects in the stored-canola seeds and other commodities.

REFERENCES

- [1] R. Mills, and J. Pedersen, A flour mill sanitation manual. Eagan Press, St. Paul, M.N, 1990.
- [2] S. L. Birla, S. Wang, J. Tang, G. Tiwari, Characterization of radio frequency heating of fresh fruits influenced by dielectric properties. *Journal of Food Engineering*, vol. 89 no 4, pp. 390-398, 2008.
- [3] J. P. Griffin, Montreal Protocol on Substances That Deplete the Ozone Layer. In *Int'l L.*, vol. 22, pp. 1261, 1988.
- [4] J. Tang, J. N. Ikediala, S. Wang, J. D. Hansen, R. P. Cavalieri, High-temperature-short-time thermal quarantine methods. *Postharvest Biology and Technology*, vol. 21 no. 1, pp. 129-145, 2000.
- [5] S. Wang, J. Tang, Radio frequency heating: a potential method for post-harvest pest control in nuts and dry products. *Journal of Zhejiang University Science*, vol. 5 no. 10, pp. 1169-1174, 2004.
- [6] S. Wang, J. N. Ikediala, J. Tang, J. D. Hansen, Thermal death kinetics and heating rate effects for fifth-instar *Cydia pomonella* (L.) (Lepidoptera: Tortricidae). *Journal of Stored Products Research*, vol. 38 no. 5, pp. 441-453, 2002.
- [7] S. Wang, J. Tang, J. A. Johnson, J. D. Hansen, Thermal-death kinetics of fifth-instar *Amyelois transitella* (Walker) (Lepidoptera: Pyralidae). *Journal of Stored Products Research*, vol. 38 no. 5, pp. 427-440, 2002.
- [8] D. Yu, B. Shrestha, O. D. Baik, Radio frequency (RF) control of red flour beetle (*Tribolium castaneum*) in stored rapeseeds (*Brassica napus* L.). Submitted to *biosystems engineering*, 2015.
- [9] A. Ben-Ialli, J. M. Méot, P. Bohuon, A. Collignan, Survival kinetics of *Ephestia kuehniella* eggs during 46–75 C heat treatment. *Journal of Stored Products Research*, vol. 45 no. 3, pp. 206-211, 2009.

A Simulation Model for Microwave-Assisted Thermal Pasteurization System

Deepali Jain¹, Frank Liu¹, Juming Tang¹, and Donglei Luan²

¹Biological Systems Engineering Department, Washington State University, Pullman, WA 99163, USA

²Shanghai Ocean University, 435 Minxing Rd, Yangpu Shanghai, China

Keywords: Microwave heating, simulation, heating pattern, computer vision assistant

INTRODUCTION

Microwave-assisted thermal pasteurization system (MAPS) is a new technology based on microwaves and hot water heating of foods that is developed at Washington State University. Determination of cold spot location and heating to reach desired lethality is a critical step in developing process schedules. In microwave processing, locations of cold spots are influenced by microwave cavity shape and size and by dielectric and thermal properties of food [1]. In the MAPS system food carrier system may also affects the heating pattern in the food. Computer simulation model aids in understanding of the electromagnetic wave propagation and effect on heating pattern by the above factors. This paper describes a computer simulation model and validation for a 915 MHz pilot scale microwave-assisted thermal pasteurization system.

METHODOLOGY

A finite difference time domain technique based software (QuickWave ver. 7.5) was used to simulate the microwave heating of food trays in a moving carrier through the pilot scale MAPS system. The system is consisted of two connected horn-shaped cavities. Dielectric properties and thermal properties of the model food were measured as described in [2]. Convective heat transfer coefficient was calculated using capacitance lumped method [3]. To validate the simulated heating patterns and temperature profiles, 16 oz. trays filled with mashed potato model food were processed in the MAPS system with 4.5 kW and 7.5 kW power with 3.8 minutes and 1.8 minutes residence time respectively. The trays were then analyzed using computer vision method for heating pattern [4].

RESULTS

Figure 1 shows experimental and simulated heating pattern of three trays processed in the MAPS. Figure 2 shows the exact location of cold and hot spots determined using computer vision method based on color parameters. Figure 3 shows the temperature profile obtained

using metallic mobile sensors at hot and cold spot. Change in electric field pattern with the presence of food carrier with and without food also showed a predictable heating pattern (Figure 4).

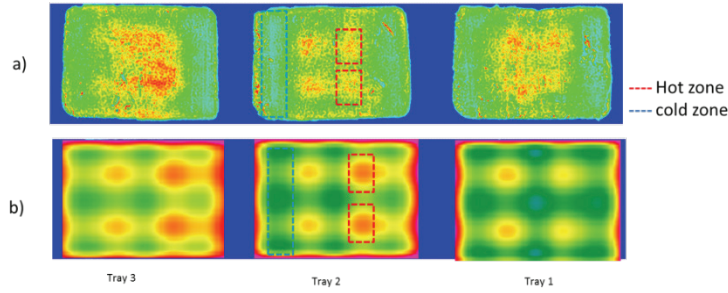


Figure 1. Heating pattern of three 16oz single compartment tray processed in the MAPS by a) chemical marker method (experiments) and b) simulation

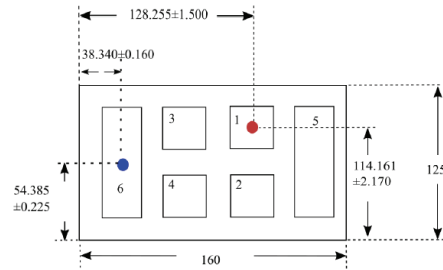


Figure 2. Location of cold and hot spot in 16oz tray

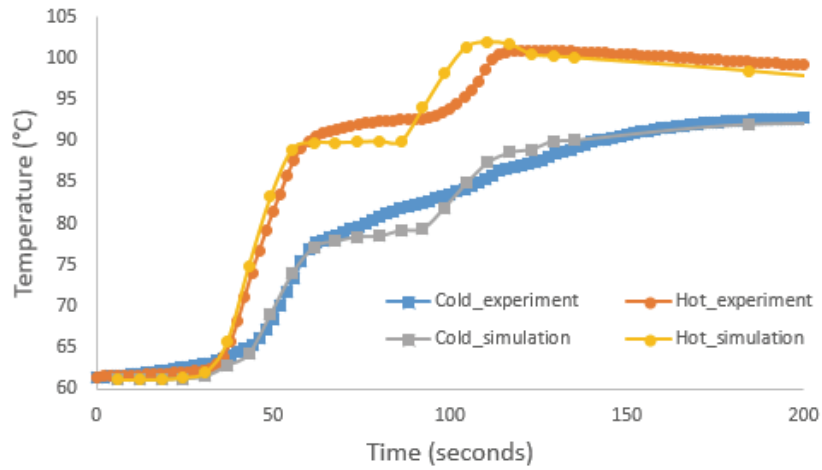


Figure 3. Temperature profile obtained from experiment and simulation at cold and hot spots in 16oz tray

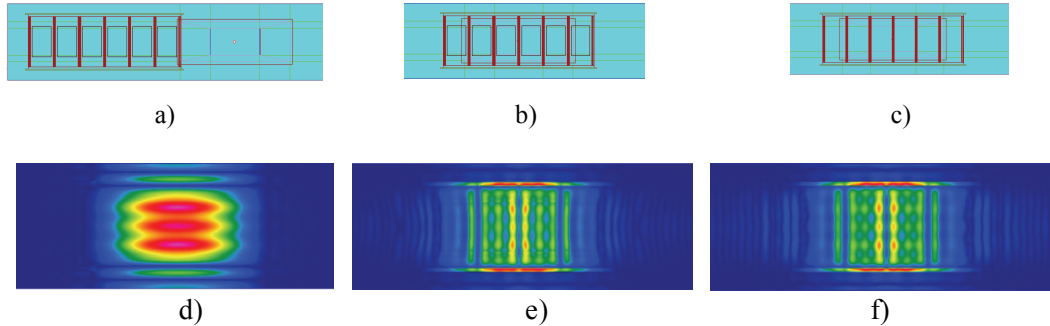


Figure 4. Simulation model and location of tray a) outside the cavity b) centre of the cavity with food c) centre of the cavity without food and corresponding simulated electric field pattern inside cavity d) empty cavity and e) tray carrier with food f) without food

DISCUSSION

Simulated heating pattern of food trays processed in the MAPS have shown good agreement with the experimental results. Based on the results there are four zones for hot spot and three zones for cold spot. Highest and lowest color value locations determined by chemical marker method are the hot and cold spot respectively. Direct measurements of temperature using metallic mobile sensors at these hot and cold spots shows that temperature at hot spot is consistently higher than at the cold spot. As seen in Figure 4, electric field pattern inside the cavity is affected by the presence of metal tray carrier and presence of food. However, the electric field pattern is the same when tray carrier is inside the cavity with or without the food.

CONCLUSION

A computer simulation of the microwave assisted thermal pasteurization system model is developed and validated. The model could be used to determine the location of cold and hot spot of the food and to study how moving metallic tray carrier affects the heating patterns. The model will further be used to improve heating uniformity.

REFERENCES

- [1] S.Yanniotis, and B. Sundén. *Heat transfer in food processing - Recent developments and applications*. Southampton: WIT press, 2007.
- [2] F.P. Resurreccion Jr, J. Tang, P. Pedrow, R. Cavalieri, F. Liu, and Z. Tang. Development of a computer simulation model for processing food in a microwave assisted thermal sterilization (MATS) system. *Journal of Food Engineering*, vol. 118, no. 4, pp. 406-416, 2013.
- [3] T. L. Bergman and P. F. Incropera. *Fundamentals of heat and mass transfer*. Hoboken, NJ: John Wiley, 2011.
- [4] B. P. Ram, J. Tang, F.Liu, and G.Mikhaylenko. A computer vision method to locate cold spots in foods in microwave sterilization processes. *Pattern Recognition* , vol 40. No 12, pp.3667-3676, 2007.

Magnetrons, Microprocessors and the Birth of Expert Cooking Intelligence

Steven J. Drucker

Droaster Laboratories LLC, Atlanta GA, USA

Keywords: microwave ovens, microprocessors, cultural cooking trends, embedded systems, artificial intelligence

ABSTRACT

The holy grail of microwave ovens is push button perfection—integral to which is instant gratification. In the process of being accorded grail status, microwave perfection has evolved into a cross-generational quest. When, where and why did it begin? If it is uniquely American, why is that? Can its roots be traced to the first appearances in the mid-nineteenth century of cookbooks for homemakers? Is the ready consumer embrace with which food processing innovations—such as canning, jars, bottles, freezing, “pod-i-zation”, popcorn bags and so forth—expressive of a cultural mindset ever more needful for what this grail promises even as society evolves from agrarian, to mercantile to industrial to post industrial?

Beginning after World War II, contemporary appliance product and feature launches, many of a faddish nature, but some so successful as to have become culturally embedded trace a line of descent down to the serial marriages—early, mid-life and late stage—of microprocessors and microwave ovens. What technologies were developed, patented and brought to market? How did they work? Why didn't they work? Did they find receptivity in the market? What are the metrics used to decide whether to introduce these technologies? How deep seated is the urge to find this grail—sufficiently so that the microwave food market exceeds billions of dollars annually even as it undergoes stagnant growth in most segments? Yet now, when its demographics exhibit marked consumption differences across age segmented market demographics, reports from the field track that this market is less robust with age groups in ascent than with mature consumers, the reasons for stagnation, contraction and segmented growth are examined. Does this mean that the quest for push button perfection is any less urgent with post-internet younger consumers? If not—what are the technological and market prospects for expert cooking intelligence? Do these prospects extend across the kitchen? Do they extend to packaged food? What role can recipes play? To what extent can microwave ovens meet millennials' preference to cook, given microwave ovens' inherent inability to effect

Maillard reactions? Given what we've learned, can artificial cooking intelligence be quantified and its worth in the microwave oven market place qualified? What is the future of Expert Cooking Intelligence within the kitchen—and what metrics shall be applied to determine its market viability?

Solid State Cooking

Robin Wesson, Advanced Application Architect

Ampleon, Nijmegen, Netherlands

Keywords: Power Amplifiers, Solid State Cooking, Practical Results, Scope for Innovation.

INTRODUCTION

Microwave oven technology is on the cusp of a revolution. Solid state electronics can now deliver comparable power levels to the magnetron which has been the engine of the microwave oven since the first products were launched seventy years ago. This new technology enables new techniques that can significantly enhance the control of energy delivery. These techniques represent scope for innovation that will change the user's experience of cooking with high power RF energy. The technical implications and possibilities are examined in this paper which should be of interest to engineers or food scientists keen to improve the results achievable with industrial or consumer RF heating appliances.

Since the 1950's the transistor has all but totally replaced electronic vacuum tubes in electronics applications. The transistor is the driving force behind ubiquitous computing and communication capabilities beyond our imagination just a decade or two ago. Moore's famous 'law' has observed that the number of transistors per square mm of silicon has doubled year on year, delivering an exponential increase in processing power. Not all transistors are better when small, however. A single large device can switch currents of hundreds of amps or broadcast television and radio signals around the world. High power transistors, while not subject to Moore's law, have gradually increased in efficiency, power density and ruggedness and can now compete with one of the last common valve applications that very few people realize they still have in their own home.

THE MAGNETRON

The magnetron is the heart of every microwave or combination oven in use today. The magnetron is a type of valve integrated with magnets and resonant chambers that generates a high power RF signal used for cooking, heating and drying in consumer and industrial applications. Discovered early in the last century, the magnetron design was improved and applied during the 1940's for radar applications, and the magnetron now delivers high power with good efficiency at relatively low cost. For cheap raw power, the magnetron remains a great solution.

Radar applications evolved beyond use of the magnetron, because the signals it generates cannot deliver the accuracy and control needed for high performance measurement systems. The entire communications industry also relies on accuracy of modulation, and in both fields a better solution was required. In stark contrast, much of the innovation in microwave cooking in recent decades has been in food additives and meal packaging techniques designed to give the best results with the existing heating technology. (IMPI conference 2013, Providence, RI). A regular complaint aired was that an innovation that delivered good performance in one oven would do something different in another. Variability from test to test was deemed to be too great. High performance microwave cooking requires a new approach.

THE MICROWAVE COOKING EXPERIENCE

Most of us are familiar with the results: microwave ovens deliver rapid heating but can result in food with overcooked, dehydrated parts and cold or raw parts. For these reasons microwaves are not widely trusted to cook raw meats, and are often used simply to reheat leftover food, or to heat a mug of water or milk for making a drink.

Regardless of the energy source, be it magnetron or solid state amplifier, the electromagnetic energy interacts with the cavity to create patterns of standing waves that are responsible for the simultaneously overcooked and raw food recognisable to our typical user. The interaction of electromagnetic energy with the food is also unchanged. Electromagnetic energy is absorbed by food depending on the frequency and the dielectric properties of the food. In most foods, contrary to the urban myth of heating from the middle, consumer microwave ovens operating around 2450 MHz directly heat only to a depth of a couple of centimetres. Microwave oven performance is characterised, as most technology is, through the use of standardised tests. Microwave ovens are specified today on their ability to heat one litre of water, which presents a large load to the system and is very easy to heat. Standards and specifications drive the performance optimisation process, which leads to products that are optimised for heating a load that will rarely be encountered in real world usage.

After this brief examination of the behaviour of magnetrons and the optimisation processes used with microwave ovens today, we will examine the capabilities of solid state systems which define the scope for innovative new solutions to RF heating applications. Taken singly, specific characteristics may be useful in some end applications and have no value in others, however together they represent the landscape of new capabilities from which breakthroughs in heating performance will emerge.

SIMULATED AND PRACTICAL RESULTS

A range of simulated and practical results will be presented, including: Pancake batter in a bowl cooked with two different algorithms, A sweep of a cavity return loss showing the changes as the food heats, and simulations showing a 1L cubic water load heated in a dual channel system at three frequencies.

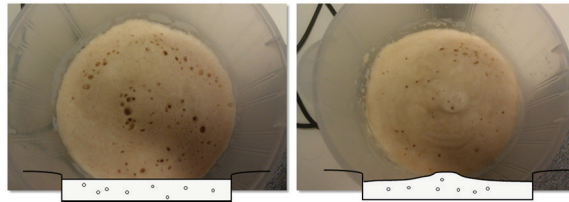


Figure 1: Pancake batter heated with two different algorithms.

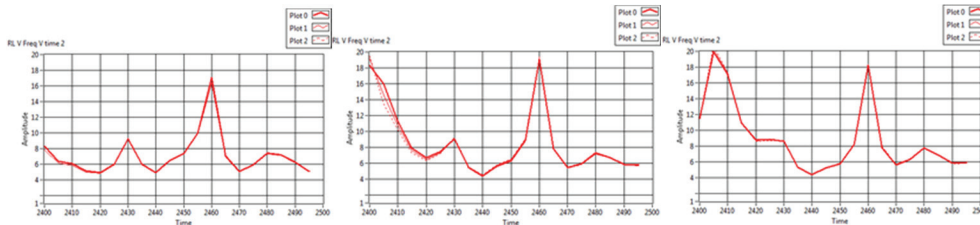


Figure 2: Sweeps of cavity return loss showing the changes as the food heats.

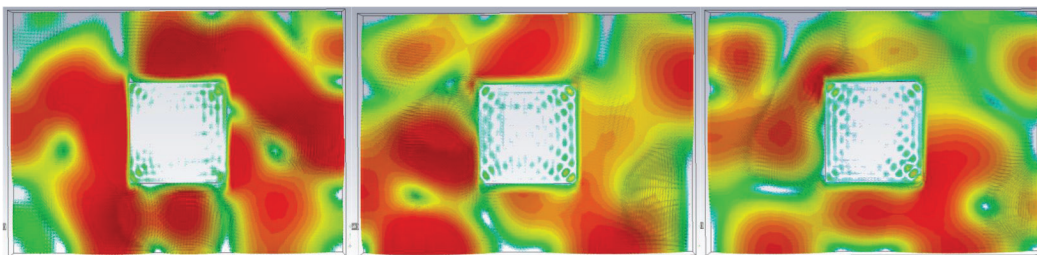


Figure 3 a,b,c: Simulation results of a 1L cube of water heated in a two channel system at three frequencies. (a = 2400 MHz, b = 2450 MHz, c = 2500 MHz)

CONCLUSION

Solid State Cooking, using high power amplifiers and highly accurate signal generation and detection, is a practical reality in the lab today. Work is quickly proceeding across the world to make it a commercial proposition, and history teaches us how fast transistor technology displaces the valve when the technology begins to be able to compete. The scope for innovation that comes with this transition will change the industry and the cooking experience of the consumer, as well as the professional and industrial heating markets. Instead of innovation in microwave heating being focused on food additives and packaging, innovation may soon be all about how to build the best new RF engine, and learning how to use it.

REFERENCES

[1] This paper is a summary of the authors own work and experience in this field

The Localized Microwave-Heating Paradigm and its Implementation in Solids, Powders, and Dusty Plasma

Eli Jerby

Faculty of Engineering, Tel Aviv University, Ramat Aviv 6997801, ISRAEL

E-mail: jerby@eng.tau.ac.il

Keywords: Microwave-heating, hotspot, dusty plasma, nano-powders

INTRODUCTION

Localized microwave-heating (LMH) effects are enabled by the intentionally-induced thermal-runaway instability [1]. The LMH and hotspot-formation effects, providing the basis for the microwave-drill operation [2], are further studied for other implementations in miniature transistor-based (LDMOS-FET) microwave heaters [3], and for ignition of thermite reactions in air and underwater [4], local sintering of metal powders, and additive-manufacturing and 3D-printing applications [5].

The LMH instability illustrated in Figs. 1a-e can be induced by various means, as for instance the open-end applicator, in materials of which the dielectric loss tends to increase (and/or the thermal conductivity to decrease) with temperature. The initial local heating near the applicator leads then to a spatial non-uniform distribution of the material properties in this vicinity; the loss factor increases (and/or the thermal conductivity decreases) there, and as the local temperature rises the power dissipated in this confined region increases. This local-heating acceleration leads to a positive-feedback response, and to the LMH instability. The temperature evolved in the confined hotspot, exceeding the melting point, enables various applications such as drilling holes.

Plasma columns and spheres can also be ejected from molten LMH hotspots in various solid substrate materials (e.g. silicon [6], glass, basalt, germanium, copper, aluminum, titanium [7]) to air atmosphere. Various potential applications of these dusty plasmas are considered, including nano-powder production, coating and deposition, material identification, plasma cooking [8], combustion and propulsion [9].

The LMH concept is reviewed in this paper and its recent developments are discussed in a paradigmatic approach. The potentials and limitations of LMH devices for various applications are considered (e.g. as low-cost substitutes for lasers).

METHODOLOGY

A typical experimental setup used for LMH-plasma experiments is schematically shown in Figs. 2a, b. It consist of a microwave cavity (made e.g. of a WR340 waveguide)

with openings (in microwave cutoff) for diagnostic purposes. A movable electrode directs the microwave energy locally into the substrate. The microwave power is generated by a 2.45 GHz, 1 kW magnetron unit, fed by a controllable switched-mode power supply (or alternatively by an LDMOS-FET oscillator as in Ref. [3]).

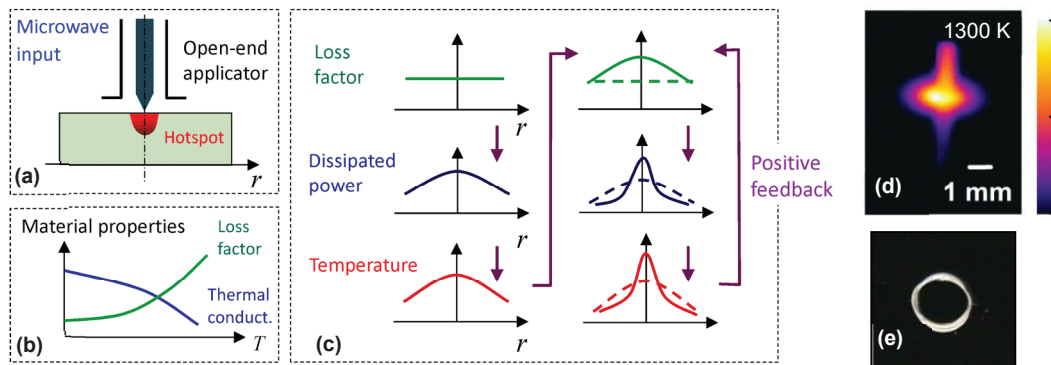


Figure 1. The thermal-runaway instability: An open-end applicator (a), directed to a substrate material with temperature-dependent properties (b), induces LMH instability (c) [1]. The molten hotspot formed e.g. in glass (d) can be removed to make a hole (e) [2].

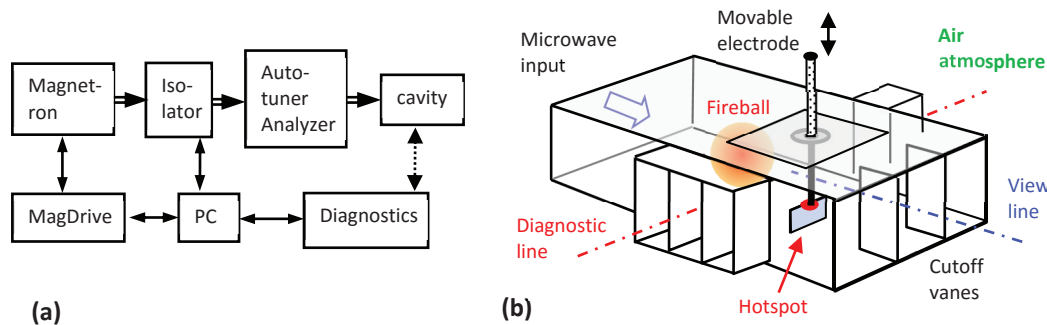


Figure 2. A typical experimental setup for LMH-plasma generation [6]: A block diagram of the experimental instrumentation (a), and the microwave cavity (b).

RESULTS

Various experimental results, as shown in Figs. 3a-f, have demonstrated the extended applicability of the LMH paradigm. These include dusty-plasma generation in forms of fire-columns and fireballs, and direct conversion of solids (e.g. silicon, copper, titanium) to nano-powders [6, 7]. Furthermore, LMH interactions with metal powders show the feasibility of incremental powder solidification in order to form solid structures [5] (possibly for 3D printing), and of LMH ignition of thermite mixtures (in air and underwater) as efficient fuels combustible in oxygen-free environments [4]. In conclusion, LMH may provide limited substitutes for lasers in various applications in which proximity is allowed between the LMH applicator and the processed object.

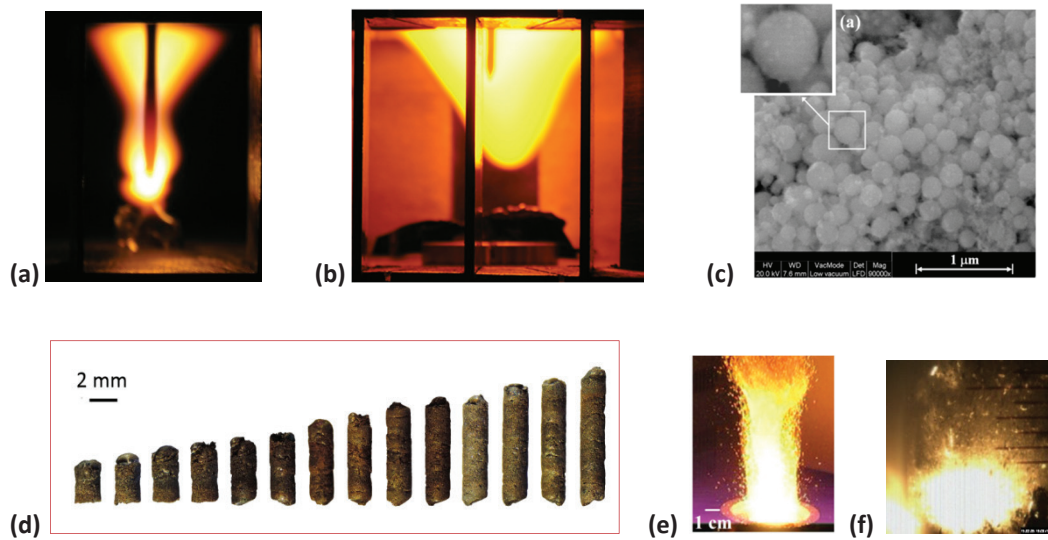


Figure 3. LMH experimental results demonstrating fire-column (a) and fireball (b) ejection from solids, and nano-powder production (c). LMH interactions with powders enable incremental solidification e.g. for 3D printing (d), as well as thermite ignition in air (e) and underwater (f).

REFERENCES

- [1] E. Jerby, O. Aktushev and V. Dikhtyar, Theoretical analysis of the microwave-drill near-field localized heating effect, *J. Appl. Phys.*, Vol. 97, 034909, 2005.
- [2] E. Jerby, V. Dikhtyar, O. Actushev and U. Groszlick, The microwave drill, *Science*, Vol. 298, pp. 587-589, 2002.
- [3] Y. Meir and E. Jerby, Localized rapid heating by low-power solid-state microwave-drill, *IEEE Trans. Microwave Theory & Tech.*, Vol. 60, pp. 2665-2672, 2012.
- [4] Y. Meir and E. Jerby, Underwater microwave ignition of hydrophobic thermite powder enabled by the bubble-marble effect, *Appl. Phys. Lett.*, Vol. 107, 054101, 2015.
- [5] E. Jerby, Y. Meir, A. Salzberg, E. Aharoni, A. Levy, J. Planta Torralba and B. Cavallini, Incremental metal-powder solidification by localized microwave-heating and its potential for additive manufacturing, *Additive Manufacturing*, Vol. 6, pp. 53-66, 2015.
- [6] Y. Meir, E. Jerby, Z. Barkay, D. Ashkenazi, J. B. A. Mitchell, T. Narayanan, N. Eliaz, J-L LeGarrec, M. Sztucki and O. Meshcheryakov, Observations of ball-lightning-like plasmoids ejected from silicon by localized microwaves, *Materials*, Vol. 6, pp. 4011-4030, 2013.
- [7] S. Popescu, E. Jerby, Y. Meir, Z. Barkay, D. Ashkenazi, J. B. A. Mitchell, J-L. Le Garrec and T. Narayanan, Plasma column and nano-powder generation from solid titanium by localized microwaves in air, *J. Appl. Phys.*, Vol. 118, 023302, 2015.
- [8] E. Jerby, Y. Meir, R. Jaffe and I. Jerby, Food cooking by microwave-excited plasmoid in air atmosphere, *Proc. 14th Int'l Conf. Microwave & High-Frequency Heating, Ampere-2013*, Nottingham, UK, Sept. 16-19, 2013, pp. 27-30 (also in these Proceedings).
- [9] Y. Meir and E. Jerby, The localized microwave-heating (LMH) paradigm – Theory, experiments, and applications, *Proc. 2th Global Congress Microwave Energy Applications, GMCEA-2, Long Beach CA*, July 23-27, 2013, pp. 131-138.

Study on an Injection-Locked Magnetron

Satoshi Fujii^{1,2}, Maitani Masato¹, Eichi Suzuki¹, Satoshi Chonan³, Miho Fukui³, and Yuji Wada¹

¹Tokyo Institute of Technology, Tokyo, Japan

²National Institute of Technology, Okinawa College, Okinawa, Japan

³Oricon Energy, Tokyo Japan

Keywords: Pidgeon process, Magnetron, Injection-locking.

INTRODUCTION

We study magnesium metal production using microwave Pidgeon process to reduce energy consumption and carbon dioxide. We have successfully obtained small amount of magnesium metal using a microwave oven with 1 kW. The microwave power supply output is expected to be over 10 kW for commercial production. In this report, an injection-locked magnetron with an external oscillator was investigated to obtain the parameters of the equivalent circuit model in order to obtain such a large output microwave power by combination of several magnetrons. The magnetron had the resonance characteristics of a parallel LCR circuit when the magnetron was locked.

EXPERIMENTAL SETUP

Fig. 1 shows a block diagram of the injection-locked continuous-wave (CW) magnetron measurement system. As the magnetron, the model 2M137A-01BTM made by Panasonic was used. The magnetron oscillates at 2.4524 GHz with an output power of 470 W, and the filament current is controlled so as to stabilize the oscillation frequency with a narrowband spectrum [1].

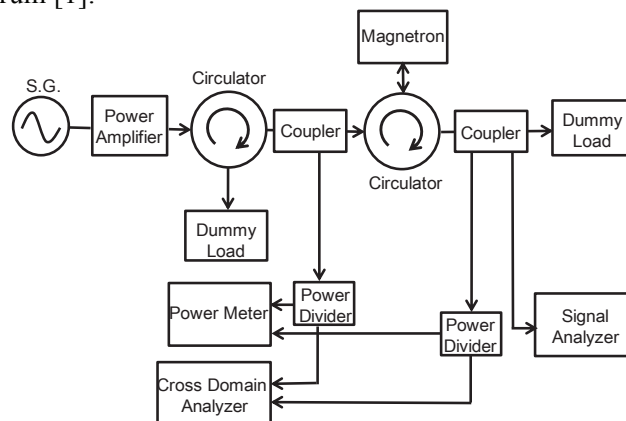


Figure 1. Block diagram of the injection-locked CW magnetron and measurement system.

RESULTS AND DISCUSSION

Fig. 2 shows the forward input power of the injection signal as a function of the frequency of the external oscillator. The magnetron could be locked within the peak-to-peak from the lowest input power to the highest. The magnetron could be locked starting with the forward input power of the injection signal 0.97 W and the ratio of the forward input power of the injection signal to the output power of the magnetron -26 dB. Increasing the input power widened the lock range.

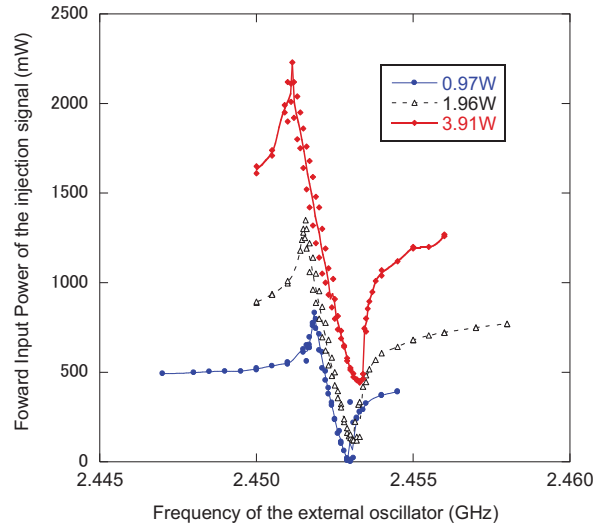


Figure 2. Forward input power of the injection signal as a function of the frequency of the external oscillator.

Fig. 3 shows the resonance characteristics of the injection-locked magnetron converted from the reflection characteristics of the input signal obtained by vector measurement as a function of input frequency of the external oscillator in dependence on the input power of the injection signal. These measurements showed that the locked magnetron has the characteristics of a parallel resonance (LCR) circuit for the injection signal [2]. The parameters of the LCR circuit model were determined. Table I presents the results. The loaded Q_L value can be derived from (1). Q_L and locking range $\delta\omega$ are interrelated as

$$\frac{\delta\omega}{\omega_0} = \frac{1}{Q_L} \sqrt{\frac{P_{IN}}{P_{OUT}}} \quad (1)$$

where $\delta\omega$, ω_0 , Q_L , P_{IN} , and P_{OUT} are the locking range and frequency of the free-running magnetron, loaded Q , input power of the injection signal, and output power of the magnetron, respectively [3].

Based on these results, increasing the input power of the injection signal causes the anti-resonance frequency, F_a , to be close to that of the unlocked magnetron at 2.4524 GHz. In addition, the resistance in the equivalent parallel circuit model of the magnetron becomes smaller. This means that the unloaded Q for the injection signal becomes smaller, which widens the locking range.

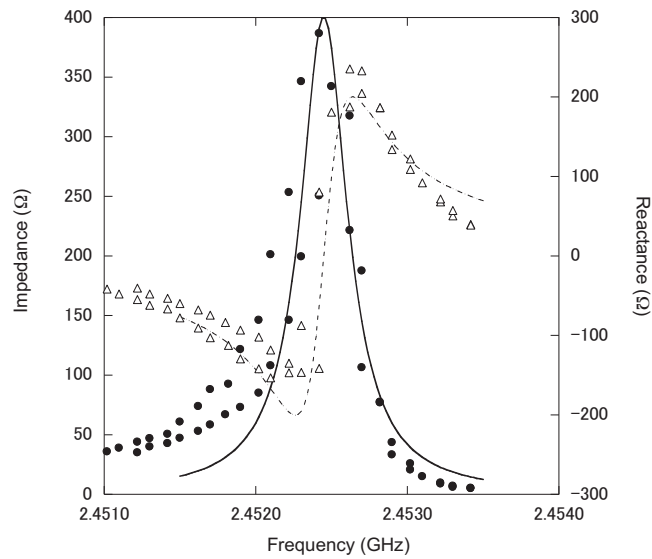


Figure 3. Resonance characteristics of the locked magnetron for input power 3.91 W.

TABLE I: SUMMARY OF THE EQUIVALENT PARAMETERS

P_{IN} (W)	F_a (GHz)	Q_L	Q_{UL}	L (pH)	C (nF)	R (Ω)
0.97	2.4528	48.8	30000	2.0	2.1	924
1.96	2.4527	48.8	12000	2.8	1.5	517
3.91	2.4525	48.5	6500	4.0	1.1	400

CONCLUSION

An injection-locked magnetron with an external oscillator was investigated to obtain the parameters of the equivalent circuit model as a function of the input power. The magnetron was locked over the ratio of the input power to the output power of -26 dB and had the resonance characteristics of a parallel LCR circuit model. Based on the derivation of these parameters, increasing the input power causes the anti-resonance frequency to become the original frequency of the magnetron, and the range of the locking frequency becomes wider because of the lower Q value.

REFERENCES

- [1] N. Shinohara, H. Matsumoto, and K. Hashimoto, "Solar power station/satellite (SPS) with phase controlled magnetrons," *IEICE Trans. Electron.*, vol. 86, pp. 1550-1555, 2003.
- [2] S. C. Chen, "Growth and frequency pushing effects in relativistic magnetron phase-locking," *IEEE Trans. Plasma Science*, vol. 18, No. 3, pp. 570-576, June 1990.
- [3] R. Adler, "A study of locking phenomena in oscillators," *Proc. IRE*, vol. 34, pp. 351-357, June 1946.

Microwave Induced Plasma for Food Sanitizing in a Technological Scale

M. Andrasch, U. Schnabel, J. Stachowiak, R. Niquet and J. Ehlbeck

Leibniz-Institut for Plasma Science and Technology e. V., Greifswald, Germany

Keywords: microwave plasma, plasma processed water, sanitation, food preservation

INTRODUCTION

Gentle sanitation of vegetables and fresh fruits is highly demanded since consumption of raw food products entails risk of food-borne illnesses. Recent outbreaks in Western Europe involved EHEC (enterohemorrhagic *Escherichia coli*) on sprouts, *Listeria monocytogenes* on meat and norovirus in frozen strawberries. Currently used disinfection or sanitation methods for fresh fruits and vegetables lack antimicrobial effectiveness, are costly and consume water or chemicals. Non-thermal atmospheric pressure microwave plasma offers a promising opportunity for fresh food preservation. Accordingly, over the last decade, different microwave plasma sources and application methods were developed and optimized to meet health requirements without decreasing product quality. This contribution describes the experiments performed to decontaminate food in a technological scale. They took place in the technical center of an industrial partner within a period of two weeks.

METHODOLOGY

The antimicrobial effects of plasma are well known and investigated for different types of plasma sources, which can be driven for instance by microwaves at 2.45 GHz. By developing a two stage microwave plasma source, which works at atmospheric pressure, 90 standard liters per minute of plasma processed air (PPA) can be continuously produced.

This plasma source and all necessary units for providing cooling water, microwave power, pressurized air and process control are combined in an auxiliary decontamination unit. Afterwards the PPA is used to produce plasma processed water (PPW) inside an international bulk container (Figure 1). The connected food treatment station then applies the PPW on different ways (bathing, spraying, and washing) to sanitize 5 kg of fresh cut endive in each experiment (Figure 2). The analysis of sanitized salad was done by three independent institutes (Fraunhofer Institute for Process Engineering and Packaging, Leibniz Institute for Agricultural Engineering Potsdam-Bornim and Leibniz Institute for Plasma Science and Technology).

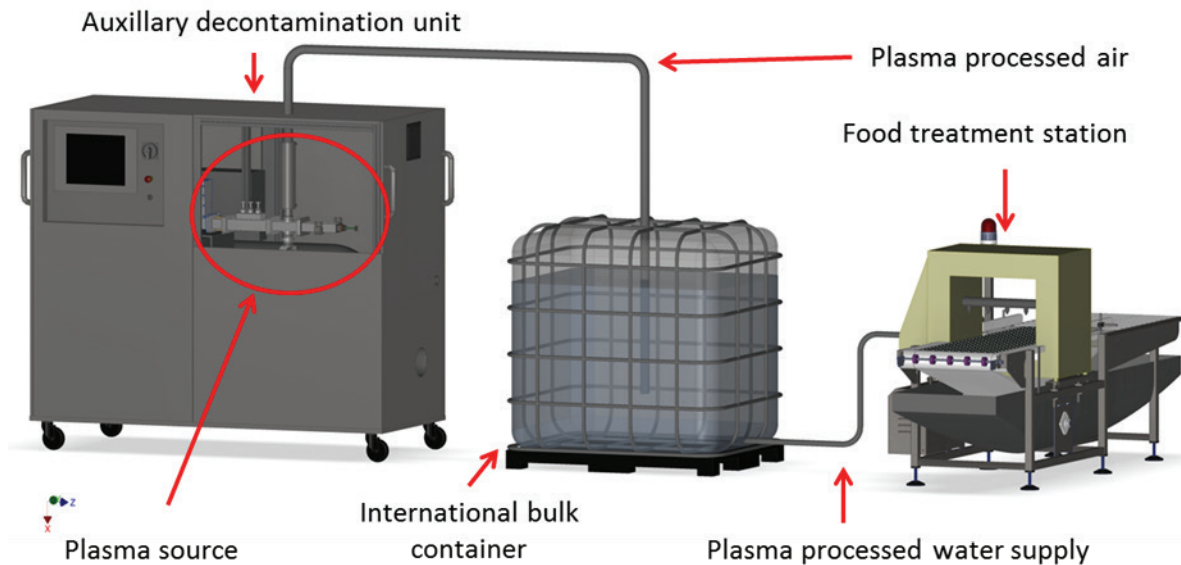


Figure 1. It shows a sketch of the experimental setup, which includes the plasma processing of air and water and their application to the food.

RESULTS

During the experiments 1.5 m³ of PPW was produced and with it 45 kg of endive was sanitized. Different combinations of tap water and PPW were tested concerning the inactivation of the native microbial load of the salad. It was found that the washing with pure water has no significant effect in inactivation (Figure 3, reduction until prewashing). This effect is mainly caused by the lack of a temperature controlled environment (Temperatures up to 25 °C) and problems in the hygienic reworking of the food treatment station. These leads to a microbial load inside the treatment station which recontaminates the processed food.

By using PPW the hygienic problems can be overcome at the local processing places and a reduction of up to two orders of magnitudes can be achieved. However, process station, which does not use PPW, will recontaminate the salad.

Furthermore, these results in inactivation of microorganisms were confirmed by all three independent research facilities.

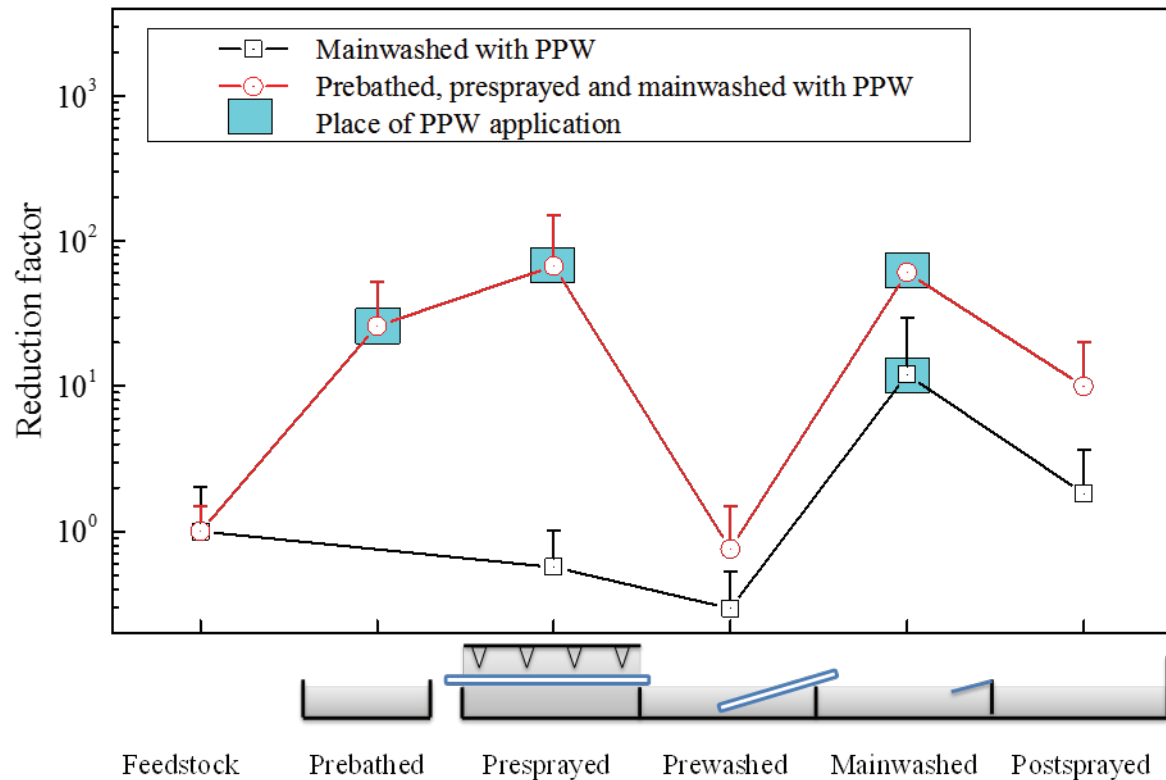


Figure 2. It shows the inactivation of the native microbial load of endive for different processes.

CONCLUSION

Based on the results of sanitizing food in a laboratory scale (10 ml) a new microwave plasma source and processes were developed. Thereby food was successfully sanitized with plasma processed water in a technological scale. 1.5 m³ of PPW were produced locally and with it 45 kg of endive was treated in different processes. Up to two orders of magnitude in reduction of the native microbial load was achieved.

ACKNOWLEDGEMENT

Gratefully, we thank the company Jürgen Lührke GmbH for providing the technical center and the Federal Ministry for Education and Research Germany (project funding reference number: 13N12428) for financial support.

The Plasma Boost in Semiconductor Industry

Tunjar Asgarli, Klaus Baumgaertner

MUEGGE GmbH, Reichelsheim, Germany

Keywords: Plasma systems, integrated circuits, etching, pyrolysis, decapsulation, technology correlation.

INTRODUCTION

The plasma technologies, a hot topic for recent scientific discussions, have actually been investigated a half century ago. However, lack of infrastructure and non-refinement of assisting technologies hindered its potential for application in numerous fields [1-2]. Since then, to keep the miraculous development rate of microfabrication rising, a need for alternative process environment emerged. It is noteworthy that the technology plasma was intended to refine had already been serving as an assisting technology for the development of plasma technology itself. Reduction in electronics' size and their efficient interface throughputs have pushed engineers to find applications for previously conducted theoretical plasma researches [3-5]. In such fashion, the plasma technologies started boosting the semiconductor industry. Else to say, small developments in the plasma field were amplified in magnitude when microfabrication was observed as output. In this paper, numerous applications of plasma processes that can be found in semiconductor industry are presented. The applications are categorized according to their methodology in the first section, followed by results and discussion about the given methods consequently. Lastly, conclusion is provided as a summary of the paper and general idea is reflected in few words.

METHODS AND APPLICATIONS

The dawn of plasma technology can be traced back to the time when the common known physical states (solid, liquid, gas) were not sufficient for development. With the further improvement on assisting fields, such as fluid dynamics and power electronics, the desired technical parameters were supplementary controlled and plasma became a manageable concept for researchers. Plasma technologies were further concentrated on according to generation method, for example, DC, RF and microwave. The latter possesses several advantages like absence of electrode, high specific power distribution, and high density of excited charge and homogeneity, which makes its use optimal for long-term, high performance applications.

The rapid growth of semiconductor industry is obvious, and it has reached ~\$350 billion in 2014. Enhanced pace in development and desire to meet the complex

requirements of post state-of-art conditions pushed the researchers to unconventional type of progress. To cut down the inflated R&D cost, researchers branched out into fabless technology and advanced fabrication. The high cost of owning and maintaining in the latter field margins out the profit to full capacity, which can only be enabled by long-term stable operated high performance sub-systems.

As a result, semiconductor industry requires high standards in terms of performance over time to supply the high demand. The advantages that microwave plasma possesses enable its usage as alternative environment generator for electronics manufacturing. Further alterations are adapted on plasma systems for its application-specific utilization in electronics field.

Plasma etching, the most abundant plasma technology, owes that fame to its compatibility with several applications. Specifically, the isotropic etching nature on different layers can be utilized for stress relief on the backside of silicon wafers after mechanical thinning, and alterable particle selection can be further applied for cleaning of the process chambers after physical or chemical vapor deposition of thin layers on semiconductor substrates. It should also be noted that the need for more functionality and further miniaturization in integrated circuits causes increasing integration density, making it hard for first-level reliability and increasing the demands for improvements in methods for failure analysis of finished integrated circuit products that are fully encapsulated. This opens a gap for a sensitive and non-destructive decapsulation tool, which is in turn filled by plasma itself.

Another emerging application for plasma is to clean the by-products from plasma semiconductor processes. In a plasma pyrolysis process based on Atmospheric Plasma System, the non-dissociated perfluorinated hydrocarbons leaving the process chamber and imposing great danger to environment, are completely transformed into environment friendly compounds and can be easily recycled in chemical industry.

Last but not least, low-pressure but also more and more atmospheric pressure plasma processes are being applied for surface activation and functionalization of semiconductor substrates.

RESULTS AND DISCUSSION

It can be surely stated that semiconductor industry is thrived by technology innovation. Plasma technology is a major part of these innovations. Plasma-based process equipment is used dominantly in present semiconductor technologies for deposition and etching. Plasma processes on these applications provide frequent cycle times and excellent uniformities. Plasma etching plays a central role to the enabling of patterning technology in semiconductor industry. Remote Plasma Source, a plasma etching device protecting the wafer from thermal impact and enabling isotropic etching, provides approximately **200 $\mu\text{m}/\text{hour}$** removal rate for silicon and organic materials when used for decapsulation purposes. More exactly, for small silicon samples up to **90 $\mu\text{m}/\text{min}$** and for 8'' silicon wafers more than **10 $\mu\text{m}/\text{min}$** etch rate was observed. It should be noted that the described etching is accomplished with high selectivity (**>500:1**), enforcing slight attack on chip passivation. Furthermore, radical rich plasma etching provides removal possibility for wide range of materials like SU-8 (**20 $\mu\text{m}/\text{min}$**), SiN & BPSG (**1 $\mu\text{m}/\text{min}$**), thermal oxide

($0.25 \mu\text{m}/\text{min}$), tungsten ($0.5 \mu\text{m}/\text{min}$) etc. It should be noted that application specific optimization is required for the system (power, working pressure, chamber & chuck size), and it can even be used for stress relief etching with silicon etch rate of $3 \mu\text{m}/\text{min}$ at uniformity of 5%.

CONCLUSION

The overview of the mutual evolution of microwave plasma technology and semiconductor industry is presented. Application-specific units of plasma processing technology in semiconductor industry are given with brief explanations. Referencing the results, it is obvious that plasma has supplied a definitive boost to the current 'well-developed' status of semiconductor industry.

REFERENCES

- [1] B. Chapman, *Glow Discharge Processes*, John Wiley & Sons, 1980.
- [2] E. Nasser, *Fundamentals of Gaseous Ionization and Plasma Electronics*, John Wiley & Sons, 1971.
- [3] R. Kumar and C. Ladas, Characterization of plasma-etching for semiconductor applications, *Electron Devices Meeting, 1975 International, 1975*, pp. 27-28.
- [4] Jen-Shih Chang, Recent development of plasma pollution control technology: a critical review, *Science and Technology of Advanced Materials*, Volume 2, Issues 3-4, pp. 571-576, 12 September 2001.
- [5] Z. J. Lemnios, Research challenges for plasma processes in the semiconductor factory of the future, *Plasma Science, 1996. IEEE Conference Record - Abstracts, 1996 IEEE International Conference on, Boston, MA, USA, 1996*, pp. 181-182.

Dielectric Properties of Concrete: An Experiment and New Model Approach

Natt Makul

Department of Building Technology, Faculty of Industrial Technology,
Phranakhon Rajabhat University, 9 Changwattana Road,
Bangkhen Bangkok, 10220, Thailand

Keywords: Dielectric permittivity; cementitious materials; hydration; microwave energy

INTRODUCTION

Microwave energy has been widely used as innovative material processing for various industrial dielectric materials such as paper, wood, etc. Basically, microwave radiation interacts with the materials through dielectric permittivity resulting in rapid heating. Consequently, dipole interaction and heat generation will take place within dielectric materials which are composed of polar molecules [1].

Can microwave energy be applied to cure cementitious materials? The answer based on theoretical feasibility, is yes. Many research groups [1] have investigated, both experimentally and numerically, the accelerated curing of cements in order to gain high strength [2]. However, the actual number of successes has been very limited. A reason for this is lack of understanding of the behavior of dielectric permittivity of cement-based materials which, in fact, are greatly affected by temperature, free moisture content and hydration time. In particular, during the first 24 h of hydration, it is critical to determine optimum conditions for high performance curing of the cementitious materials using microwave energy [3].

In this paper, the dielectric permittivity of cement-based materials during the initial period of hydration at 2.45 GHz has been investigated by using a network analyzer with an open-ended probe technique based on the influences of water-cementitious ratios, cement types, pozzolan materials and aggregates.

METHODOLOGY

Three groups of 117 specimens having a cubical shape in size of $55 \cdot 55 \cdot 110 \text{ mm}^3$ were tested for dielectric permittivity, temperature rise and setting time, They were made from Types I and III Portland cements in accordance with the ASTM C 150 [4] pulverized fuel ash in a class of low calcium (Type F) in accordance with the ASTM C 618 [4], and silica fume in accordance with the ASTM C 1240 [4]. River sand (FM.=2.58) and crushed

limestone rock (Max. Size = 10 mm), having a grade conforming with the ASTM C 33 [4], were mixed with tap water to form pastes, mortars and concretes with various proportions.

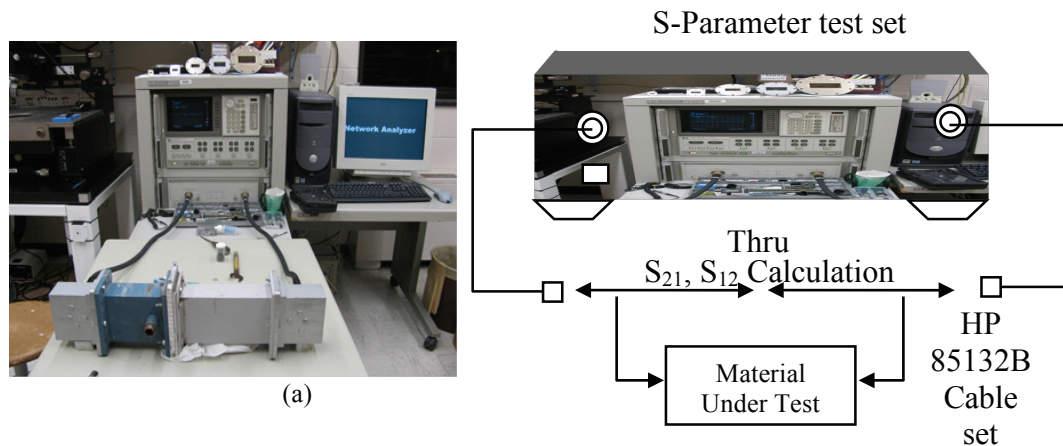


Figure 1 Network analyzer [5].

RESULTS

Figure 2 shows the evolution of dielectric permittivity and simultaneous temperature rise of concretes. It can be observed that the dielectric permittivity at the initial stage is relatively high in comparison with the later stage, and also increases with the increasing water content (higher w/c) in the concrete. This is due to the fact that immediately after the contact between water and cement they start to react and then dissolve Ca^{2+} , OH^- and SO_4^{2-} ions into the system. In addition, during the dormant period, the dielectric permittivity changes very little because the chemical compositions of the aqueous remains remain nearly constant [6].

At early stage of 24 h hydration reaction period, permittivity remains at a high level and decreases at the end of the dormant period, approaching to a constant value when the internal structure has been stabilized. The dielectric permittivity of Type III pastes is higher than the Type I pastes because Portland cement Type III has finer grains of tri-calcium aluminate (C_3A) [6] than in the Type I causing it to dissolve with a high rate and maintaining an ion-rich system. In addition, the rate of the decrease of dielectric permittivity of Type III paste is higher than that of Type I. In the acceleratory period, the Type III paste reacts faster than the Type I paste. This coincides with temperature rise and shorter dormant period. For setting time, the dielectric constant is maintained until the final setting time because of the high dissolution rate, however the dielectric constant drops dramatically with the high hydration rate. At the later stage after formation of the C-S-H structure, the dielectric permittivity tends to remain constant because of strong constraints imposed by its structure.

CONCLUSION

Dielectric permittivity of cement-based materials is affected by initial water-cement ratio, cement types, pozzolan and aggregate types. However, although the volumetric fraction of water and superplasticizer in a given mixture is small, it strongly affects the dielectric permittivity of the cement due to its high dielectric permittivity. The change in the dielectric permittivity is relatively high and remains constant during the dormant period; after that it decreases rapidly when the hydration reaction resumes, and it continues to decrease during the acceleratory period.

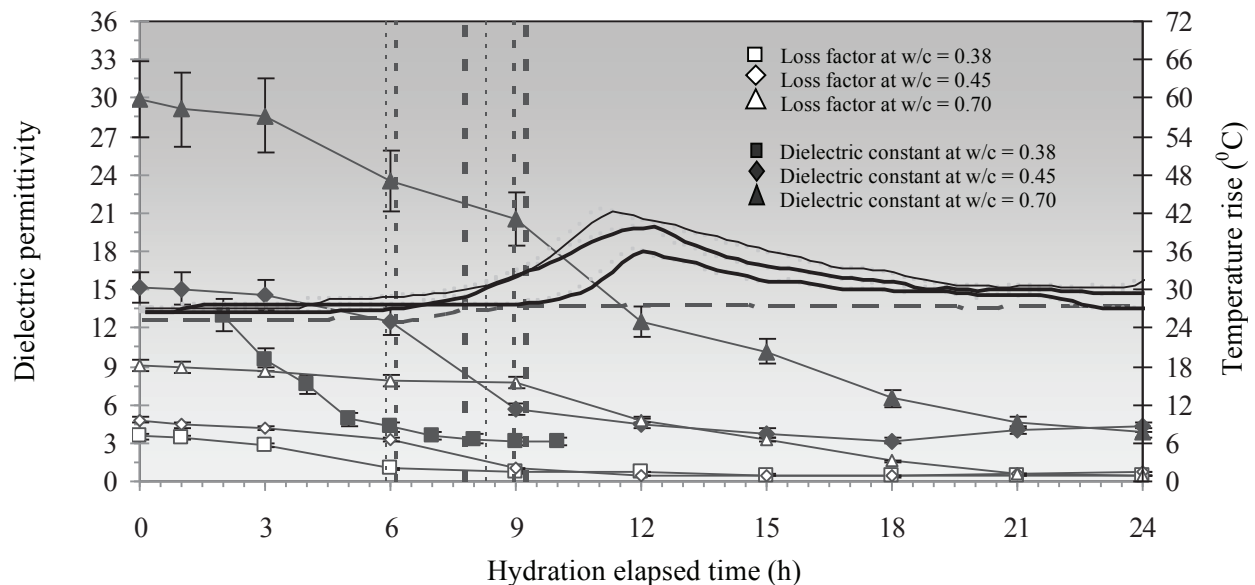


Figure 2 Dielectric permittivity of concretes with different w/c ratios.

ACKNOWLEDGEMENTS

The author appreciates the financial support of the Thailand Research Fund (Contract No. TRG5780255) and Phranakhon Rajabhat University #2558 for providing financial support for this project.

REFERENCES

- [1] Metaxas, A.C. Microwave heating. *J. Power Eng.*, 1991(5), pp. 237- 247.
- [2] Leung, K.Y.C. and Pheeraphan, Microwave curing of Portland cement concrete: experimental results and feasibility for practical applications. *Cons. Build. Mat.*, 1995, 9 (2), pp. 67 - 73.
- [3] Hutchinson, R.G., et al. *Thermal acceleration of Portland cement mortars with microwave energy.* *Cem. Con. Res.*, 1991, 21, pp. 795 - 799.
- [4] ASTM. *Annual Book of ASTM Standard Vol. 4.01*, Philadelphia, PA, USA, 2008.
- [5] Hewlett Packard Corporation. *Dielectric Probe Kit 85070A*. Palo Alto, CA: Research and Development Unit, Test and Measurements Laboratories, 1992.
- [6] Hewlett, P. C. *Lea's chemistry of cement and cementitious material*. 4th Edition, New York: John Wiley & Sons Inc.

Microwave Aided Plasma Generation

Margarita Baeva, Mathias Andrasch, Andre Bösel, Jörg Ehlbeck, Detlef Loffhagen and Klaus-Dieter Weltmann

Leibniz Institute for Plasma Science and Technology, INP Greifswald e.V., Felix-Hausdorff-Str. 2, 17489 Greifswald, Germany

Keywords: Self-consistent modeling, plasma ignition, microwave-plasma interaction.

INTRODUCTION

Microwaves offer the opportunity of generating traveling-wave or localized gas discharges used in many applications since they enable lower costs equipment and processing. Treatment of thermal sensitive materials, antimicrobial processing of samples and food, gas purification, detection of heavy elements and compounds, and crystal growth are some of the aspects that have been in the focus of experimental and theoretical research. The further development and potential applications demand a better understanding of the physical processes involved. Complementary studies benefit from advanced modeling and diagnostic techniques.

In this work, results of self-consistent modeling are presented related to microwave aided plasma generation at 2.45 GHz. The MiniMIP source (Figure 1a) is aimed at analytical applications and is operated in argon and helium at atmospheric pressure. The PLexc family (Figure 1b) operates at pressures from millibar up to atmospheric pressure in air-like mixtures and rare gases. A high-temperature plasma jet is provided for surface treatment and sterilization.

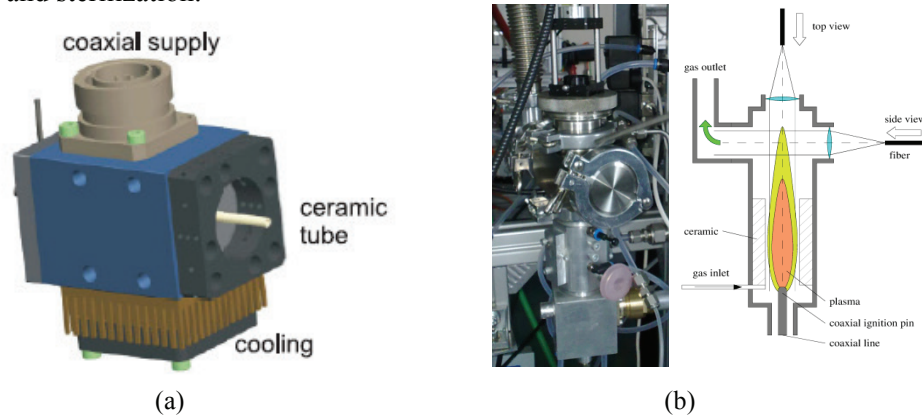


Figure 1. View and schematic diagram of the microwave plasma sources: (a) MiniMIP – working gases Ar, He 200-400 ml/min, 1 atm, forwarded power 20 - 200 W, plasma size \varnothing 1.5mm, length 7 mm, (b) The PLexc family- working gas Ar, Air-like mixtures 30 – 1000 ml/min, pressure 5-80 mbar/1 atm, forwarded power 100 – 400 W, 1 kW, min plasma size. \varnothing 16 mm, length 20 mm.

METHODOLOY

A time-dependent 2D fluid model has been used in combination with different diagnostics for instance optical emission spectroscopy. The model has been described in detail in [1, 2]. The plasma behaves like a fluid containing electrons and heavy particles of argon. Navier-Stokes equations provide a solution of the mass density and the mass-averaged velocity of the fluid. Separate energy conservation equations are solved for the electron and the heavy particles plasma components. The species transport is described by diffusion equations for excited atoms and ions. The electron density is found from the condition of plasma quasi-neutrality. The electromagnetic field is determined by solving Maxwell equations, accounting for the electric conductivity of the induced plasma. The model delivers the gas flow parameters, the spatial distributions of the heavy particles and electron temperature, the species density, and the electromagnetic field in the entire computational domain.

RESULTS

The computed electric field distribution in the computational domain corresponding to the MiniMIP source is shown in Figure 2a. Prior to the plasma ignition, the microwave is guided to the upper end the metal source head. In the presence of plasma, the microwave is guided along the plasma boundary and is capable of propagating so that a plasma jet with gas temperatures of over 2000 K is generated. Depending on the absorbed microwave power, the plasma is sustained in diffuse or constricted mode as shown in Figure 2b. This behavior is explained by the nonlinear dependence of the molecular ion density on the gas temperature. For gas temperatures over 1200 K, the molecular ion density is less than the atomic ion density due to dissociation and dissociative recombination of the molecular ion in collisions with electrons. Excited atoms produced in the latter process further contribute to the production of atomic ions. In the plasma periphery, the gas is colder and correspondingly, the molecular ion density increases as a result of the process of ion conversion and the larger neutral atom density.

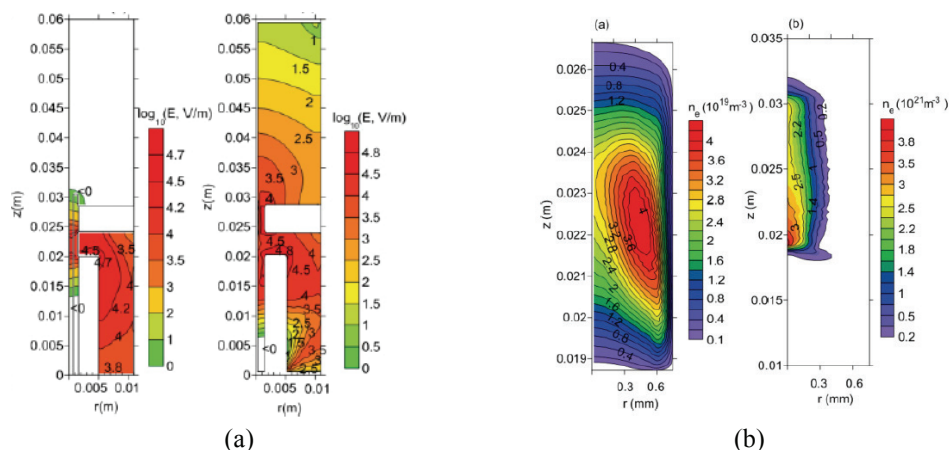


Figure 2. Simulated spatial distributions in MiniMIP: a) Electric field without plasma (lhs) and in a presence of plasma (rhs), b) Electron density at absorbed power of 2 W (lhs) and 20 W (rhs) [1].

The self-consistent model does not only provide the plasma characteristics but it allows us as well to have a look at the plasma-wave interaction. The evolution of the plasma and the propagation of the microwave in the PLe_{xc} source is illustrated in Figure 3. At the start of the pulse, there are only the background electrons and ions. The microwave is guided approximately to the end of the inner electrode. The electric field has a maximum around the pin-shaped edge where the plasma ignition starts. The electron density, the volume occupied by the plasma, and the absorbed power increase with increasing incident microwave power. The generated core plasma expands and approaches the wall. Microwave propagation and plasma expansion occur along the walls approaching the end of the source head. The plasma plays the role of an extension of the inner electrode in the propagation of the microwave. Power in-coupling occurs in the region of the highest electron density during the early stage of the discharge. In the steady state phase, however, the power in-coupling occurs close to the source walls where the electron density is significantly lower than at the discharge axis.

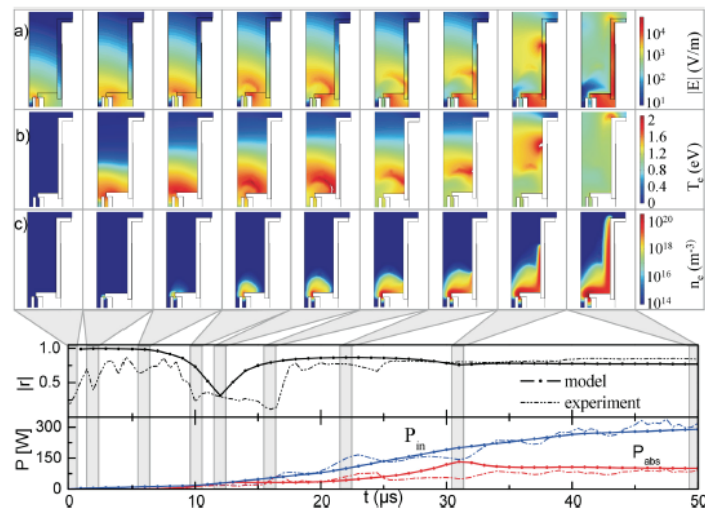


Figure 3. Simulated evolution in PLe_{xc} source – electric field, electron temperature and density in argon at 20 mbar related to the measured reflection coefficient, incident and absorbed power [2].

CONCLUSION

Self-consistent modeling is a powerful tool to understanding basic processes, development of plasma sources and the optimum application of microwave plasma.

REFERENCES

- [1] M. Baeva, A. Bösel, J. Ehlbeck, and D. Loffhagen, Modeling of microwave-induced plasma in argon at atmospheric pressure, *Phys. Rev. E*, vol. 85, 056404 (9 p.), 2012.
- [2] M. Baeva, M. Andrasch, J. Ehlbeck, D. Loffhagen, and K.-D. Weltmann, Temporally and spatially resolved characterization of microwave induced argon plasmas: Experiment and modelling, *J. Appl. Phys.*, vol. 115, 143301 (13 p.), 2014.

A Novel Microwave-Low Pressure Process for Strengthening High Performance Concrete Paste

Natt Makul

Department of Building Technology, Faculty of Industrial Technology, Phranakhon Rajabhat University, 9 Changwattana Road, Bangkok Bangkok, 10220, Thailand

Keywords: Concrete, Paste, Microwave, Processing, Low-pressure, Strength

INTRODUCTION

The use of microwave (MW) energy to make high performance concrete paste (HPC), which is associated with a low pressure system, is an innovative method that will become increasingly important in the near future in the production of HPC. Research in this area is necessary to understand the processing mechanism with dielectric properties and to establish the characteristics of HPC.

The concept for determining the parameters of MW processing and the vacuum system of HPC is based on the hydration reaction of HPC, which comprises three main periods: [1,2]

- Period 1: The early period, which is also referred to as the dormant period, begins with contact between the cement grains and the water molecules.
- Period 2: The accelerated or middle period begins with the formation of calcium and hydroxide ions until the system is saturated. Once the system has become saturated, the calcium hydroxide begins to crystallize.
- Period 3: The final period is referred to as the decelerated or late period. In this period, the hydrate products begin to slowly form and continue to form so long as both water and unhydrated silicates are present.

As noted in the conceptual outline, two principal parameters are employed to control the hydration reaction of HPC: the time-dependent dielectric properties of HPC throughout the hydration process and the water–cement (w/c) mass ratio; the latter influences the temperature (i.e., causes it to increase) and the properties of the MW-cured HPC.

METHODOLOGY

Type 1 Portland cement (ASTM C150) was mixed with deionized water with a pH of 7.5 in specific water–cement (w/c) mass ratios of 0.22, 0.38, and 0.60. MW was used to assist the processing as shown in Fig. 1. The MW power was generated at a frequency of 2.45 GHz, and the power setting was calibrated at 780 W. The MW power was conveyed via a rectangular waveguide to a 0.13 m³ metallic low-pressure cavity, in

which the materials were rotated by a rotary drum. The drum was composed of polypropylene with a diameter of approximately 30 cm and a length of approximately 50 cm, and had a full load capacity of 30 kg. The drum rotation speed was 10 rpm. The maximum low-pressure level was approximately 30 kPa.

The work pieces were maintained at a specific maximum temperature; for the HPC with w/c ratios of 0.22, 0.38, and 0.60, these temperatures were 96.8°C, 70.4°C, and 52.8°C, respectively). After obtaining the given maximum temperatures, the work pieces were maintained at these temperatures for 60 min, i.e., until the MW processing was completed. After step 3 was completed, the work pieces were cooled at room temperature, and the pressure was simultaneously reduced to normal using a convection method that was based on air flow.

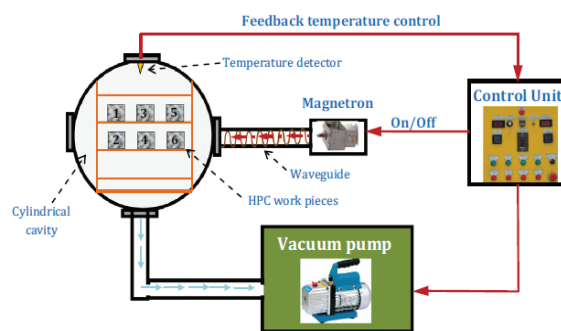


Figure 1 A combined unsymmetrical MW and vacuum system

RESULTS

The compressive strengths of the HPC work pieces with w/c ratios of 0.22, 0.38, and 0.60 after the application of MW processing are shown in Fig. 2. When cured at elevated temperatures, HPC can rapidly develop strength. At the age of 2 hours after MW curing, the HPC work pieces with a w/c ratio of 0.22 attained a compressive strength of 20.1 MPa (129% higher than the compressive strengths of the water-cured HPC). At 24 h of curing, the compressive strength of the MW-cured HPC was 35.3 MPa; at 7 days and 28 days, the compressive strengths were 45.2 and 42.6 MPa, respectively. However, for subsequent 7-day and 28-day stages, the compressive strengths of the MW-cured work pieces were 21.1 to 41.9% lower than the compressive strengths of the water-cured HPC due to a reduction of less than 0.25 in the w/c of the MW-cured HPC. When the water content is 0.25, all water molecules exist as gel and combined water in the C-S-H structure, that is, no capillary water exists after complete hydration has occurred. However, some capillary pores should be preserved as paths through which water molecules can enter and react with cement grains near the pores. These pores can serve as a space for the gel to expand. The existence of a few capillary pores may support the structure and strength of the hardened concrete paste, which is consistent with our experimental results, that is, if the w/c ratio is less than 0.40, full hydration of the cement may not occur and the strength development is undermined.

With regard to the HPC with a w/c ratio of 0.22, the compressive strength of the water-cured HPC work pieces almost continuously developed, because the remaining w/c

for the work pieces exceeded the minimum w/c (0.25). Consequently, the strength continuously developed compared with the water-cured HPC at a subsequent age. In the case of the work pieces with a w/c ratio of 0.60, the strength development at subsequent ages (7 and 28 days) was lower than the strength development of the water-cured HPC because high w/c ratios affect the high porosity of the internal structure of HPC. As a result, the water with high HPC content can be transported from the work pieces, causing a decrease in compressive strength.

CONCLUSION

MW heating of HPC produced compressive strength that was higher than that produced by normal water curing.

ACKNOWLEDGMENTS

The author appreciates the financial support of the Thailand Research Fund (Contract No. TRG5780255). The author is also grateful for the permission and facilities extended by Professor Dr. Phadungsak Rattanadecho.

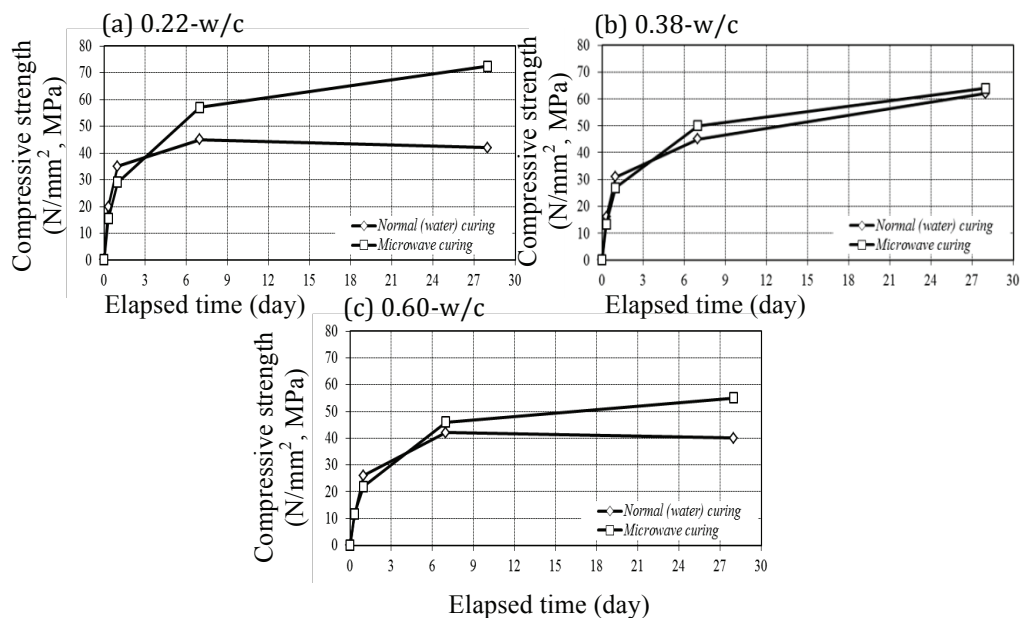


Figure 2. Compressive strength development of HPC with w/c ratios of 0.22, 0.38, and 0.60 after application of MW power at 780 watt for 15 min and low pressure of 30 kPa compared with compressive strength development with normal (water) curing.

REFERENCES

- [1] Neelakantan, T. R.; Ramasundaram, S.; Vinoth, R. Accelerated curing of M30 grade concrete specimen using microwave energy. *Asian Journal of Applied Sciences* 2014, 7, 256–261.
- [2] Xuequan, W.; Jianbo, D.; Mingshu, T. Microwave curing technique in concrete manufacture. *Cement and Concrete Research* 1987, 17, 205–210.

Cooking by Microwave Fireball Excited from Salty-Water Jet

Rafi Jaffe and Eli Jerby*

Tel Aviv University, Ramat Aviv 6997801, Israel

* E-mail: jerby@eng.tau.ac.il

Keywords: Plasma cooking, microwave heating, food browning, microwave fireballs

INTRODUCTION

Microwave ovens are well known for their rapid, low-cost, easy-to-use, and safe heating of food. A major issue in conventional microwave heating and cooking is the non-uniformity of the heating pattern. This inherent feature of microwave heating [1] manifests itself in two major forms, namely hotspot generation within the bulk, and relatively cold outer surfaces. Plasma heating has been studied as a method for the disinfection of solid food items [2]. Microwave induced plasma has been recently developed for food sanitizing in a technological scale [3].

This paper presents methods of cooking using microwave plasma fireballs [4] excited from salty water in air atmosphere. The experiments aim to address the topics of heating patterns and effects by studying the plasma spectral emission and energy balance, scanning-electron microscope (SEM) analyses, and toxicological aspects concerning the contact between the plasma and the food item.

METHODS AND MATERIALS

Various conceptual schemes for cooking by microwave-induced fireballs ejected from salty-water jets are presented in the examples shown in Fig 1a and b [5]. The microwave energy generated by a conventional magnetron at 2.45 GHz (as in a domestic microwave oven) is radiated into a cavity containing a water injector. The momentary injection provides both liquid electrode attracting the electromagnetic fields, and thus enabling the localized microwave breakdown process, and forms the hotspot from which the plasma is excited [4]. The plasmoid in a form of fireball or fire-column is evolved then from the salty-water jet and elevates towards the cavity ceiling.

The cooked objects in these experiments are chicken breast filet cut into cubes (~15 mm, weighing ~3.5 g) or slices (~50x40x4 mm). The substrate from which the plasmoid is excited is a salty-water solution (1:5 sodium chloride to water by weight) injected momentarily into the microwave cavity to ignite the fireball.

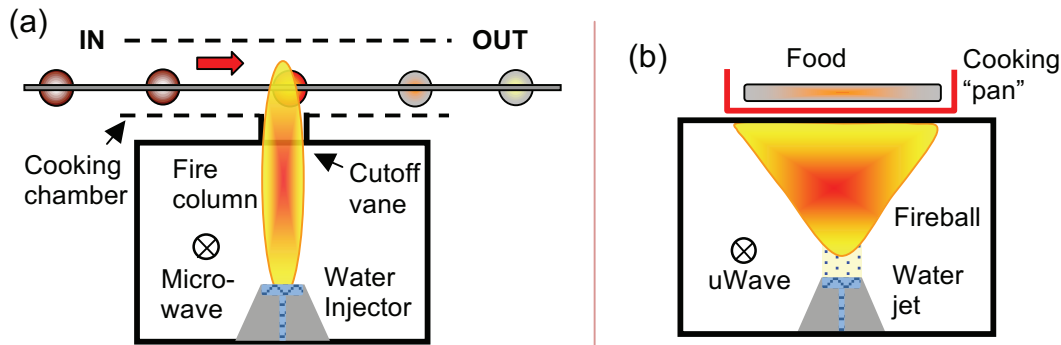


Figure 1: Conceptual schemes for direct (a) and indirect (b) cooking by microwave-generated plasmas. A hybrid mode of both microwave and plasma heating combined is accomplished by inserting the food into the plasma within the microwave cavity.

An impedance-matching tuner and reflectometer provides microwave power and scattering parameters, while a thermal camera measures the temperature in the 0-400°C range. An optical spectrometer is used to analyze the spectral emission of the plasmoid. The cooked food surface is analyzed ex-situ by environmental SEM. Its elemental content is revealed by energy dispersive spectroscopy (EDS) analysis with an X-ray detector. These SEM and EDS analyses aim to examine the effect of the plasma cooking on the meat's surface. These concern both structural aspects (fibers and other formations) and elemental changes that the meat undergoes due to the plasma processing (deposition from the plasma substrate, etc.).

Calorimetric methods are used to measure the heat output of the plasma. The calorimeter is modeled using COMSOL-MultiphysicsTM, and the experimental results are compared to simulation in order to compute the estimated heat output of the fireball.

RESULTS

Figure 2 shows, for example, cross sections of chicken cubes cooked by either sole-plasma cooking, standard microwave cooking, or hybrid microwave-plasma cooking modes. The standard microwave oven cooks mainly the inner bulk of the chicken cube (Figs. 2a, b), whereas the sole-plasma cooking rapidly cooks the surface in contact with the plasma (Figs. 2c, d). The combined mode is achieved by first exposing the chicken to microwaves and then to plasma, utilizing the complementary inner-and-outer effects of the two mechanisms. The results (e.g. Fig 2e) show better uniformity, surface browning and richer grilled-like flavor.

Slices of chicken cooked by the indirect plasma cooking scheme have been presented in Ref. [5]. The fireball heats the pan, thus cooking the slice through is roughly one minute. The cooking is quite uniform, also throughout the bulk. This resembles cooking on a standard household frying pan on a stove, except that the heat source is not a carbon-based burning flame, but rather a detached plasmoid energized by microwave power in a cavity.

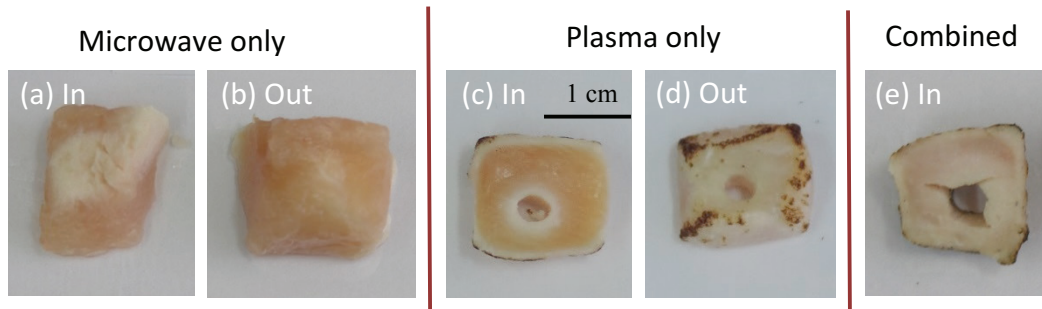


Figure 2. Inner (cross-section) and outer parts of chicken cubes cooked by the various methods. The microwave mostly cooks the inside (a, b) whereas the plasma scorches the outside (c, d). Their combination provides more uniform grilled-flavored cooking (e).

DISCUSSION AND CONCLUSIONS

The sole-plasma method presented here shows extremely quick browning of the surface which came in contact with the fireball. It may provide therefore a method for quickly searing meat. The hybrid microwave and plasma method shows the complementary cooking effect achieved while cooking the inner bulk with microwaves and the outer surface with plasma. This demonstrates the potential of a versatile microwave-plasma cooker with various modes of operation (e.g. microwave/plasma/hybrid). While using the heat from the plasma through a metallic "pan", a similar cooking to that of a conventional frying pan on a stovetop is achieved. This mode might be more efficient though because the fireball can potentially utilize non-standard fuel sources to increase its heat output efficiency (as demonstrated e.g. in [6]). Since the fireball originates here from a salty-water substrate with no metallic electrode, it does not contain toxic metallic particles (found in other plasmoids) and hence is considered as safer for food processing. The cooking techniques introduced in this paper show the feasibility of utilizing plasma generated by microwaves from salty-water jets, which could be incorporated in microwave ovens modified for this purpose.

REFERENCES

- [1] R. Vadivambal and D. S. Jayas, Non-uniform temperature distribution during microwave heating of food materials - a review, *Food Bioprocess Technology*, vol. 3, pp. 161-171, 2010.
- [2] C. S. Yah, G. S. Simate, and S. E. Iyuke, Nanoparticles toxicity and their routes of exposures. *Iranian Jour. Pharmaceutical Sci.*, vol. 8, pp. 299-314, 2011.
- [3] M. Andrasch, Microwave induced plasma for food sanitizing in a technological scale, in these Proceedings.
- [4] V. Dikhtyar and E. Jerby, Fireball ejection from a molten hot-spot to air by localized microwaves. *Phys. Rev. Lett.*, vol. 96, pp. 045002-1-4, 2006.
- [5] E. Jerby, R. Jaffe, Y. Meir, and I. Jerby, Food cooking by microwave-excited plasmoid in air atmosphere, Proc. 14th Conf. Microwave & High Freq. Heating, Ampere-2013, Nottingham, UK, 2013, pp. 27-30.
- [6] Y. Meir and E. Jerby, Thermite-powder ignition by electrically-coupled localized microwaves, *Combust. Flame*, vol. 159, pp. 2474-2479, 2012.

Inversion of the Mixture Models for Materials of Required Complex Permittivity

Hannah Yeung and Vadim V. Yakovlev

Worcester Polytechnic Institute, Worcester, MA

Keywords: Complex permittivity, homogenization of dissipated power, inversed mixture models, microwave heating, power-law mixing rule

Among numerous methods aiming to homogenize microwave processing, there is a group of techniques attempting to improve the heating profile through deformation of the pattern of the electric field by partially filling the cavity with appropriate dielectric slabs (e.g., [1], [2]). Recently, this approach has been revisited and an original technique was reported for determination of geometry and complex permittivity of a dielectric insert which, when placed inside a microwave applicator, homogenizes distribution of dissipated power in the processed material [3], [4]. However, while machining the shape of the filling may not be a problem, the material with required dielectric constant ϵ' and the loss factor ϵ'' is usually not readily available. This may make this technique impractical especially for those many applications in which high values of ϵ' and ϵ'' are needed to guarantee heating uniformity.

In this paper, we present a computational part of a new technique capable of producing a material characterized by a desired complex permittivity. The material is produced from several (3 or more) thoroughly mixed prime materials with known complex permittivities; in the course of the production, depending on their state, the materials may be heated/melted, cooled and shaped. Our computation determines in which proportions/ volume fractions the prime substances should be taken to get the resulting material with desirable ϵ' and ϵ'' .

Computation relies on the power-law mixing rule [5] which can be written for complex permittivity of the mixture $\epsilon_m = \epsilon_m' - i\epsilon_m''$ as

$$\epsilon_m^\alpha = \sum_{i=1}^n V_i \epsilon_i^\alpha, \quad \sum_{i=1}^n V_i = 1, \quad n \geq 3, \quad (1)$$

where ϵ_i are complex permittivities of the prime materials and V_i are their volume fractions. Inverting the rule (1) for different models, i.e., for different values of $\alpha = -1$ (serial model), 0 (Lichtenecker), 1/2 (Kraszewski), 1/3 (Looyenga), $(V_1-0.35)$ (Wakino), $(1.65V_1+0.265, \text{ for } V_1 \leq 0.25)$ (Stölzle), and 1 (parallel model), we compute V_1, \dots, V_n for different topologies, shapes and orientations of the particles, etc. for which corresponding models were found to be the best fit.

In order to illustrate functionality of our computational tool, we determine volume fractions of three prime materials necessary to get optimal values of complex permittivity of the dielectric insert in the system for microwave fixation [3]: $\epsilon_I = 52.7 - i2.53$ and $\epsilon_{II} = 65.0 - i2.08$. Twelve prime materials (denoted here as A, B, C, ..., L) are taken from the class of Li-Nb-Ti-O ceramics [6] to form two groups such that $50.1 \leq \epsilon_{A...F}' \leq 58.5$, $1.0 \leq \epsilon_{A...F}'' \leq 4.0$ and $62.4 \leq \epsilon_{G...L}' \leq 70.0$, $0.5 \leq \epsilon_{G...L}'' \leq 3.5$. Each set of the prime materials, A to F and G to L, is chosen such a way that the target material is located inside the domain formed on the complex permittivity plane by those prime materials. Our computational procedure finds all possible combinations of prime triples that lead to ϵ_I and ϵ_{II} . In this case, the problem of determination of V_i has multiple solutions associated with different triples; typical results for both target materials are shown in Table 1.

Table 1. Volume Fractions of the Prime Materials Required for Production of Mixtures I and II: Inversion of the Parallel, Kraszewski, and Looyenga Models

Target mixture	$\epsilon_I = 52.7 - i2.53$			Target mixture	$\epsilon_{II} = 65.0 - i2.08$		
Set of three prime materials	V_1	V_2	V_3	Set of three prime materials	V_1	V_2	V_3
A+C+D	$\alpha = 1$ 0.375	0.138	0.487	G+J+K	$\alpha = 1$ 0.377	0.443	0.180
	$\alpha = 1/2$ 0.386	0.111	0.503		$\alpha = 1/2$ 0.409	0.345	0.246
	$\alpha = 1/3$ 0.389	0.103	0.508		$\alpha = 1/3$ 0.418	0.315	0.267
A+C+F	$\alpha = 1$ 0.420	0.350	0.230	H+I+K	$\alpha = 1$ 0.539	0.264	0.197
	$\alpha = 1/2$ 0.463	0.285	0.252		$\alpha = 1/2$ 0.587	0.201	0.212
	$\alpha = 1/3$ 0.477	0.265	0.258		$\alpha = 1/3$ 0.602	0.181	0.217
B+C+F	$\alpha = 1$ 0.427	0.419	0.154	H+J+L	$\alpha = 1$ 0.673	0.241	0.086
	$\alpha = 1/2$ 0.489	0.346	0.165		$\alpha = 1/2$ 0.721	0.165	0.114
	$\alpha = 1/3$ 0.508	0.323	0.169		$\alpha = 1/3$ 0.735	0.142	0.123

One can see that, as expected, the values of V_i obtained by inversion of different models are not the same; for those particular Li-Nb-Ti-O ceramics used to produce the materials with ϵ_I and ϵ_{II} , the volume fractions are distinct by 2 to 14%. This means that the choice of the inverted model for determination of V_i should be conditioned by data on the physical structure and particles constituting the prime materials. Forthcoming implementation of the production part of the proposed technique (including measurement of complex permittivity of produced mixtures) will provide specific guidelines to this end.

- [1] J.T. Bernhard and W.T. Joines, Dielectric slab-loaded resonant cavity for applications requiring enhanced field uniformity, *IEEE Trans. Microwave Theory & Tech.*, vol. 44, pp. 457-460, 1996.
- [2] K.A. Lurie and V.V. Yakovlev, Control over electric field in traveling wave applicators, *J. Engng Math*, vol. 44, no. 2, pp. 107-123, 2002.
- [3] E.M. Moon, J.F. Gerling, C.W. Scouten, and V.V. Yakovlev, Modeling-based optimization of thermal processing in microwave fixation, *Proc. 49th IMPI's Microwave Power Symp. (San Diego, CA, June 2015)*, pp. 54-55.

- [4] E.M. Moon and V.V. Yakovlev, CAD of a dielectric insert supporting uniformity of microwave heating, *Proc. 3rd Global Congress on Microwave Energy Applications (Cartagena, Spain, July 2013)* (to be published).
- [5] A. Sihvola, *Electromagnetic Mixing Formulas and Applications*, IFT, 1999.
- [6] Z. Liu, Y Wang, W. Wu, and Y. Li, Li-Nb-Ti-O microwave dielectric ceramics, *J. of Asian Ceramic Soc.*, vol. 1, pp. 2-8, 2013.